Westinghouse Non-Proprietary Class 3

WCAP-17360-NP
Revision 0

May 2012

Small Scale Unbuffered and Buffered Boric Acid Nucleate Boiling Heat Transfer Tests with Sump Debris in a Vertical 3x3 Rod Bundle

Westinghouse

WCAP-17360-NP
Revision 0

Small Scale Unbuffered and Buffered Boric Acid Nucleate Boiling Heat Transfer Tests with Sump Debris in a Vertical 3x3 Rod Bundle

W. A. Byers*
Materials Center of Excellence

J. P. Spring*
LOCA Integrated Services II

May 2012

Reviewers: B. E. Kellerman*
LOCA Integrated Services II

Y. J. Song
Nuclear Systems/NPP

A. E. Hawk
LOCA Integrated Services II

Approved: D. M. Crytzer,* Manager
LOCA Integrated Services II

This work is performed under PWROG Project Number PA-ASC-0689, Revision 3.

*Electronically approved records are authenticated in the electronic document management system.

Westinghouse Electric Company LLC
1000 Westinghouse Drive
Cranberry Township, PA 16066, USA

LEGAL NOTICE

This report was prepared as an account of work performed by Westinghouse Electric Company LLC. Neither Westinghouse Electric Company LLC, nor any person acting on its behalf:

A. Makes any warranty or representation, express or implied including the warranties of fitness for a particular purpose or merchantability, with respect to the accuracy, completeness, or usefulness of the information contained in this report, or that the use of any information, apparatus, method, or process disclosed in this report may not infringe privately owned rights; or

B. Assumes any liabilities with respect to the use of, or for damages resulting from the use of, any information, apparatus, method, or process disclosed in this report.

COPYRIGHT NOTICE

DISTRIBUTION NOTICE

This report was prepared for the PWR Owners Group. This Distribution Notice is intended to establish guidance for access to this information. This report (including proprietary and non-proprietary versions) is not to be provided to any individual or organization outside of the PWR Owners Group program participants without prior written approval of the PWR Owners Group Program Management Office. However, prior written approval is not required for program participants to provide copies of Class 3 Non Proprietary reports to third parties that are supporting implementation at their plant, and for submittals to the NRC.

PWR OWNERS GROUP DOMESTIC MEMBER PARTICIPATION* FOR PROJECT/TASK PA-ASC-0689 REV. 3			
		Participant	
Utility Member	**Plant Site(s)**	**Yes**	**No**
AmerenMissouri	Callaway (W)	X	
American Electric Power	D.C. Cook 1&2 (W)	X	
Arizona Public Service	Palo Verde Unit 1, 2, & 3 (CE)	X	
Constellation Energy Group	Calvert Cliffs 1 & 2 (CE)	X	
Constellation Energy Group	Ginna (W)	X	
Dominion Connecticut	Millstone 2 (CE)	X	
Dominion Connecticut	Millstone 3 (W)	X	
Dominion Kewaunee	Kewaunee (W)	X	
Dominion VA	North Anna 1 & 2, Surry 1 & 2 (W)	X	
Duke Energy	Catawba 1 & 2, McGuire 1 & 2 (W), Oconee 1, 2, 3 (B&W)	X	
Entergy	Palisades (CE)	X	
Entergy Nuclear Northeast	Indian Point 2 & 3 (W)	X	
Entergy Operations South	Arkansas 2, Waterford 3 (CE), Arkansas 1 (B&W)	X	
Exelon Generation Co. LLC	Braidwood 1 & 2, Byron 1 & 2 (W), TMI 1 (B&W)	X	
FirstEnergy Nuclear Operating Co	Beaver Valley 1 & 2 (W), Davis-Besse (B&W)	X	
Florida Power & Light \ NextEra	St. Lucie 1 & 2 (CE)	X	
Florida Power & Light \ NextEra	Turkey Point 3 & 4, Seabrook (W)	X	
Florida Power & Light \ NextEra	Pt. Beach 1&2 (W)	X	
Luminant Power	Comanche Peak 1 & 2 (W)	X	
Omaha Public Power District	Fort Calhoun (CE)	X	
Pacific Gas & Electric	Diablo Canyon 1 & 2 (W)	X	
Progress Energy	Robinson 2, Shearon Harris (W), Crystal River 3 (B&W)	X	
PSEG – Nuclear	Salem 1 & 2 (W)	X	
Southern California Edison	SONGS 2 & 3 (CE)	X	
South Carolina Electric & Gas	V.C. Summer (W)	X	
So. Texas Project Nuclear Operating Co.	South Texas Project 1 & 2 (W)	X	
Southern Nuclear Operating Co.	Farley 1 & 2, Vogtle 1 & 2 (W)	X	
Tennessee Valley Authority	Sequoyah 1 & 2, Watts Bar (W)	X	

PWR OWNERS GROUP DOMESTIC MEMBER PARTICIPATION* FOR PROJECT/TASK PA-ASC-0689 REV. 3			
		Participant	
Utility Member	**Plant Site(s)**	**Yes**	**No**
Wolf Creek Nuclear Operating Co.	Wolf Creek (W)	X	
Xcel Energy	Prairie Island 1&2 (W)	X	

* Project participants as of the date the final deliverable was completed. On occasion, additional members will join a project. Please contact the PWR Owners Group Program Management Office to verify participation before sending this document to participants not listed above.

PWR OWNERS GROUP INTERNATIONAL MEMBER PARTICIPATION* FOR PROJECT/TASK PA-ASC-0689 REV. 3			
		Participant	
Utility Member	**Plant Site(s)**	**Yes**	**No**
Axpo AG	Beznau 1 & 2 (W)	X	
EDF Energy	Sizewell B	X	
Electrabel (Belgian Utilities)	Doel 1, 2 & 4, Tihange 1 & 3	X	
Electricite de France	54 Units	X	
Eleconuclear-Eletrobras	Angra 1	X	
Hokkaido	Tomari 1 & 2 (MHI)	X	
Japan Atomic Power Company	Tsuruga 2 (MHI)	X	
Kansai Electric Co., LTD	Mihama 1, 2 & 3, Ohi 1, 2, 3 & 4, Takahama 1, 2, 3 &4 (W & MHI)	X	
Korea Hydro & Nuclear Power Corp.	Kori 1, 2, 3 & 4 Yonggwang 1 & 2 (W)	X	
Korea Hydro & Nuclear Power Corp.	Yonggwang 3, 4, 5 & 6 Ulchin 3, 4 , 5 & 6 (CE)	X	
Kyushu	Genkai 1, 2, 3 & 4, Sendai 1 & 2 (MHI)	X	
Nuklearna Electrarna KRSKO	Krsko (W)	X	
Ringhals AB	Ringhals 2, 3 & 4 (W)	X	
Shikoku	Ikata 1, 2 & 3 (MHI)	X	
Spanish Utilities	Asco 1 & 2, Vandellos 2, Almaraz 1 & 2 (W)	X	
Taiwan Power Co.	Maanshan 1 & 2 (W)	X	

* This is a list of participants in this project as of the date the final deliverable was completed. On occasion, additional members will join a project. Please contact the PWR Owners Group Program Management Office to verify participation before sending documents to participants not listed above.

TABLE OF CONTENTS

LEGAL NOTICE ii
COPYRIGHT NOTICE ii
DISTRIBUTION NOTICE ii
TABLE OF CONTENTS vi
LIST OF TABLES x
LIST OF FIGURES xiii
LIST OF ACRONYMS AND ABBREVIATIONS xx
NOMENCLATURE xxi
EXECUTIVE SUMMARY 1-1
1 INTRODUCTION 1-2
1.1 MOTIVATION 1-3
1.2 OBJECTIVES 1-4
1.3 HIGH RANKED PIRT ITEMS 1-5
2 TEST APPARATUS 2-1
2.1 FACILITY COMPONENTS AND SETUP 2-1
2.2 CORE POWER CONTROL 2-6
2.3 SIMULATED FUEL ROD 2-6
2.4 TEST VESSEL 2-7
2.5 COOLANT FEED SYSTEM 2-7
2.6 COMPUTER MONITORING SYSTEM 2-7
2.7 VISUALIZATION SYSTEM 2-8
2.8 GRAB SAMPLE COLLECTION AND PROCESSING 2-8
3 SOLUTION AND DEBRIS PREPARATION 3-1
3.1 SOLUTION PREPARATION 3-1
3.1.1 Water 3-1
3.1.2 Boric Acid 3-1
3.1.3 Sodium Hydroxide Buffered Boric Acid 3-1
3.1.4 Trisodium Phosphate Buffered Boric Acid 3-1
3.2 DEBRIS PREPARATION 3-1
3.2.1 [ ]^{c} 3-1

3.2.2 [ ]^c 3-1
3.2.3 [ ]^c 3-3
3.3 DEBRIS ADDITION 3-4
3.4 PARTICULATE ADDITION PROCEDURE 3-4
3.5 FIBER ADDITION PROCEDURE 3-4
3.6 CHEMICAL ADDITION PROCEDURE 3-5
4 SCALING DISTORTIONS ON HIGH RANKED PIRT ITEMS 4-1
4.1 HIERARCHICAL TWO-TIER SCALING APPROACH 4-1
4.2 SYSTEM LEVEL SCALING (TOP-DOWN) 4-2
4.2.1 Momentum Equation Scaling 4-2
4.2.2 Energy Equation Scaling 4-6
4.3 DETERMINATION OF PI GROUPS 4-7
4.3.1 Calculation of Pi Groups 4-8
5 TEST RESULTS 5-1
5.1 RUN NRL01 5-4
5.1.1 Power Measurement 5-4
5.1.2 Concentration Measurements 5-5
5.1.3 Precipitation and Debris Observations 5-5
5.1.4 Temperature Measurements 5-5
5.1.5 Two-Phase Flow Visualizations 5-8
5.2 RUN NRL02 5-9
5.2.1 Power Measurement 5-10
5.2.2 Concentration Measurements 5-10
5.2.3 Precipitation and Debris Observations 5-11
5.2.4 Temperature Measurements 5-16
5.2.5 Two-Phase Flow Visualizations 5-19
5.3 RUN NRL03 5-25
5.3.1 Power Measurement 5-26
5.3.2 Concentration Measurements 5-27
5.3.3 Precipitation and Debris Observations 5-28
5.3.4 Temperature Measurements 5-32

5.3.5 Two-Phase Flow Visualizations 5-36
5.4 RUN NRL04 5-41
5.4.1 Power Measurement 5-41
5.4.2 Concentration Measurements 5-42
5.4.3 Precipitation and Debris Observations 5-42
5.4.4 Temperature Measurements 5-42
5.4.5 Two-Phase Flow Visualizations 5-45
5.5 RUN NRL05 5-51
5.5.1 Power Measurement 5-52
5.5.2 Concentration Measurements 5-53
5.5.3 Precipitation and Debris Observations 5-54
5.5.4 Temperature Measurements 5-58
5.5.5 Two-Phase Flow Visualizations 5-61
5.6 RUN NRL06 5-66
5.6.1 Power Measurement 5-67
5.6.2 Concentration Measurements 5-68
5.6.3 Precipitation and Debris Observations 5-69
5.6.4 Temperature Measurements 5-71
5.6.5 Two-Phase Flow Visualizations 5-73
5.6.6 Core Uncovery and Recovery Cycles 5-78
5.7 RUN NRL07 5-84
5.7.1 Power Measurement 5-85
5.7.2 Concentration Measurements 5-86
5.7.3 Precipitation and Debris Observations 5-86
5.7.4 Temperature Measurements 5-88
5.7.5 Two-Phase Flow Visualizations 5-90
5.8 RUN NRL08 5-92
5.8.1 Power Measurement 5-93
5.8.2 Concentration Measurements 5-94
5.8.3 Precipitation and Debris Observations 5-95
5.8.4 Temperature Measurements 5-98

5.8.5 Two-Phase Flow Visualizations 5-101
5.8.6 Core Uncovery and Recovery 5-106
5.9 RUN NRL09 5-111
5.9.1 Power Measurement 5-112
5.9.2 Concentration Measurements 5-112
5.9.3 Precipitation and Debris Observations 5-113
5.9.4 Temperature Measurements 5-114
5.9.5 Two-Phase Flow Visualizations 5-117
5.9.6 Core Uncovery and Recovery Tests 5-126
6 DISCUSSION 6-1
6.1 NUCLEATE BOILING WITH DEBRIS AND CHEMICALS 6-2
6.1.1 Unbuffered Boric Acid with and without Debris 6-3
6.1.2 Trisodium Phosphate Buffered Boric Acid with and without Debris 6-9
6.1.3 Sodium Hydroxide Buffered Boric Acid with Debris 6-14
6.2 BUOYANCY DRIVEN EXCHANGE 6-16
6.3 BORIC ACID PRECIPITATION AND DISSOLUTION 6-19
6.4 IMPACT OF BORIC ACID CONCENTRATION ON TWO-PHASE MIXTURE LEVEL 6-22
7 CONCLUSIONS AND RECOMMENDATIONS 7-1
8 REFERENCES 8-1
APPENDIX A RESOLUTION OF ISSUES NOT ADDRESSED IN PREVIOUS BOILING CHANNEL TESTS. A-1
APPENDIX B BORIC ACID SOLUBILITY B-1
APPENDIX C VISCOSITY DATA OF BUFFERED BORIC ACID SOLUTION WITH AND WITHOUT DEBRIS C-1
APPENDIX D SURFACE TENSION DATA OF BUFFERED BORIC ACID SOLUTION WITH AND WITHOUT DEBRIS D-1

LIST OF TABLES

Table 1-1: High Ranked PIRT Items 1-5

Table 2-1: Elevation of Vessel Fluid and Heater Rod Thermocouples 2-4

Table 3-1: Values Specified for Fiber Length 3-2

Table 4-1: Normalization Parameters for Fluid Momentum Equation 4-5

Table 4-2: Individual Pi Groups from Fluid Momentum Equation 4-5

Table 4-3: Normalization Parameters for Fluid Energy Equation 4-7

Table 4-4: Individual Pi Groups from Fluid Energy Equation 4-7

Table 4-5: Round #4 Test Reference Conditions 4-8

Table 4-6: Subcooled and Saturated Fluid Properties 4-8

Table 4-7: Values of Yeh Void Fraction Correlation Constants 4-9

Table 4-8: Summary of Pi Group Calculations 4-11

Table 4-9: Numerical Values of Pi Groups 4-13

Table 5-1: Summary of Test Parameters 5-2

Table 5-2: Run NRL01 Test Parameters 5-4

Table 5-3: Run NRL02 Test Parameters 5-9

Table 5-4: Run NRL02 Concentration Measurements 5-11

Table 5-5: Run NRL02 Video Collected for Flow Visualization 5-20

Table 5-6: Run NRL03 Summary of Debris Loading Times 5-25

Table 5-7: Run NRL03 Test Parameters 5-26

Table 5-8: Run NRL03 Concentration Measurements 5-28

Table 5-9: Run NRL03 Summary of Time Lapse Videos Showing Debris Accumulation in the Lower Plenum 5-30

Table 5-10: Run NRL03 Video Collected for Flow Visualization 5-37

Table 5-11: Run NRL04 Test Parameters 5-41

Table 5-12: Run NRL04 Video Collected for Flow Visualization 5-47

Table 5-13: Run NRL05 Summary of Debris Loading Times 5-51

Table 5-14: Run NRL05 Test Parameters 5-52

Table 5-15: Run NRL05 Concentration Measurements 5-54

Table 5-16: Run NRL05 Video Collected for Flow Visualization 5-62

Table 5-17: Run NRL06 Summary of Debris Loading Times 5-66

Table 5-18: Run NRL06 Test Parameters....5-67
Table 5-19: Run NRL06 Concentration Measurements....5-69
Table 5-20: Run NRL06 Video Collected for Flow Visualization....5-74
Table 5-21: Run NRL06 Cladding Temperatures, Turnaround and Recovery Times during Uncovery and Recovery Cycles....5-78
Table 5-22: Run NRL06 Video Collected during Uncovery and Recovery Cycles....5-80
Table 5-23: Run NRL07 Summary of Debris Loading Times....5-84
Table 5-24: Run NRL07 Test Parameters....5-85
Table 5-25: Run NRL07 Video Collected for Flow Visualization....5-90
Table 5-26: Run NRL08 Summary of Debris Loading Times....5-92
Table 5-27: Run NRL08 Test Parameters....5-93
Table 5-28: Run NRL08 Concentration Measurements....5-94
Table 5-29: Run NRL08 Video Collected for Flow Visualization....5-102
Table 5-30: Run NRL08 Cladding Temperatures, Turnaround and Recovery Times during Uncovery and Recovery Cycle....5-106
Table 5-31: Run NRL08 Video Collected during Uncovery and Recovery Cycle....5-108
Table 5-32: Run NRL09 Test Parameters....5-111
Table 5-33: Run NRL09 Concentration Measurements....5-113
Table 5-34: Run NRL09 Video Collected for Flow Visualization (Images Presented)....5-117
Table 5-35: Run NRL09 Additional Video Collected for Flow Visualization (No Images Presented)....5-119
Table 5-36: Run NRL09 Cladding Temperatures, Turnaround and Recovery Times during Uncovery and Recovery Cycles....5-127
Table 5-37: Run NRL09 Video Collected during Uncovery and Recovery Cycles....5-129
Table 6-1: Solution Composition and Debris Loading Test Matrix....6-1
Table 6-2: Calculated Heat Fluxes for given Experimental Times and Bundle Powers....6-3
Table 6-3: Physical Properties of Buffered (TSP) Boric Acid....6-23
Table C-1: Chemical Additions for Solutions without Debris....C-2
Table C-2: Chemical Additions for Solutions with Debris....C-2
Table C-3: Chemical Additions for AlOOH....C-2
Table C-4: Viscosity of Buffered (NaOH) Boric Acid without Debris....C-3
Table C-5: Viscosity of Buffered (NaOH) Boric Acid with Debris....C-7

Table C-6: Viscosity of Buffered (TSP) Boric Acid without Debris C-11
Table C-7: Viscosity of Buffered (TSP) Boric Acid with Debris C-15
Table D-1: Chemical Additions for Solutions without Debris D-1
Table D-2: Chemical Additions for Solutions with Debris D-1
Table D-3: Chemical Additions for AlOOH D-2
Table D-4: Surface Tension of Buffered Boric Acid Solutions with and without Debris D-2

LIST OF FIGURES

Figure 1-1: Sodium Borate Saturation Limits 1-4

Figure 1-2: Simulation of High Ranked PIRT Items in 3x3 Test Apparatus 1-6

Figure 2-1: Schematic of Test Facility 2-2

Figure 2-2: Schematic of Test Facility Vessel 2-3

Figure 2-3: Cross-Section of Test Facility Vessel and Heater Rod Thermocouple Locations 2-4

Figure 2-4: Photograph of Test Facility Vessel 2-5

Figure 2-5: Photograph of Data Acquisition System and Supply Tanks 2-5

Figure 2-6: Bundle Power as a Function of Time for Simulated Core Power and 10CFR50 Appendix K Decay Heat Curve 2-6

Figure 2-7: Heater Rod Designs 2-7

Figure 3-1: Equipment Necessary for Preparing the Fiber Debris 3-3

Figure 3-2: Resulting Fiber under Optical Microscope 3-4

Figure 4-1: Schematic of PWR Vessel 4-3

Figure 5-1: Run NRL01 Power Transient 5-5

Figure 5-2: Run NRL01 Sump, Downcomer, and Lower Plenum Fluid Temperatures 5-7

Figure 5-3: Run NRL01 Lower Plenum and Core Fluid Temperatures 5-7

Figure 5-4: Run NRL01 Cladding Temperatures 5-8

Figure 5-5: Run NRL02 Power Transient 5-10

Figure 5-6: Run NRL02 Boric Acid Precipitation Observed on the Lower Plenum Walls after [ ]^{c} 5-13

Figure 5-7: Run NRL02 Boric Acid Precipitation Observed on the Lower Plenum Walls and within the Bulk Fluid Contained in the Lower Plenum after [ ]^{c} 5-14

Figure 5-8: Run NRL02 Boric Acid Precipitation Observed on the Walls within the Core Region at the Top of the Heated Length after [ ]^{c} 5-15

Figure 5-9: Run NRL02 Sump, Downcomer and Lower Plenum Fluid Temperatures 5-17

Figure 5-10: Run NRL02 Lower Plenum and Core Fluid Temperatures 5-18

Figure 5-11: Run NRL02 Cladding Temperatures 5-18

Figure 5-12: Run NRL02 Flow Visualization of Bubbly Flow 5-21

Figure 5-13: Run NRL02 Flow Visualization of Bubble Motion 5-22

Figure 5-14: Run NRL02 Flow Visualization of Vapor Slugs 5-23

Figure 5-15: Run NRL02 Formation of Vapor Slug 5-24

Figure 5-16: Run NRL03 Power Transient 5-27

Figure 5-17: Run NRL03 Crystalline Precipitate on the Vessel Walls near the Two-Phase Mixture Level after [ ]^{c} 5-29

Figure 5-18: Run NRL03 Suspension of Fibrous Debris in Downcomer 5-30

Figure 5-19: Run NRL03 Debris Accumulation in the Lower Plenum after: [ ]^{c} 5-31

Figure 5-20: Run NRL03 Fiber Accumulation on the Outer Edge of a Spacer Grid Observed after [ ]^{c} 5-32

Figure 5-21: Run NRL03 Sump Tank, Downcomer, and Lower Plenum Fluid Temperatures 5-34

Figure 5-22: Run NRL03 Lower Plenum and Core Fluid Temperatures 5-34

Figure 5-23: Run NRL03 Cladding Temperatures (Heater Rod 7) 5-35

Figure 5-24: Run NRL03 Cladding Temperatures (Heater Rod 8) 5-35

Figure 5-25: Run NRL03 Cladding Temperatures (Heater Rod 9) 5-36

Figure 5-26: Run NRL03 Breakup of a Cap Bubble at 18 Inch Elevation and a Bundle Power of 1441W 5-38

Figure 5-27: Run NRL03 Formation of Distorted Cap Bubbles at the Downstream Edge of a Spacer Grid at 22 Inch Elevation and a Bundle Power of 1437W 5-39

Figure 5-28: Run NRL03 Formation of a Large Vapor Slug at the Downstream Edge of a Spacer Grid at 34.5 Inch Elevation and a Bundle Power of 1396W 5-40

Figure 5-29: Run NRL04 Power Transient 5-42

Figure 5-30: Run NRL04 Sump, Downcomer, and Lower Plenum Fluid Temperatures 5-44

Figure 5-31: Run NRL04 Lower Plenum and Core Fluid Temperatures 5-44

Figure 5-32: Run NRL04 Cladding Temperatures 5-45

Figure 5-33: Run NRL04 Flow Visualizations at 2900W Power 5-48

Figure 5-34: Run NRL04 Flow Visualizations at 1400W Power 5-49

Figure 5-35: Run NRL04 Flow Visualizations at 1212W Power 5-50

Figure 5-36: Run NRL05 Power Transient 5-53

Figure 5-37: Run NRL05 Two-Phase Mixture Level at the End of the Experiment Indicating No Visible Precipitation 5-55

Figure 5-38: Run NRL05 Debris Accumulation in the Lower Plenum Roughly [ ]^{c} into the Experiment 5-56

Figure 5-39: Run NRL05 Debris Clumps Swept into the Core Region after Breaking from the Debris Bed Formed in the Lower Plenum 5-56

Figure 5-40: Run NRL05 Debris Accumulation on Outer Edge of a Spacer Grid Observed at the End of the Experiment....5-57

Figure 5-41: Run NRL05 Debris that Settled in the Lower Plenum after Termination of the Experiment which Indicates that Debris was Present in the Core Region....5-57

Figure 5-42: Run NRL05 Debris that Settled at the Core Inlet after Termination of the Experiment which Indicates that Debris was Present in the Core Region....5-58

Figure 5-43: Run NRL05 Sump Tank, Downcomer, and Lower Plenum Fluid Temperatures....5-60

Figure 5-44: Run NRL05 Lower Plenum and Core Fluid Temperatures....5-60

Figure 5-45: Run NRL05 Cladding Temperatures....5-61

Figure 5-46: Run NRL05 Two-Phase Flow Regimes at Three Elevations and Powers Early in the Experiment....5-63

Figure 5-47: Run NRL05 Two-Phase Flow Regimes at Three Elevations and an Average Power of 1390W....5-64

Figure 5-48: Run NRL05 Two-Phase Flow Regimes at Three Elevations and an Average Power of 1284W....5-65

Figure 5-49: Run NRL06 Power Transient....5-68

Figure 5-50: Run NRL06 Debris Accumulation in the Lower Plenum, Downcomer, and Core Inlet Region after [ ]^{c}....5-70

Figure 5-51: Run NRL06 Rod Bundle after Experiment and Disassembly; (a) Debris Accumulation on Outer Edge of a Spacer Grid, (b) White Haze on Heater Rod Surfaces where Precipitation Formed During Core Uncovery....5-70

Figure 5-52: Run NRL06 Sump Tank, Downcomer, and Lower Plenum Fluid Temperatures....5-72

Figure 5-53: Run NRL06 Lower Plenum and Core Fluid Temperatures....5-72

Figure 5-54: Run NRL06 Cladding Temperatures....5-73

Figure 5-55: Run NRL06 Two-Phase Flow Regimes at Three Elevations and Powers Early in the Experiment....5-75

Figure 5-56: Run NRL06 Two-Phase Flow Regimes at Three Elevations and Powers Later in the Experiment....5-76

Figure 5-57: Run NRL06 Two-Phase Flow Regimes at Three Elevations and a Power of Approximately 1427W....5-77

Figure 5-58: Run NRL06 Cladding Temperature Measured at the Top of the Bundle during the Two Uncovery and Recovery Cycles....5-79

Figure 5-59: Run NRL06 Core Fluid Temperature Measured at the Top of the Bundle during the Two Uncovery and Recovery Cycles....5-79

Figure 5-60: Run NRL06 Core Uncovery with High Boric Acid Concentration (Cycle 1)....5-81

Figure 5-61: Run NRL06 Core Uncovery with High Boric Acid Concentration (Cycle 2) 5-82
Figure 5-62: Run NRL06 Core Recovery with High Boric Acid Concentration (Cycle 1).....5-83
Figure 5-63: Run NRL07 Power Transient.....5-86
Figure 5-64: Run NRL07 Debris Accumulation in the Lower Plenum at Experiment Termination Following Debris Injection at the Top of the Core 5-87
Figure 5-65: Run NRL07 Sump, Downcomer, and Lower Plenum Fluid Temperatures.....5-89
Figure 5-66: Run NRL07 Lower Plenum and Core Fluid Temperatures.....5-89
Figure 5-67: Run NRL07 Cladding Temperatures.....5-90
Figure 5-68: Run NRL07 Two-Phase Flow Regimes at Three Elevations and Powers Early in the Experiment.....5-91
Figure 5-69: Run NRL08 Power Transient.....5-94
Figure 5-70: Run NRL08 Debris Accumulation in the Lower Plenum, Downcomer, and Core Inlet Region after [ ]^{c}.....5-96
Figure 5-71: Run NRL08 Debris Accumulation on the Bottom of the Lower Plenum after the Experiment and Disassembly.....5-97
Figure 5-72: Run NRL08 Debris Buildup on the Outer Edges of a Spacer Grid after the Experiment and Disassembly 5-97
Figure 5-73: Run NRL08 Lower Plenum, Downcomer, and Core Inlet Region: (a) Initial Injection of [ ]^{c}, (b) [ ]^{c} into the Experiment 5-98
Figure 5-74: Run NRL08 Sump, Downcomer, and Lower Plenum Fluid Temperatures.....5-100
Figure 5-75: Run NRL08 Lower Plenum and Core Fluid Temperatures.....5-100
Figure 5-76: Run NRL08 Cladding Temperatures.....5-101
Figure 5-77: Run NRL08 Two-Phase Flow Regimes at Three Elevations and Powers Early in the Experiment.....5-103
Figure 5-78: Run NRL08 Two-Phase Flow Regimes at Three Elevations and Powers Later in the Experiment.....5-104
Figure 5-79: Run NRL08 Formation of a Small Vapor Slug by the Coalescence of Several Distorted Bubbles at a Power of 1848W 5-105
Figure 5-80: Run NRL08 Cladding Temperature Measured at the Top of the Bundle during the Uncovery and Recovery Cycle 5-107
Figure 5-81: Run NRL08 Fluid Temperature Measured at the Top of the Bundle during the Uncovery and Recovery Cycle.....5-107
Figure 5-82: Run NRL08 Core Uncovery with High Boric Acid Concentration 5-109

Figure 5-83: Run NRL08 Top of the Heated Length Roughly [ ]^{c} Minutes after Core Recovery Indicating that all Precipitate Formed during Core Uncovery has Dissolved Back into Solution 5-110

Figure 5-84: Run NRL09 Power Transient 5-112

Figure 5-85: Run NRL09 Sump, Downcomer, and Lower Plenum Fluid Temperatures 5-115

Figure 5-86: Run NRL09 Lower Plenum and Core Fluid Temperatures 5-116

Figure 5-87: Run NRL09 Cladding Temperatures 5-116

Figure 5-88: Run NRL09 Flow Visualization of Lower Plenum and Flow Stratification in the Bottom of Downcomer 5-119

Figure 5-89: Run NRL09 Flow Visualization of a Vapor Slug at 34 Inch Elevation 5-120

Figure 5-90: Run NRL09 Flow Visualization of Dispersed Bubbly Flow at 34 Inch Elevation 5-120

Figure 5-91: Run NRL09 Flow Visualization of a Vapor Slug at 32 Inch Elevation 5-121

Figure 5-92: Run NRL09 Flow Visualization of Dispersed Bubbly Flow at 32 Inch Elevation 5-121

Figure 5-93: Run NRL09 Flow Visualization of Bubbly Flow (Large Bubble Generation) at 22 Inch Elevation 5-122

Figure 5-94: Run NRL09 Flow Visualization of Dispersed Bubbly Flow (after Large Bubble Breakup) at 22 Inch Elevation 5-122

Figure 5-95: Run NRL09 Flow Visualization of Bubbly Flow (Large Distorted Bubble) at 18 Inch Elevation 5-123

Figure 5-96: Run NRL09 Flow Visualization of Dispersed Bubbly Flow at 18 Inch Elevation 5-123

Figure 5-97: Run NRL09 Estimated Rise Velocity of a Small Spherical Bubble 5-125

Figure 5-98: Run NRL09 Cladding Temperature Measured at the Top of the Bundle during the Four Uncovery and Recovery Cycles 5-127

Figure 5-99: Run NRL09 Core Fluid Temperature Measured at the Top of the Bundle during the Four Uncovery and Recovery Cycles 5-128

Figure 5-100: Run NRL09 Two-Phase Mixture Level during Core Uncovery 5-130

Figure 5-101: Run NRL09 Core Uncovery with Low Boric Acid Concentration (Cycle 1) 5-131

Figure 5-102: Run NRL09 Core Uncovery with High Boric Acid Concentration (Cycle 2) 5-132

Figure 5-103: Run NRL09 Core Uncovery with High Boric Acid Concentration (Cycle 3) 5-133

Figure 5-104: Run NRL09 Core Uncovery with High Boric Acid Concentration and [ ]^{c} ... 5-134

Figure 5-105: Run NRL09 Core Recovery and Precipitate Dissolution Process (Cycle 3) 5-136

Figure 6-1: Comparison of Experimental Boiling Curves for Runs NRL01, NRL02, and NRL03 Calculated at the [ ]^{c} Bundle Elevation 6-5

Figure 6-2: Comparison of Experimental Boiling Curves for Runs NRL01, NRL02, and NRL03 Calculated at the [ ]^{c} Bundle Elevation 6-5

Figure 6-3: Comparison of Experimental Boiling Curves for Runs NRL01, NRL02, and NRL03 Calculated at the [ ]^{c} Bundle Elevation 6-6

Figure 6-4: Comparison of Core Fluid Temperature for Runs NRL01, NRL02, and NRL03 Measured at the [ ]^{c} Bundle Elevation 6-6

Figure 6-5: Comparison of Core Fluid Temperature for Runs NRL01, NRL02, and NRL03 Measured at the [ ]^{c} Bundle Elevation 6-7

Figure 6-6: Comparison of Core Fluid Temperature for Runs NRL01, NRL02, and NRL03 Measured at the [ ]^{c} Bundle Elevation 6-7

Figure 6-7: Comparison of Heater Rod Temperature for Runs NRL01, NRL02, and NRL03 Measured at the [ ]^{c} Bundle Elevation 6-8

Figure 6-8: Comparison of Heater Rod Temperature for Runs NRL01, NRL02, and NRL03 Measured at the [ ]^{c} Bundle Elevation 6-8

Figure 6-9: Comparison of Heater Rod Temperature for Runs NRL01, NRL02, and NRL03 Measured at the [ ]^{c} Bundle Elevation 6-9

Figure 6-10: Comparison of Experimental Boiling Curves for Runs NRL01, NRL06, and NRL09 Calculated at the [ ]^{c} Bundle Elevation 6-11

Figure 6-11: Comparison of Experimental Boiling Curves for Runs NRL01, NRL06, and NRL09 Calculated at the [ ]^{c} Bundle Elevation 6-11

Figure 6-12: Comparison of Core Fluid Temperature for Runs NRL01, NRL06, and NRL09 Measured at the [ ]^{c} Bundle Elevation 6-12

Figure 6-13: Comparison of Core Fluid Temperature for Runs NRL01, NRL06, and NRL09 Measured at the [ ]^{c} Bundle Elevation 6-12

Figure 6-14: Comparison of Heater Rod Temperature for Runs NRL01, NRL06, and NRL09 Measured at the [ ]^{c} Bundle Elevation 6-13

Figure 6-15: Comparison of Heater Rod Temperature for Runs NRL01, NRL06, and NRL09 Measured at the [ ]^{c} Bundle Elevation 6-13

Figure 6-16: Comparison of Experimental Boiling Curves for Runs NRL01, NRL05, and NRL08 Calculated at the [ ]^{c} Bundle Elevation 6-15

Figure 6-17: Comparison of Core Fluid Temperatures for Runs NRL01, NRL05, and NRL08 at the [ ]^{c} Bundle Elevation 6-15

Figure 6-18: Comparison of Heater Rod Temperatures for Runs NRL01, NRL05, and NRL08 at the [ ]^{c} Bundle Elevation 6-16

Figure 6-19: Run NRL01 Fluid Temperature Measurements Made in the Core and Lower Plenum Regions 6-18

Figure 6-20: Run NRL02 Fluid Temperature Measurements Made in the Core and Lower Plenum Regions 6-18
Figure 6-21: Run NRL03 Fluid Temperature Measurements Made in the Core and Lower Plenum Regions 6-19
Figure 6-22: Cladding Temperature Response during Core Uncovery and Recovery 6-21
Figure 6-23: Run NRL09 Two-Phase Mixture Level at Similar Powers and Different Concentrations: (a) Low Boric Acid Concentration, (b) High Boric Acid Concentration 6-23
Figure B-1: Boric Acid (H_3BO_3) Solubility Limit as a Function of Temperature (Reference 11) B-1
Figure C-1: Viscosity of Buffered (NaOH) Boric Acid at 140°F C-4
Figure C-2: Viscosity of Buffered (NaOH) Boric Acid at 158°F C-4
Figure C-3: Viscosity of Buffered (NaOH) Boric Acid at 176°F C-5
Figure C-4: Viscosity of Buffered (NaOH) Boric Acid at 194°F C-5
Figure C-5: Viscosity of Buffered (NaOH) Boric Acid at 212°F C-6
Figure C-6: Viscosity of Buffered (NaOH) Boric Acid with Debris at 140°F C-8
Figure C-7: Viscosity of Buffered (NaOH) Boric Acid with Debris at 158°F C-9
Figure C-8: Viscosity of Buffered (NaOH) Boric Acid with Debris at 176°F C-9
Figure C-9: Viscosity of Buffered (NaOH) Boric Acid with Debris at 194°F C-10
Figure C-10: Viscosity of Buffered (NaOH) Boric Acid with Debris at 212°F C-10
Figure C-11: Viscosity of Buffered (TSP) Boric Acid at 140°F C-12
Figure C-12: Viscosity of Buffered (TSP) Boric Acid at 158°F C-12
Figure C-13: Viscosity of Buffered (TSP) Boric Acid at 176°F C-13
Figure C-14: Viscosity of Buffered (TSP) Boric Acid at 194°F C-13
Figure C-15: Viscosity of Buffered (TSP) Boric Acid at 212°F C-14
Figure C-16: Viscosity of Buffered (TSP) Boric Acid with Debris at 140°F C-16
Figure C-17: Viscosity of Buffered (TSP) Boric Acid with Debris at 158°F C-17
Figure C-18: Viscosity of Buffered (TSP) Boric Acid with Debris at 176°F C-17
Figure C-19: Viscosity of Buffered (TSP) Boric Acid with Debris at 194°F C-18
Figure C-20: Viscosity of Buffered (TSP) Boric Acid with Debris at 212°F C-18
Figure D-1: Surface Tension of Buffered (NaOH) Boric Acid D-3
Figure D-2: Surface Tension of Buffered (NaOH) Boric Acid with Debris D-3
Figure D-3: Surface Tension of Buffered (TSP) Boric Acid D-4
Figure D-4: Surface Tension of Buffered (TSP) Boric Acid with Debris D-4

LIST OF ACRONYMS AND ABBREVIATIONS

AlOOH	Aluminum Oxyhydroxide
B	Boron
BA	Boric Acid
B&W	Babcock and Wilcox
CCFL	Counter Current Flow Limitation
CE	Combustion Engineering
DC	Direct Current
DI	De-Ionized
ECCS	Emergency Core Cooling System
H2TS	Hierarchical Two-Tier Scaling
LOCA	Loss of Coolant Accident
LTCC	Long Term Core Cooling
MUT	Make-Up Tank
Na	Sodium
NaOH	Sodium Hydroxide
NRC	Nuclear Regulatory Commission
P	Phosphorous
PIRT	Phenomena Identification and Ranking Table
PSU	The Pennsylvania State University
PWR	Pressurized Water Reactor
PWROG	Pressurized Water Reactor Owners Group
RBHT	Rod Bundle Heat Transfer
RCS	Reactor Coolant System
SiC	Silicon Carbide
SI	Safety Injection
TSP	Trisodium Phosphate
WCAP	Westinghouse Technical Report Number Preface (formerly Westinghouse Commercial Atomic Power)

NOMENCLATURE

General

A	Flow Area
C	Specific Heat
D_h	Hydraulic Diameter
e	Internal Energy
f	Friction Factor
g	Gravitational Constant
h	Enthalpy
j	Volumetric Flux
K	Form Loss
L	Length
MF	Momentum Flux
P	Pressure
P/P_o	Decay Heat Ratio
PWL	Full Power Level
Q	Power
Q'''	Volumetric Power
R	Flow Resistance
Re	Reynolds Number
t	Time
T	Temperature
V	Volume
V_{bcr}	Bubble Critical Rise Velocity
W	Flow Rate

Greek Letters

α	Void Fraction
Δ	Difference
Ø	Two-Phase Friction Multiplier
Π	Pi Group
μ	Viscosity
ρ	Density
τ	Residence Time
σ	Surface Tension
Φ	Power

Subscripts

b	Boiling
C	Core
DC	Downcomer
e	Exit
f	Liquid Phase
g	Gas Phase
i	Inlet
LP	Lower Plenum
m	Two-Phase Mixture or Model
o	Initial Condition
p	Property at Constant Pressure or Prototypic
sat	Saturation
sub	Subcooling
UP	Upper Plenum
v	Property at Constant Volume
1Ø	Single-Phase
2Ø	Two-Phase

EXECUTIVE SUMMARY

Following a LOCA in a PWR, the RCS begins to depressurize and, for all but the smallest breaks, significant boiling occurs in the core. The ECCS injects borated water into the reactor vessel to keep the core fuel temperatures at acceptably low levels. All three U.S. PWR nuclear plant designs (Westinghouse, CE, and B&W, advanced plant designs excluded) have ECCS features that, with or without operator action, initiate a core dilution mechanism to prevent the core region boric acid concentration from reaching the precipitation point. The U.S. NRC staff has often cited the disparity of methods and assumptions used to address long-term cooling boric acid control across the U.S. PWR fleet, and the NRC has requested that the industry develop conformity in this area. In response, the PWROG funded a program to develop a LOCA boric acid precipitation control analytical approach, applicable to all PWR designs that would be acceptable to the NRC staff. An early objective in this program was to develop a phenomena identification and ranking table (PIRT) that would provide guidance as to what phenomena the methodology needed to address and how sophisticated of a methodology was needed. While developing the PIRT, it became apparent that there is a relatively low state-of-knowledge regarding the properties of unbuffered and buffered boric acid solutions in the areas of the convective boiling heat transfer, surface tension, and viscosity. Since any new LOCA boric acid precipitation evaluation methodology must consider relevant phenomena, the PWROG boric acid precipitation control program funded tests to investigate the heat transfer behavior of buffered and unbuffered boric acid solutions with and without debris under conditions simulating that expected during the long-term cooling phase following a LOCA. The results of these tests are summarized in this report.

Section 1 provides an introduction including background, motivation for performing the tests, test objectives, and a discussion of the PIRT high ranked phenomena for unbuffered and buffered boric acid solution mixing and transport in a reactor vessel during post-LOCA conditions. Sections 2 and 3 provide the facility description and procedures for preparing chemical solutions and debris loadings. Section 4 presents a scaling analysis performed after the test facility was constructed to quantify any major distortions due to the reduced size of the test facility. Section 5 summarizes the results including temperature transients, precipitation and debris observations, concentration measurements from physical grab samples, and high-speed video collected for two-phase flow visualization. Section 6 contains the discussion of experimental results and includes boiling curve and saturation temperature comparisons as well as discussions on core to lower plenum transport and mixing, precipitation and dissolution during the core uncovery and recovery cycles, and the effect of solute concentration on two-phase mixture level. Section 7 contains the conclusions and recommendations which point toward the need for a full height test facility as well as additional physical properties testing for unbuffered and buffered boric acid solutions with and without debris. Appendix A discusses the resolution of issues not resolved during previous testing. Appendices B, C and D contain physical properties data collected for buffered and unbuffered boric acid solutions with and without debris and include boric acid solubility limit, viscosity, and surface tension.

Results from this experimental series indicate that the presence of debris had no major adverse effects on [ ]^{c} for the debris loadings tested. Further, it was observed that for the range of conditions investigated, the addition of buffering agents (sodium hydroxide or trisodium phosphate) to the boric acid solution appeared to increase the solubility limit such that the onset of precipitation is delayed. This behavior was observed in experiments conducted [ ]^{c}

1 INTRODUCTION

All U.S. pressurized water reactor (PWR) designs use boron coolant to control core reactivity and are subject to concerns regarding potential boric acid precipitation in the core for scenarios that preclude direct safety injection through the core for extended periods following a loss of coolant accident (LOCA). All plant designs have emergency core cooling system (ECCS) features that, with appropriate operator action, initiate a flow through the core to prevent the core region boric acid concentration from reaching the boric acid solubility limit. Up to this point in time, simple models using conservative boundary conditions have been used to demonstrate adequate boric acid dilution. These simplified methods are used to determine the time at which appropriate operator action must be taken to initiate an active boron dilution flow path. All three U.S. PWR suppliers (Westinghouse, CE, and B&W) have different ECCS designs, different procedures for preventing boric acid precipitation, and different methodologies for evaluating the potential for boric acid precipitation. Nevertheless, there are common approaches, assumptions and simplifications that have been used in virtually all PWR post-LOCA calculations that address the potential for boric acid precipitation. Recent extended power uprate (EPU) programs have provided the opportunity for the NRC to challenge some of these common approaches, assumptions and simplifications with regards to regulatory compliance and technical justification.

In August of 2005, shortly after the Waterford EPU was approved, the NRC staff made known to the industry an extensive list of questions related to the potential for boric acid precipitation after a LOCA event. In response to these questions and the NRC's concerns regarding the methodologies used by industry to analyze the potential for boric acid precipitation, the PWROG funded a long-term program to develop a LOCA boric acid precipitation control methodology, applicable to all PWR designs that would be acceptable to the NRC staff. Phase 1 of the long-term program is to establish evaluation model scenarios, assumptions and acceptance criteria that would be acceptable to the NRC. The initial task of Phase 1 was to develop a phenomena identification and ranking table (PIRT) that would provide guidance as to what phenomena the methodology needs to address and how sophisticated the methodology needs to be (Reference 5). In the series of PIRT expert panel sessions that followed, it became clear that there is a relatively low state-of-knowledge in the area of the physical properties of unbuffered and buffered boric acid solutions that would be typical of those found in a PWR containment sump after a LOCA. A follow-up study of LOCA coolant chemistry and possible post-LOCA chemical reactions provided insights on how different chemistries might affect long-term core cooling (LTCC) of the reactor (Reference 6). The study concluded that a variety of different coolant chemistries could exist after a LOCA. For plants which add sodium hydroxide for pH control, the coolant would contain a variety of dissolved species which may behave quite differently than simple boric acid solutions. Such solutions, depending on pH, would tend to precipitate sodium borates rather than boric acid and would do so at different concentration levels. Likewise, plants adding trisodium phosphate or sodium tetraborate would also have different properties than boric acid solutions. The presence of pH control agents will affect not only precipitation from solution, but also other properties such as surface tension, and viscosity. Changes in these properties may in turn affect heat transfer characteristics as well as two-phase flow regimes and mixture level. Since the system codes currently used for predicting post-LOCA boric acid precipitation and heat transfer consider only water and boric acid solutions, it was decided that electrical heater rod testing should be performed to make sure that the pH control agents do not unfavorably alter the heat transfer or two-phase flow structure. Since the boiling and heat transfer characteristics of concentrated sump solutions have ramifications beyond the PWROG boric acid precipitation program, Westinghouse internally funded an initial Round #1 of tests to investigate boric acid buffered with sodium hydroxide (to form a sodium

borate solution) at intermediate and low pH levels.

The results of the initial round of tests indicated that a second series of tests, Round #2, were warranted. The Round #2 tests, again funded by Westinghouse, investigated boric acid buffered with sodium hydroxide (sodium borate solution) at high pH levels, boric acid buffered with trisodium phosphate, and unbuffered boric acid. After the second round of tests, it was determined that concentrated sodium borate solutions were [

]^{c}

After the Round #2 tests, it became apparent that buffered boric acid boiling tests could provide valuable support for justifying a new boric acid precipitation analysis methodology. For example, knowledge obtained from the tests will increase the state-of-knowledge of medium and high ranked phenomena identified in the PIRT for unbuffered boric acid and buffered boric acid solutions. The results could also be used to address potential NRC concerns over the ability of a concentrated sump solution to remove decay heat without a significant clad heatup. Finally, the tests will provide insights for subsequent transport and mixing tests and provide data to support assumptions regarding the potential for precipitation in the boiling region for buffered and unbuffered boric acid solutions. With this perspective, the PWROG approved a revision to PA-ASC-0264 that funded a third round of tests and the documentation of all three rounds of tests in a formal report. This report would then be available to all PWROG members participating in project PA-ASC-0264. One recommendation that came out of the Round #3 testing was to confirm previous observations with an improved apparatus that is more prototypic of the post-LOCA core boiling conditions. This recommendation will be followed during the design of the Round #4 test rig.

1.1 MOTIVATION

Heated beaker tests were performed with buffered boric acid solutions such as sodium borate.
[

]^{c}

It is known that boiling point elevation may occur with the addition of solute to a solvent. The presence of solute, especially if it is non-volatile, will reduce the ability of solvent molecules at the surface of the liquid-vapor interface to escape (overcome intermolecular bonds) and increase the vapor pressure. Due to the intermolecular bonds, a higher vapor pressure is needed to reach the boiling point. This effect can be reduced through agitation (such as turbulence imparting additional energy to the liquid molecules to overcome intermolecular bonds) and/or by creating more effective nucleation near the liquid-vapor interface.

Solubility curves for buffered boric acid solutions suggest the possibility of a lower solubility limit at higher pH levels or higher Na/B mol ratios as shown in Figure 1-1which depicts saturation lines for various forms of sodium borate (Reference 8). Solubility characteristics above mol ratio Na/B = 0.5 cannot be extrapolated from the data available in open literature.

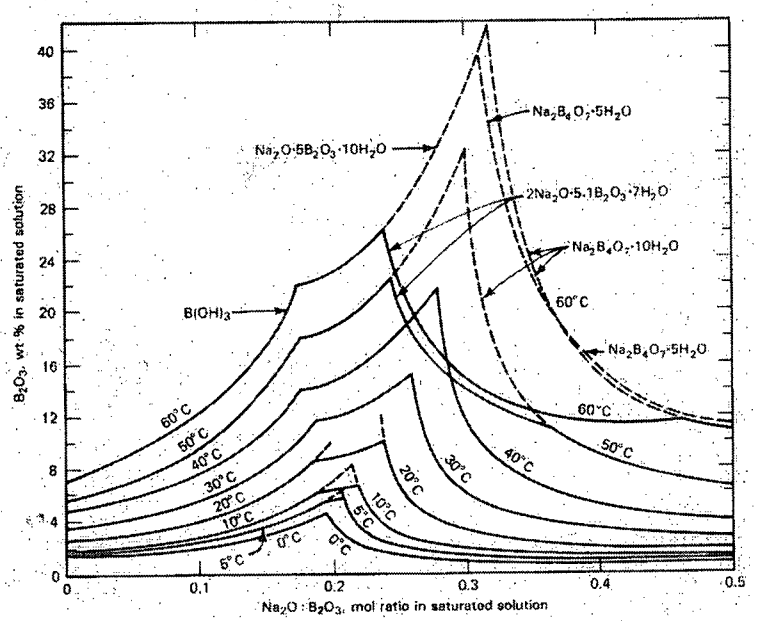

Figure 1-1: Sodium Borate Saturation Limits

Information from open literature (Reference 1) supports the ability of chemical solutions such as sodium borate to provide boiling heat transfer comparable to water. However, no such data has been found demonstrating the performance of chemical solutions in boiling channel geometries at various combinations of pH and boric acid concentrations. To further elaborate, no such data exists pertaining to the precipitation and/or deposition of the solute in such solutions expected to occur during post-LOCA conditions in a nuclear core.

1.2 OBJECTIVES

The primary objective of the Round #4 nucleate boiling heat transfer tests is to extend the knowledge of solute concentration buildup, its impact on nucleate boiling, and the effects of sump debris (GSI-191) on nucleate boiling and boric acid precipitation. The second objective is to investigate unbuffered and buffered boric acid mixing phenomena and concentration distribution under nucleate boiling conditions. To complete these objectives, the testing will be broken into two major parts such that a complete set of nucleate boiling test data can be obtained. First, tests will be conducted using both unbuffered and buffered boric acid solutions without debris. Second, tests will be conducted using the same solutions as in part 1 but with debris loadings representative of those expected to occur in the actual plant. To summarize, the Round #4 testing is expected to:

1. Improve the understanding of nucleate boiling heat transfer and two-phase flow structures in rod bundle geometries under post-LOCA conditions with and without sump debris.

2. Increase the state-of-knowledge of precipitation modes in rod bundle geometries with unbuffered and buffered boric acid solutions with and without sump debris.

3. Provide information to help develop the boric acid precipitation with debris PIRT.

1.3 HIGH RANKED PIRT ITEMS

During the PIRT process, phenomena are ranked for importance through the various periods identified for the event and the state-of-knowledge is assessed based upon the diverse experience of the PIRT review team. For specific phenomena to receive a ranking of HIGH it must be considered crucial to obtain the correct or conservative prediction of the event during the particular period being investigated relative to the other phenomena in question. In the PIRT report, (Reference 5) HIGH ranked phenomena are identified and are of great interest for future study. The Round #3 test report (Reference 3) provides a summary of the PIRT items that received the ranking of HIGH and are listed in Table 1-1.

Table 1-1: High Ranked PIRT Items	
1.	Decay Heat Level
2.	Boiling Heat Transfer Regime (nucleate)
3.	Boiling Channel Hydraulic Geometry
4.	Subcooling of Fluid entering Boiling Channel
5.	Two-Phase Flow Regime (bubbly, slug, etc.) including Bubble Size/Motion
6.	Nucleation Characteristics of Heated Surface (zircaloy tube)
7.	Precipitation in Boiling Regime a. Impact of chemical solution solubility b. Impact of chemical solute transport/mixing (concentration distribution)
8.	Deposition of solute material on heated surfaces above two-phase mixture level a. Impact of surface temperature on evaporation of solvent (i.e., water) b. Impact of solute concentration in liquid phase c. Impact of liquid entrainment or transport of liquid phase onto heated surfaces
9.	Nucleation characteristics of chemical solution a. Impact of dissolved gases in chemical solution b. Impact of nucleation particles from sump in chemical solution
10.	Chemical solution thermo-fluid properties (latent heat of vaporization, surface tension, etc.) 1. Impact of chemical solution pH 2. Impact of chemical solution concentration 3. Impact of system pressure

However, previous tests did not study or only provided limited information of those phenomena and did not include the impact of sump debris. A new PIRT that will consider the effects of sump debris (GSI-191) is currently under development and will use results from this round of testing. Figure 1-2 shows the high ranked phenomena that will be simulated in the 3x3 rod bundle heat transfer tests and includes some possible high ranked phenomena that could be included in the debris PIRT currently under development.

- ● Simulated
- o Partially Simulated
- - Not Simulated

			Test Type						
			1	2	3	4	5	6	7
			De-ionized Water (Large LP)	Unbuffered Boric Acid (Large LP)	Unbuffered Boric Acid + Debris (Large LP)	TSP Buffered Boric Acid (Small LP)	TSP Buffered Boric Acid + Debris (Small LP)	NaOH Buffered Boric Acid + Debris (Large LP)	NaOH Buffered Boric Acid + Debris (Small LP)
			NRL01	NRL02	NRL03	NRL09	NRL06	NRL05	NRL08
Phenomena	1	Decay Heat Level	●	●	●	●	●	●	●
	2	Boiling Heat Transfer Regime (nucleate)	●	●	●	●	●	●	●
	3	Boiling Channel Hydraulic Geometry	●	●	●	●	●	●	●
	4	Subcooling of Fluid Entering Boiling Channel	o	o	o	o	o	o	o
	5	Two-Phase Flow Regime	o	o	o	o	o	o	o
	6	Nucleation Characteristics of Heated Surface	●	●	●	●	●	●	●
	7	Precipitation in Boiling Regime	-	o	o	o	o	o	o
	8	Precipitation on Unheated Surfaces	-	o	o	o	o	o	o
	9	Deposition of Solute Material on Heated Surfaces during Core Uncovery	-	-	-	o	o	-	o
	10	Nucleation Characteristics of Chemical Solution	●	●	●	●	●	●	●
	11	Chemical Solution Physical Properties	●	●	●	●	●	●	●
	12	Solute/Thermal Transport and Mixing	o	o	o	o	o	o	o
	13	Impact of Sump Debris on Boiling Heat Transfer	-	-	o	-	o	o	o
	14	Impact of Sump Debris on Precipitation Modes	-	-	o	-	o	o	o
	15	Impact of Sump Debris on Simulated Fuel Rod Temperature	-	-	●	-	●	●	●
	16	Impact of Sump Debris on Solute/Thermal Transport and Mixing	-	-	o	-	o	o	o

Figure 1-2: Simulation of High Ranked PIRT Items in 3x3 Test Apparatus

2 TEST APPARATUS

In this section, the details of the test apparatus are discussed. This includes a description of the facility components, power simulator, heater rod design, and coolant feed system. The types of instrumentation along with measurement locations and capabilities are also discussed.

2.1 FACILITY COMPONENTS AND SETUP

The test facility is composed of the following four main parts:

- RWST and Sump Tanks
- Coolant Feed and Overflow System
- Vessel (Downcomer, Lower Plenum, Core, and Steam Stack)
- Data Acquisition and Control System

[

]^{c}

[

]c

c

Figure 2-1: Schematic of Test Facility

c

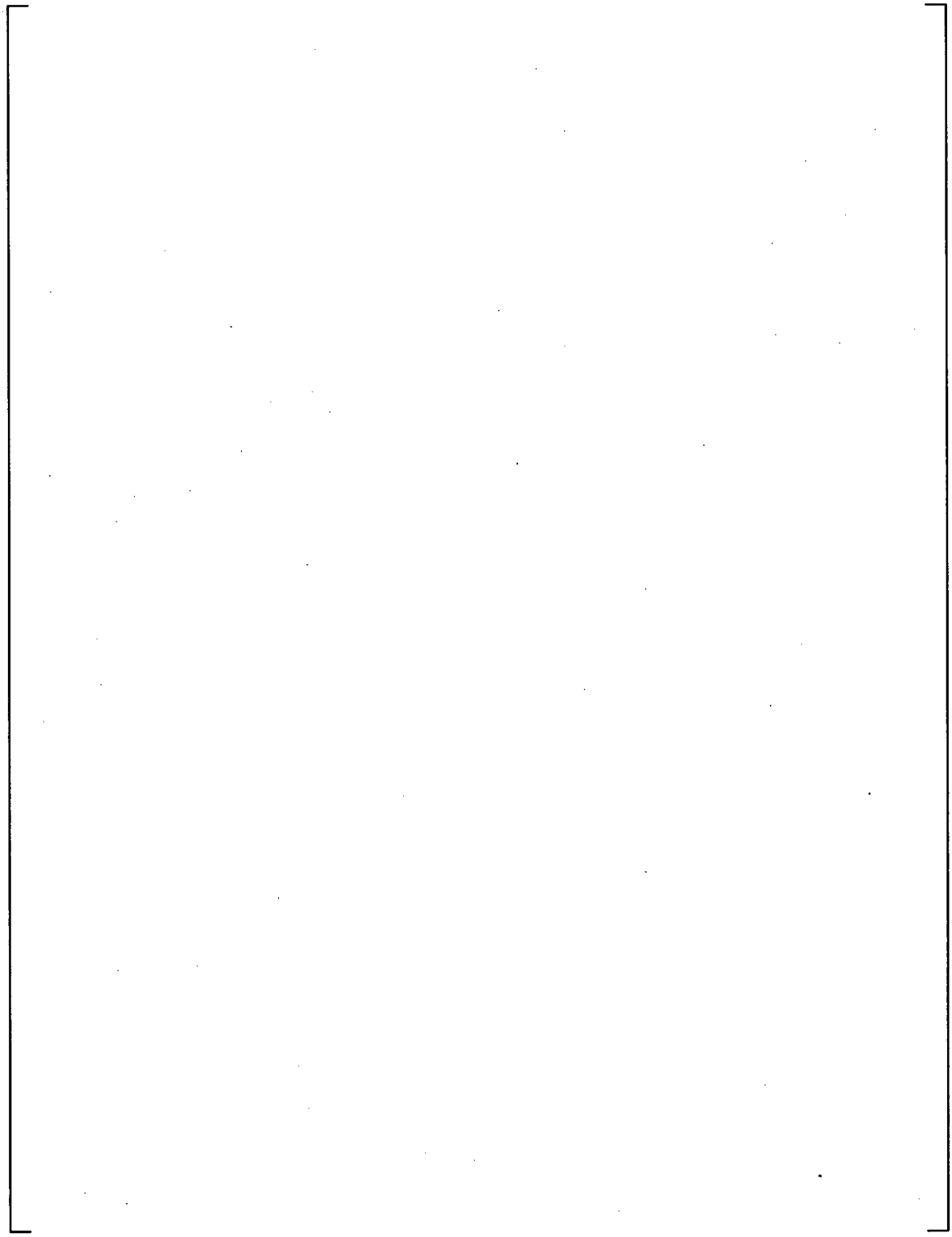

Figure 2-2: Schematic of Test Facility Vessel

c

Figure 2-3: Cross-Section of Test Facility Vessel and Heater Rod Thermocouple Locations

Table 2-1: Elevation of Vessel Fluid and Heater Rod Thermocouples

c

c

Figure 2-4: Photograph of Test Facility Vessel

c

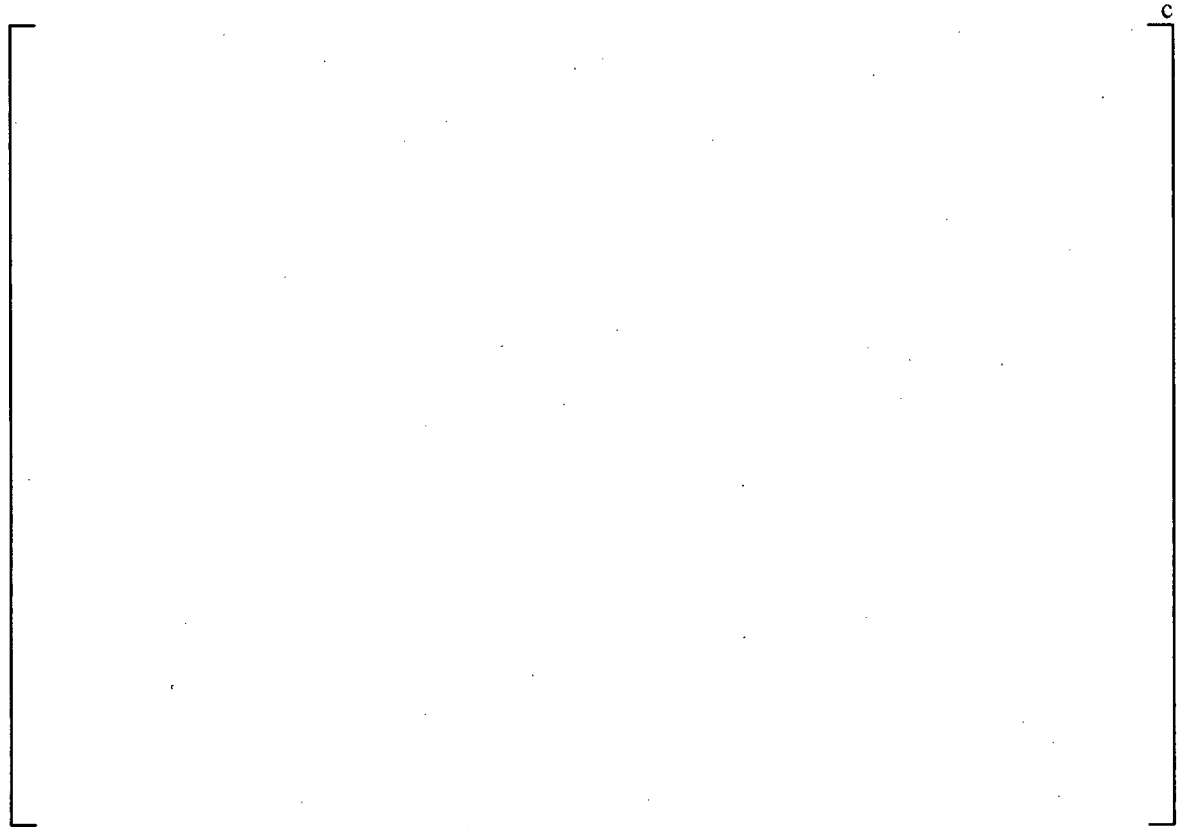

Figure 2-5: Photograph of Data Acquisition System and Supply Tanks

2.2 CORE POWER CONTROL

Power to the simulated core is provided by two power supplies wired in series. The power supplies are controlled by a waveform generator that can be programmed to produce a core power that varies with time. For the majority of tests, the power supplied to the cartridge heaters simulates the 10CFR50 Appendix K decay heat curve. The startup power is [ ]^{c} which corresponds to a [ ]^{c} decay heat ratio (equivalent to approximately [ ]^{c} after a reactor trip). Figure 2-6 shows a comparison between the 10CFR50 Appendix K decay heat curve and the supplied power to the nine cartridge heater rods. Alternatively, the power supplies can be controlled manually to create constant power levels as well.

c

Figure 2-6: Bundle Power as a Function of Time for Simulated Core Power and 10CFR50 Appendix K Decay Heat Curve

2.3 SIMULATED FUEL ROD

The heater rods used in the Round #4 test facility are fabricated from [

]^{c}

c

Figure 2-7: Heater Rod Designs

2.4 TEST VESSEL

The test vessel is designed to simulate a prototypic reactor vessel following a large cold leg break. Coolant and debris enter the test vessel through the downcomer and flow through the lower plenum into the core region. The coolant boils in the core and steam exits through the top of the vessel after passing through a moisture separator. Most of the vessel is made from [

]^{c}

2.5 COOLANT FEED SYSTEM

The injected flow into the test vessel is accomplished with a [

]^{c}

Two tanks are used to supply simulated coolant to the vessel [

]^{c}

2.6 COMPUTER MONITORING SYSTEM

The computer monitoring system continuously records the following data:

- Fluid temperature at six axial locations within the vessel.
- Fluid temperature in the sump tank.
- Fluid temperature in the downcomer.
- Heater rod cladding temperature at four axial, four circumferential, and three lattice positions within the vessel.
- Atmospheric pressure at the test facility.
- Liquid level in the RWST and sump tank.
- Heater rod voltage and current.

This data can be recorded at a time interval chosen by the operator. [
]^{c}

2.7 VISUALIZATION SYSTEM

A high-speed video camera (Model STV-LRC, Serial 15022) manufactured by Southern Vision Systems, Inc. (SVSi) is used to record two-phase flow patterns, precipitation, and debris transport in the vessel during testing. The maximum speed of the camera is 200 frames per second. In addition, a SONY camcorder is also used to record the test process at moments of interest. Still photographs are taken using a digital camera.

2.8 GRAB SAMPLE COLLECTION AND PROCESSING

Samples were collected through the ports on the side of the vessel. [

]^{c}

3 SOLUTION AND DEBRIS PREPARATION

In this section, the methods and procedures for preparing unbuffered and buffered boric acid solutions, sump debris contents, and chemicals for the Round #4 testing are discussed.

3.1 SOLUTION PREPARATION

3.1.1 Water

The water used for this round of testing is tap water that was run through a de-mineralizer to produce de-ionized (DI) water.

3.1.2 Boric Acid

The boric acid solution is prepared by adding [

]^{c}

3.1.3 Sodium Hydroxide Buffered Boric Acid

The boric acid solution buffered with sodium hydroxide (NaOH) is prepared by adding [

]^{c}

3.1.4 Trisodium Phosphate Buffered Boric Acid

The boric acid solution buffered with trisodium phosphate (TSP) is prepared by adding [

]^{c}

3.2 DEBRIS PREPARATION

3.2.1 [ ]^{c}

The particulate [

]^{c}

3.2.2 [ ]^{c}

[ ]^{c}

[ ]^{c}

[

]c

Table 3-1: Values Specified for Fiber Length c

The following equipment is required for producing the fiber and is shown in Figure 3-1:

- Analytical balance with at least a one gram precision
- Blender
- Assorted large beakers and crystallizing dishes
- Filter holder funnel for vacuum filtration
- Vacuum flask
- Vacuum tubing
- Vacuum system
- Filters
- Oven or furnace with adequate ventilation

[

]c

[ ]c

3.2.3 [ ]c

[

]c

1. [ ]c
2. [ ]c
3. [ ]c
4. [ ]c
5. [ ]c

c

Figure 3-1: Equipment Necessary for Preparing the Fiber Debris

[ ]c

Figure 3-2: Resulting Fiber under Optical Microscope

3.3 DEBRIS ADDITION

Debris will be added in the following sequence: particulate, fiber, and chemical. Debris is to be added to the sump tank. Amounts and timing for each experimental run are given in Section 5.0.

3.4 PARTICULATE ADDITION PROCEDURE

1. [ ]c
2. [ ]c
3. [ ]c
4. [ ]c
5. [ ]c

3.5 FIBER ADDITION PROCEDURE

1. [ ]c

2. [ ]^{c}

3. [ ]^{c}

4. [ ]^{c}

5. [ ]^{c}

3.6 CHEMICAL ADDITION PROCEDURE

1. [ ]^{c}

4 SCALING DISTORTIONS ON HIGH RANKED PIRT ITEMS

A generalized scaling approach has been developed for complex thermal-hydraulic systems by Zuber (Reference 15). The objective of this analysis, identified as the hierarchical two-tier scaling (H2TS) analysis, is to show the extent to which the experimental data can be applied to improving the state of knowledge about the phenomena that were ranked highly in the PIRT. In some respects, the experiments in the nine-rod apparatus capture the phenomena that would be prototypic of a PWR, and hence provide data that can be used for model development and computer code validation, while in other respects, scaling issues limit the applicability of the data. One important aspect of Zuber's approach is that the scaling process can be used to help identify the most important phenomena as well as the less important phenomena such that when compromises are made, the important phenomena are represented in the most feasible prototypic fashion and their distortions minimized. It should be noted that the detailed two-tier scaling analysis reported in this chapter was performed after the facility and test program had been completed and thus the conclusions could not be used to improve the experimental design. The results will be useful in planning further testing where distortions are minimized.

The H2TS methodology has been used for the scaling analysis for the Oregon State University low-pressure integral systems test facility (Reference 16) as well as other thermal hydraulic experiments to assess possible test distortions relative to the full size reactor system (Reference 17). It has also been utilized in the design of the PSU/NRC Rod Bundle Heat Transfer (RBHT) Facility (Reference 18). The H2TS scaling approach is the current state-of-the-art methodology for scaling thermal-hydraulic systems and will be used here to identify any distortions on the high ranked phenomena relevant to the Round #4 testing.

4.1 HIERARCHICAL TWO-TIER SCALING APPROACH

The two-tier scaling approach consists of a "top-down" scaling approach which gives a scaling group for each transfer process as derived from the dimensionless control volume equations for the conservation of mass, momentum, and energy as written for the thermal-hydraulic system. The scaling groups which result from the normalization of the control volume equations are time ratios for the different processes which occur in the system. These groups are called "pi" parameters. Therefore, top-down scaling or systems approach provides a method for identifying the high ranked phenomena, deriving similarity groups, weighting of the different groups to establish priorities, and providing a basis for decoupling fast and slow acting processes which have different time scales. The top-down scaling approach, which is used for both the experiment and the prototype, or full scale system, can identify the lack of similarity between the test and the prototype which indicates scaling distortions. Top-down scaling also identifies those thermal-hydraulic processes which require additional detailed analysis using a "bottom-up" scaling approach.

The bottom-up scaling approach, or process approach, addresses only those thermal-hydraulic processes which are identified as being important or can have distortions which could impact the experiment. Bottom-up scaling will focus on specific pi terms in the system equations which govern the particular phenomena of interest. The bottom-up scaling can be used to characterize the transport terms in the control volume equations (transport of mass, momentum or energy), to establish the relationships for calculating these terms and to compare the scaled experiment to the prototypic PWR.

The bottom-up scaling approach is primarily used to analyze any highly ranked distorted pi groups such that the model can be designed or modified to minimize such distortions. Since the scaling analysis presented in this chapter was conducted after the Round #4 tests were completed modifications to the test design cannot be made and therefore, the bottom-up scaling analysis will not be performed for the Round

#4 test rig. Instead, the focus of this scaling analysis will be on the top-down approach since it is the part of H2TS that determines the pi groups and identifies the dominant phenomena as well as any highly distorted items. In terms of the H2TS methodology, this approach is completely valid and is an example of the versatility of the analysis method. Note that a bottom-up scaling analysis will be used in conjunction with the design of any future test facilities used to study boron precipitation phenomena.

4.2 SYSTEM LEVEL SCALING (TOP-DOWN)

The PIRT phenomena that have been developed (Reference 5) are based on the phenomena associated with a component during a specific time period within a PWR vessel. In addition to the component level phenomena, there are vessel-wide phenomena which couple the individual components. The vessel or system-wide phenomena are at a level above the components since they relate the interaction of the different components to determine the system flows, pressures, overall heat removal, and cooling. The vessel (system) components considered in this analysis are:

- Core regions (single and two-phase)
- Core support region
- Lower head region
- Upper plenum region
- Downcomer region

A schematic of the system under consideration is shown in Figure 4-1.

The method for determining the dominant terms for the system behavior is to write conservation equations for the system. There are two equations which are examined for the Round #4 test rig: (1) the fluid momentum equation; (2) the fluid energy equation. Each conservation equation is derived in the fashion as recommended by Zuber (Reference 15). The equations are normalized with respect to boundary and initial conditions and divided by the "driver term" such that the resulting pi groups are dimensionless. This approach is applied to both the Round #4 test rig as well as to a reference 3 loop PWR to indicate possible non-prototypic effects and distortions in the test facility relative to the actual plant system.

4.2.1 Momentum Equation Scaling

The complete derivation of the dimensionless momentum equation used for scaling purposes can be found in Reference 23. In this section, a summary of the derivation is provided starting with the generalized one-dimensional integral form of the momentum equation as given by Shames (Reference 19) with the addition of a term to account for the change in momentum flux due to boiling in the core:

$$P_i - P_e = \frac{1}{g_c}\int_i^e \frac{dW}{dt}\frac{dz}{A} + \frac{1}{g_c}\left[\frac{1}{A^2}\left(\frac{W_e^2}{\rho_e} - \frac{W_i^2}{\rho_i}\right)\right] - \frac{g}{g_c}\int_i^e \rho \cdot dz + \frac{f}{2 \cdot D_h \cdot \rho \cdot A^2 g_c}\int_i^e W|W|dz + \frac{K \cdot W^2}{2 \cdot \rho \cdot A^2 \cdot g_c} + \frac{\Delta M \cdot F_{cb}}{g_c} \quad (4\text{-}1)$$

where the subscripts i and e represent the vessel inlet and exit and the terms on the right hand side represent the:

- Inertial effects of the fluid in the control volume
- Momentum flux of the fluid into and out of the volume
- Gravitational forces
- Frictional losses
- Form losses within the volume
- Momentum flux change due to boiling in the two-phase region

The nomenclature is given at the beginning of this report for these equations. The momentum equation can be written for the complete vessel from the inlet to the exit. Since the system is considered an open loop, the pressure drop on the left hand side of the equation is maintained throughout the analysis. The

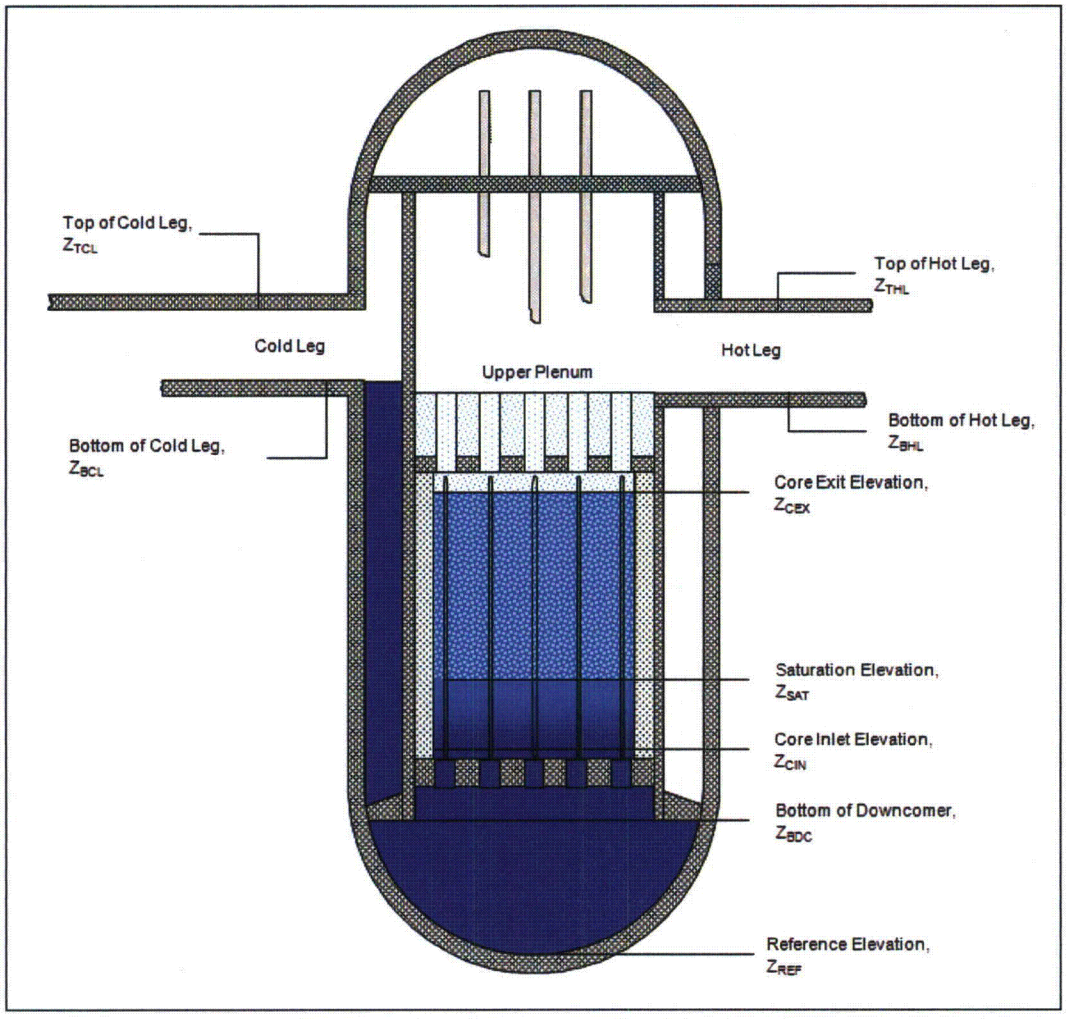

Figure 4-1: Schematic of PWR Vessel

flow in the core is single-phase for some length and two-phase over the remaining length. The inlet is assumed to be single-phase while the exit has a two-phase mixture. The saturation point is assumed to be at some elevation in the core throughout the experiment. Thus, the total core length can be split into a single-phase region (from z_{ci} to z_{sat}) and a two-phase region (from z_{sat} to z_{ce}). It is also assumed that the mass flow rate is only time dependent and does not vary across any component cross sections or lengths.

Using the normalization parameters given in Table 4-1, the dimensionless fluid momentum equation is:

$$\begin{aligned}\pi_1 \cdot \Delta P^* = {} & \pi_2 \frac{dW^*}{dt^*}\frac{L^*}{A^*}\bigg|_{1\phi} + \pi_2 \frac{dW_m^*}{dt^*}\frac{L^*}{A^*}\bigg|_{2\phi} + \pi_2 \frac{W^{*2}}{A^{*2}} \cdot \left[\frac{1}{\rho_m^*} - \frac{1}{\rho_f^*}\right] \\ & + \pi_3 \cdot \overline{\rho_f^*} \cdot \left[L_{DC}^* - L_{C,1\phi}^*\right] - \pi_4 \cdot \left[\overline{\alpha^*} \cdot \rho_g^* + \left(1 - \overline{\alpha^*}\right) \cdot \rho_f^*\right] \cdot L_{C,2\phi}^* \\ & + \pi_5 \cdot \sum_i^N \frac{R_{1\phi}^*}{A_i^{*2} \cdot \overline{\rho_{f,1}^*}} \cdot W^{*2} + \pi_5 \cdot \sum_i^M \frac{R_{2\phi}^*}{A_i^{*2} \cdot \overline{\rho_{f,1}^*}} \cdot W_m + \pi_6 \cdot \frac{W_m^{*2}}{A_c^{*2} \cdot \rho_{f,c}^*}\end{aligned} \tag{4-2}$$

where the individual pi groups are given in Table 4-2.

π_1 and π_2 are not independent and represent the velocity head or kinetic energy of the flow relative to the maximum gravity head.

π_3 is the gravity head term relative to itself and is equal to one.

π_4 represents the single-phase gravity head term relative to the maximum gravity head term. The same pi group can be used to represent the two-phase gravity head term relative to the maximum gravity head term because of the normalization used.

π_5 represents the ratio of the single-phase frictional and form pressure losses in the bundle to the maximum gravitational head. Again, because of the normalization used, the same pi group can be used to represent the ratio of the two-phase frictional and form pressure losses in the bundle to the maximum gravitational head.

π_6 represents the change in momentum flux due to boiling in the core relative to the maximum gravitational head.

Table 4-1: Normalization Parameters for Fluid Momentum Equation

$$W^* = \frac{W}{W_i}, \quad L^* = \frac{L}{L_T}, \quad A^* = \frac{A}{A_c}, \quad \rho_m{}^* = \frac{\rho_m}{\rho_i},$$

$$\alpha^* = \frac{\alpha}{\alpha_{c,e}}, \quad t^* = \frac{t}{\tau}, \quad \tau^* = \rho_i \frac{V_T}{W_i}, \quad R_{1\phi}{}^* = \frac{R_{1\phi}}{R_{T,1\phi}}, \quad R_{2\phi}{}^* = \frac{R_{2\phi}}{R_{T,1\phi}}$$

$$\Delta P^* = \frac{\Delta P}{\frac{W_i^2}{2A_c{}^2 \rho_i g_c}}, \quad \left.\frac{L}{A}\right|_{1\phi} = \left[\left.\frac{L}{A}\right|_{DC} + \left.\frac{L}{A}\right|_{LP} + \left.\frac{L}{A}\right|_{C,1\phi}\right], \quad \left.\frac{L}{A}\right|_{2\phi} = \left[\left.\frac{L}{A}\right|_{C,2\phi} + \left.\frac{L}{A}\right|_{UP}\right]$$

where $R_{T,1\phi}$ refers to the total frictional and form resistance for the entire vessel in single-phase flow.

Table 4-2: Individual Pi Groups from Fluid Momentum Equation

$$\pi_1 = \frac{W_i^2}{2 \cdot g \cdot A_c{}^2 \cdot \rho_i{}^2 \cdot L_T} = \frac{velocity\ head}{gravity\ head}$$

$$\pi_2 = \frac{W_i^2}{g \cdot A_c{}^2 \cdot \rho_i{}^2 \cdot L_T} = \frac{velocity\ head}{gravity\ head}$$

$$\pi_3 = \frac{g \cdot A_c{}^2 \cdot \rho_i{}^2 \cdot L_T}{g \cdot A_c{}^2 \cdot \rho_i{}^2 \cdot L_T} = 1 = \frac{gravity\ head}{gravity\ head}$$

$$\pi_4 = \alpha_{c,e} = \frac{vapor\ head}{gravity\ head}$$

$$\pi_5 = \frac{W_i^2 \cdot R_{T,1\phi}}{2 \cdot g \cdot A_c{}^2 \cdot \rho_i{}^2 \cdot L_T} = \frac{single\ phase\ resistance}{gravity\ head}$$

$$\pi_6 = \frac{W_i^2 \cdot N_{cb}}{g \cdot A_c{}^2 \cdot \rho_i{}^2 \cdot L_T} \cdot \left[N_{cb} \cdot \left(\frac{N_p + 1}{N_p}\right) - 2\right] = \frac{boiling\ momentum\ flux}{gravity\ head}$$

4.2.2 Energy Equation Scaling

The complete derivation of the dimensionless fluid energy equation used for scaling purposes is also presented in Reference 23. In this section, a summary of the derivation is provided for completeness. The one-dimensional fluid energy equation can also be written for the system, assuming negligible heat loss from the structures and that kinetic and potential energies are small relative to the internal energy of the fluid. Boiling is occurring in the core and a two-phase mixture is vented out the vessel exit. Again, the single and two-phase regions in the system are treated separately and the energy equation for the vessel becomes:

$$V_{1\phi} \cdot \frac{d}{dt}(\rho e)_{1\phi} + V_{2\phi} \cdot \frac{d}{dt}(\rho_m e_m) = W_i h_i - W_e h_e + Q \qquad (4\text{-}3)$$

where the subscripts i and e represent the vessel inlet and exit and the terms in the equation represent:

- Rate of energy change in the single-phase region
- Rate of energy change in the two-phase region
- Energy flow into the vessel at the inlet
- Energy flow out of the vessel at the exit
- Energy release to the fluid from the core.

The nomenclature is given at the beginning of this report for these equations.

(Eq. 4-3) can be normalized using the values in Table 4-3 and the resulting dimensionless fluid energy equation is:

$$\pi_7 \cdot V_{1\phi}^* \cdot \frac{d}{dt}\left(\rho^* \cdot C_v^* \cdot \Delta T^*\right) + \pi_8 \cdot V_{2\phi}^* \cdot \frac{d}{dt}\left(\rho_m^* \cdot e_m^*\right) = \pi_9 \cdot \left(W_i^* \cdot h_i^* - W_e^* \cdot h_e^*\right) - \pi_{10} \cdot Q^* \qquad (4\text{-}4)$$

where the individual pi groups are given in Table 4-4.

π_7 and π_9 are equal and represent the ratio of sensible heat rate to core power which is the fraction of core power required for the fluid to reach saturation temperature.

π_8 is the ratio of boiling heat rate to core power. It represents the fraction of core power put toward vapor generation in the core due to boiling.

π_{10} is the core power divided by itself and equals one.

Table 4-3: Normalization Parameters for Fluid Energy Equation

$$W^* = \frac{W}{W_i},\quad V^* = \frac{V}{V_T},\quad \rho^* = \frac{\rho}{\rho_i},\quad Q^* = \frac{Q}{Q_c}$$

$$t^* = \frac{t}{\tau},\quad \tau^* = \rho_i \frac{V_T}{W_i},\quad C_v^* = \frac{C_v}{C_{v,i}},\quad h^* = \frac{h}{\Delta h_{sub}}$$

$$\Delta T^* = \frac{\Delta T}{\Delta T_{sub}},\quad \rho_m^* e_m^* = \frac{\rho_m e_m}{\alpha_{c,e}\rho_g e_g + (1-\alpha_{c,e})\cdot \rho_f e_f}$$

where ΔT_{sub} refers to the inlet subcooling $(T_{sat} - T_i)$ and Δh_{sub} refers to the enthalpy difference between the inlet and saturated $(h_f - h_i)$.

Table 4-4: Individual Pi Groups from Fluid Energy Equation

$$\pi_7 = \frac{W_i \cdot C_{v,i} \cdot \Delta T_{sub}}{Q_c} = \quad \frac{sensible\ heat\ rate}{core\ power}$$

$$\pi_8 = \frac{W_i \cdot (\alpha_{c,e} \cdot e_g \cdot \rho_g + (1-\alpha_{c,e}) \cdot e_f \cdot \rho_f)}{\rho_i \cdot Q_c} = \quad \frac{boiling\ heat\ rate}{core\ power}$$

$$\pi_9 = \frac{W_i \cdot \Delta h_{sub}}{Q_c} = \frac{W_i \cdot C_{v,i} \cdot \Delta T_{sub}}{Q_c} = \quad \frac{sensible\ heat\ rate}{core\ power}$$

$$\pi_{10} = \frac{Q_c}{Q_c} = 1 = \quad \frac{core\ power}{core\ power}$$

4.3 DETERMINATION OF PI GROUPS

The fluid momentum equation includes 4 unique pi groups defined in Section 4.2.1. The fluid energy equation includes 2 unique pi groups defined in Section 4.2.2. Here, the numerical values of these groups are calculated for the Round #4 test rig and a typical Westinghouse 3 loop PWR vessel.

The round #4 test rig reference conditions used for scaling purposes are given in Table 4-5. The experiments were conducted at atmospheric pressure with 62°F subcooling. The total power supplied to the heaters is simulating the 10CFR50 Appendix K decay heat curve. The startup power is [ ]^c,

which corresponds to a [ ]^{c} decay heat ratio (approximately [ ]^{c} after reactor trip). Although the inlet flow rate was varied during some of the test runs to simulate core uncovery and recovery, it will be assumed for the scaling analysis that inlet flow is supplied at a rate equal to the boil-off rate such that quasi-equilibrium is maintained.

Table 4-5: Round #4 Test Reference Conditions

Parameter	Value
Inlet Flow Rate (lbm/s)	Boil-off rate
Pressure (psia)	14.7
Inlet Subcooling (°F)	62
Initial Bundle Power (W)	[ ]^{c}
Initial Decay Heat Ratio	[ ]^{c}

In order to calculate the pi groups, fluid properties are needed for the vessel inlet condition (subcooled) as well as at saturation. The necessary fluid properties used for the scaling analysis are shown in Table 4-6.

Table 4-6: Subcooled and Saturated Fluid Properties

Parameter	Value
ρ_i (lbm/ft^3)	61.195
e_i (Btu/lbm)	118.05
h_i (Btu/lbm)	118.1
$C_{v,i}$ (Btu/lbm-R)	0.94361
μ_i (lbm/ft-s)	2.89×10^{-4}
ρ_f (lbm/ft^3)	59.829
e_f (Btu/lbm)	180.25
h_f (Btu/lbm)	180.3
ρ_g (lbm/ft^3)	0.0373
e_g (Btu/lbm)	1078.1
h_g (Btu/lbm)	1151
σ (lbf/ft)	4.037×10^{-3}
C_p (Btu/lbm-R)	1.0076
h_{fg} (Btu/lbm)	970.7
$\Delta h_{sub} = h_f - h_i$ (Btu/lbm)	62.2

4.3.1 Calculation of Pi Groups

The first step is to determine the initial boil-off rate which will be used for the initial inlet flow. The boil-off rate is determined by multiplying the core power (PWL) by the initial decay heat ratio and dividing by the sum of the latent heat of vaporization and subcooling:

$$W_i = W_{boil} = \frac{\frac{P}{P_0} \cdot (PWL)}{h_{fg} + \Delta h_{sub}} \tag{4-5}$$

To determine the core exit void fraction, the three regime Yeh correlation (Reference 13) is utilized:

$$\alpha_i = C \cdot \left(\frac{\rho_g}{\rho_f}\right)^{0.239} \left(\frac{j_g(z)}{V_{bcr}}\right)^a \left(\frac{j_g(z)}{j_g(z) + j_f(z)}\right)^{0.6} \tag{4-6}$$

where V_{bcr} (ft/s) is the critical bubble rise velocity correlated as:

$$V_{bcr} = 1.53 \cdot \left[\frac{\sigma \cdot (\rho_f - \rho_g) \cdot g \cdot g_c}{\rho_f^{\,2}}\right]^{0.25} \tag{4-7}$$

and j_f, j_g (ft^3/ft^2-s) are the volumetric fluxes of the liquid and vapor phases, respectively. The variables b and C vary by regime and are defined in Table 4-7.

Table 4-7: Values of Yeh Void Fraction Correlation Constants

Regime	C	a
$j_g / V_{bcr} \leq 1$	0.925	0.67
$1 < j_g / V_{bcr} < 4.31$	0.925	0.47
$j_g / V_{bcr} \geq 4.31$	1.035	0.393

In order to determine the single-phase resistance through the system, it is necessary to determine an appropriate friction factor for each component. To accomplish this, a Reynolds number for each component is first calculated with:

$$\mathrm{Re} = \frac{W_i \cdot D_h}{\mu \cdot A} \tag{4-8}$$

where D_h is the component hydraulic diameter, A the component flow area, and μ the liquid viscosity. Based on the Reynolds number, if the flow through the component is laminar, the friction factor is calculated by (Reference 20):

$$f = \frac{64}{\mathrm{Re}} \tag{4-9}$$

If the flow is turbulent the friction factor is determined using the Blasius relation (Reference 20):

$$f = 0.316 \cdot \mathrm{Re}^{-0.25} \tag{4-10}$$

Both of the above correlations for friction factor assume a smooth surface within the component.

Using the pi group equations presented in Table 4-2 and Table 4-4 along with the equations presented in this section, it is possible to calculate the pi group values for the fluid momentum and energy equations for the Round #4 test rig and reference PWR geometries. Table 4-8 shows the system geometry and calculation results for determining the Round #4 test rig and reference PWR pi groups.

Numerical values of the 10 pi groups are shown in Table 4-9 for the Round #4 test rig (model) and reference PWR (prototypic). The pi group model to prototypic ratio given as:

$$\pi_{M/P} = \frac{\pi_M}{\pi_P} \tag{4-11}$$

is also presented in Table 4-9. Ideally, all pi group model to prototypic ratios should equal or be very close to unity, however, this will never be the case even if a scaling analysis is performed prior to designing the test facility (Reference 21). The goal is to achieve a test facility in which the high ranked pi groups are scaled well against the prototypic system. Review of Table 4-9 indicates that the high ranked pi groups for this scenario from the fluid momentum equation are the [ ]^c The high ranked pi groups from the fluid energy equation are the [ ]^c The other pi group's numerical values are [ ]^c In addition, since all the pi group numerical values are [ ]^c

In terms of experimental distortion, it can be observed that the [ ]^c The vapor head, represented by the core exit void fraction is [ ]^c and the change in momentum flux due to boiling is [ ]^c In addition, the boiling heat rate in the model [ ]^c

Although this scaling analysis has identified several major [ ]^c

The boiling momentum flux represented by pi group six is related to the [ ]^c

Table 4-8: Summary of Pi Group Calculations

c

[

]

Table 4-8: Summary of Pi Group Calculations (cont.)

[c

]

Table 4-9: Numerical Values of Pi Groups c

5 TEST RESULTS

In this chapter the data collected for nine valid test runs is presented. Table 5-1 provides a summary of the test parameters used for each run. The table provides information about the injection flow including temperature and flow rate. The composition of the prepared solution for each run is presented by providing the total mass which is the summation of water, boric acid, and any buffering agents added to the solution. For runs that had debris loadings, the quantity of each debris type is also presented. Finally, a description of the lower plenum geometry used for each run is given along with the total run time.

Runs NRL01 and NRL04 were conducted using de-ionized water and serve as baseline tests that can be compared to runs conducted with boric acid solutions and debris. Run NRL01 follows the 10CFR50 Appendix K decay heat curve while run NRL04 is run at three constant power levels. The primary purpose of run NRL04 was to collect flow visualization videos that can be compared to videos collected during periods of high boric acid and/or debris concentrations from other runs.

Runs NRL02 and NRL03 were conducted using unbuffered boric acid. Both runs follow the 10CFR50 Appendix K decay heat curve. During run NRL03, the power was lost to one of the heater rods roughly 2 hours into the experiment. This resulted in an 11% decrease in bundle power. Run NRL03 was conducted with a debris loading and comparing these two runs identifies any effects debris has on the boiling and two-phase flow characteristics when the solution is unbuffered boric acid. Precipitation was observed on the lower plenum surfaces as well as the vessel walls around the two-phase mixture level during both of these runs.

Runs NRL05, NRL07, and NRL08 were conducted using boric acid buffered with sodium hydroxide (NaOH). All runs had debris loadings and followed the 10CFR50 Appendix K decay heat curve. Runs NRL05 and NRL07 were conducted using the large lower plenum volume while run NRL08 was conducted using the small lower plenum volume. Run NRL07 was terminated after roughly 3 hours because of a leaking pump and therefore, the concentration levels achieved are lower compared to the other runs which ran for longer periods of time. Since the large lower plenum was used during run NRL05, a large amount of debris was observed to settle in the lower plenum volume which indicates that the debris concentration in the core region was lower during this run. One core uncovery and recovery cycle was performed at the end of run NRL08 and it was observed that precipitation formed on the exposed heater rod surfaces during core uncovery. When the core was recovered, the precipitate dissolved back into solution. This was the only precipitation observed during these tests.

Runs NRL06 and NRL09 were conducted using boric acid buffered with trisodium phosphate (TSP). Both runs followed the 10CFR50 Appendix K decay heat curve and run NRL06 was conducted with a typical debris loading added at the beginning of the experiment. Run NRL09 was conducted without a debris loading however, [ ]^{c} was added near the end of the experiment prior to performing the last core uncovery and recovery cycle. Two core uncovery and recovery cycles were performed during run NRL06 and 4 uncovery and recovery cycles were performed during run NRL09. Precipitation was observed on the exposed heater rod surfaces during core uncovery and this was the only precipitation observed during these runs. The precipitate dissolved back into solution when the core was recovered.

Table 5-1: Summary of Test Parameters c

Data collected during the experimental runs includes; bundle power, heater rod inside cladding temperature at various locations, fluid temperature in the supply tank, lower plenum, and core region, mixture level in the supply tanks, grab samples for concentration measurements, and various high-speed videos used for two-phase flow and precipitation visualization.

The bundle power is calculated by the data acquisition system by multiplying the voltage drop across the heaters by the current through the heaters. Time traces of the bundle power are presented for each experimental run.

Grab samples were collected at various times and locations during each experiment. In general, if precipitation was observed during the run (not including precipitation during core uncovery), grab samples were taken from the core and lower plenum regions. If precipitation was not observed during the experiment (buffered boric acid runs), grab samples were collected at the end of the experiment. Grab samples were also collected from the supply tanks at the end of each experiment to compare the actual solution concentration to the theoretical value calculated during preparation of the source solutions. The grab samples were analyzed by an independent lab and concentrations were determined. The concentration results showing weight percent boron (B), sodium (Na), phosphorous (P), and debris (% solids) are presented for each run in which grab samples were collected.

Observations were made for each test regarding precipitation and debris. For runs in which precipitation was observed, images showing the formation of precipitates are presented. Likewise, images showing the characteristics of debris accumulation are presented for each run in which a debris loading was used.

Temperature measurements are presented for each run. These include the fluid temperatures measured in the supply tank, lower plenum, and core region. Heater rod temperatures from at least three locations are also presented for each run.

High-speed videos collected for two-phase flow visualization were recorded at various times during each experimental run. Images taken from these videos are presented to show the two-phase flow regimes and structures present during the experiments.

For runs in which core uncovery and recovery cycles were performed, heater rod and fluid temperatures measured at the top of the heated length are presented for the time during uncovery and recovery. Images taken from the high-speed videos collected during the uncovery and recovery cycles that show the buildup of precipitation and the dissolution are shown for each cycle.

5.1 RUN NRL01

Run NRL01 is a calibration run conducted using de-ionized water without any debris loading. The purpose of this run is to obtain baseline heat transfer data that can be compared to runs conducted using boric acid solutions with and without debris loadings such that any effect on the boiling heat transfer can be determined.

The temperature of the injection water in the sump tank is controlled at an average temperature of 149°F and the injection flow rate is set at 1600 ml/min. After a short preheating period, the power controller is set to follow the 10CFR50 Appendix K decay curve as discussed in Section 2.2. Temperature measurements are recorded for the heater rod cladding and fluid within the sump, downcomer, lower plenum, and core regions. The total run time for this experiment is roughly 10 hours. Table 5-2 summarizes the test parameters used for run NRL01.

Table 5-2: Run NRL01 Test Parameters c

[ ]

5.1.1 Power Measurement

The power transient for run NRL01 is shown in Figure 5-1. As the figure shows, the power is held constant at around [ ]^{c} for several minutes to allow some preheating of the vessel. After the short preheating period, the power controller is set to simulate the 10CFR50 Appendix K decay heat curve for the remainder of the experiment.

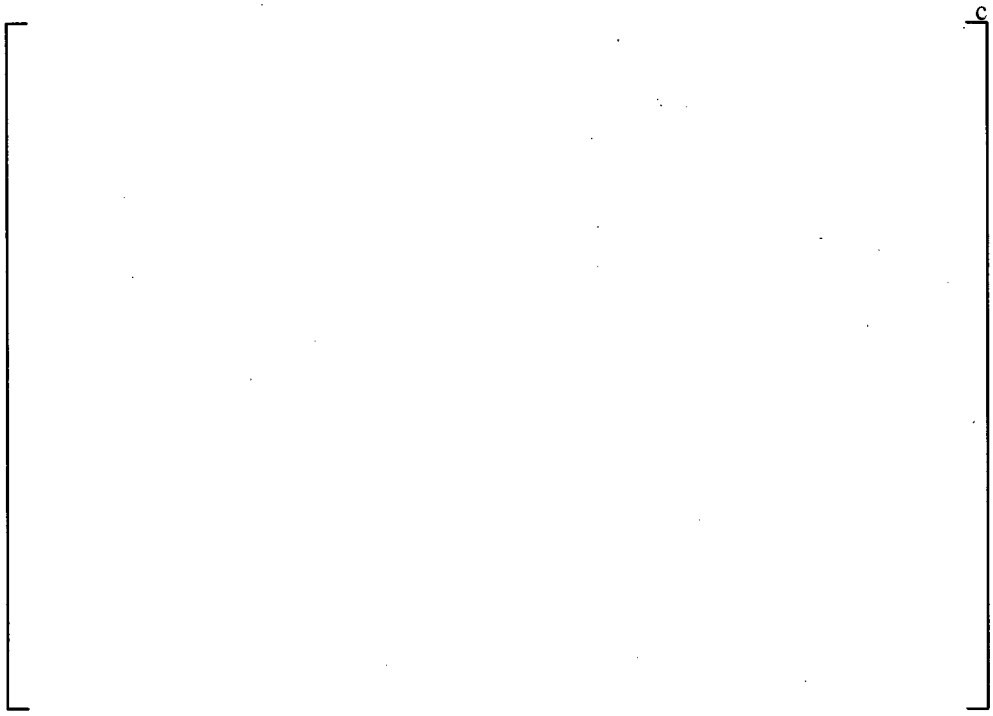

Figure 5-1: Run NRL01 Power Transient

5.1.2 Concentration Measurements

Since Run NRL01 was conducted with de-ionized water no samples were taken to measure the solution concentration.

5.1.3 Precipitation and Debris Observations

No precipitation will occur in run NRL01 since it was conducted with de-ionized water. There was no debris loading used in run NRL01 and therefore, no observations related to debris behavior are made.

5.1.4 Temperature Measurements

Fluid temperatures measured in the sump tank, downcomer, and lower plenum are shown in Figure 5-2. Based on this figure, the following observations can be made:

- [
  ]
- [ ]
- [ ]

[

]^{c}

- [

]^{c}

Fluid temperatures measured in the lower plenum and core region are shown in Figure 5-3. From the figure, the following observations can be made:

- [

]^{c}

- [

]^{c}

The cladding temperatures measured during run NRL01 are shown in Figure 5-4. Using this figure, the following observations can be made:

- [

]^{c}

- [

]^{c}

Figure 5-2: Run NRL01 Sump, Downcomer, and Lower Plenum Fluid Temperatures

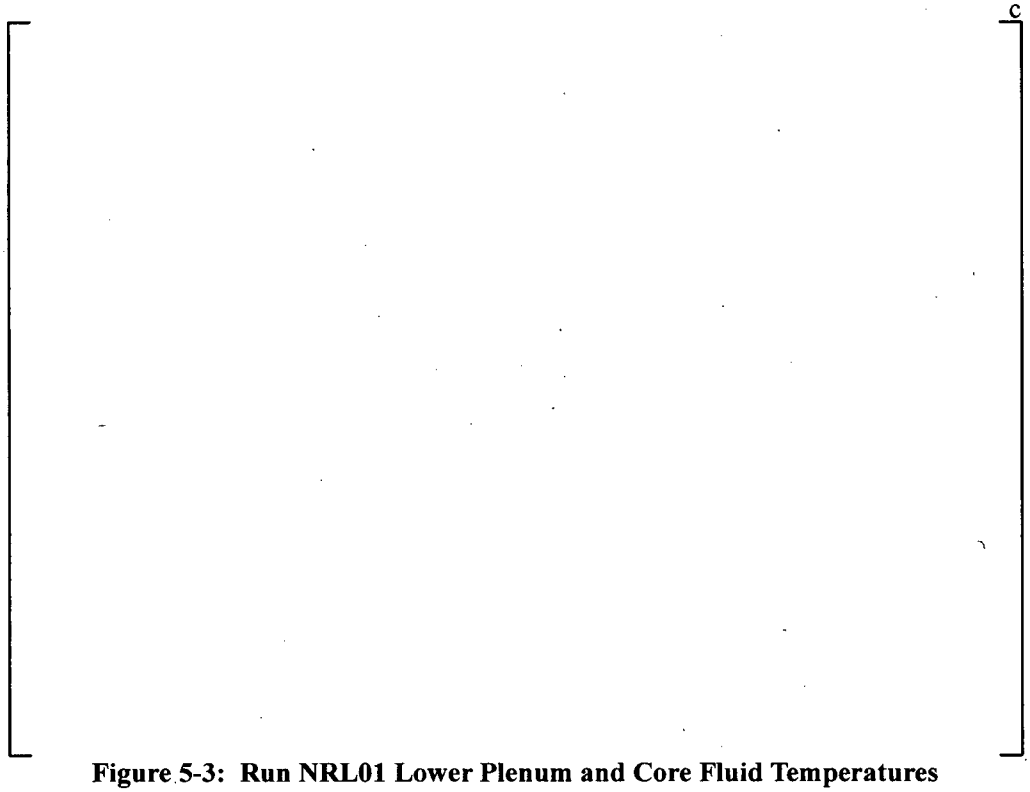

Figure 5-3: Run NRL01 Lower Plenum and Core Fluid Temperatures

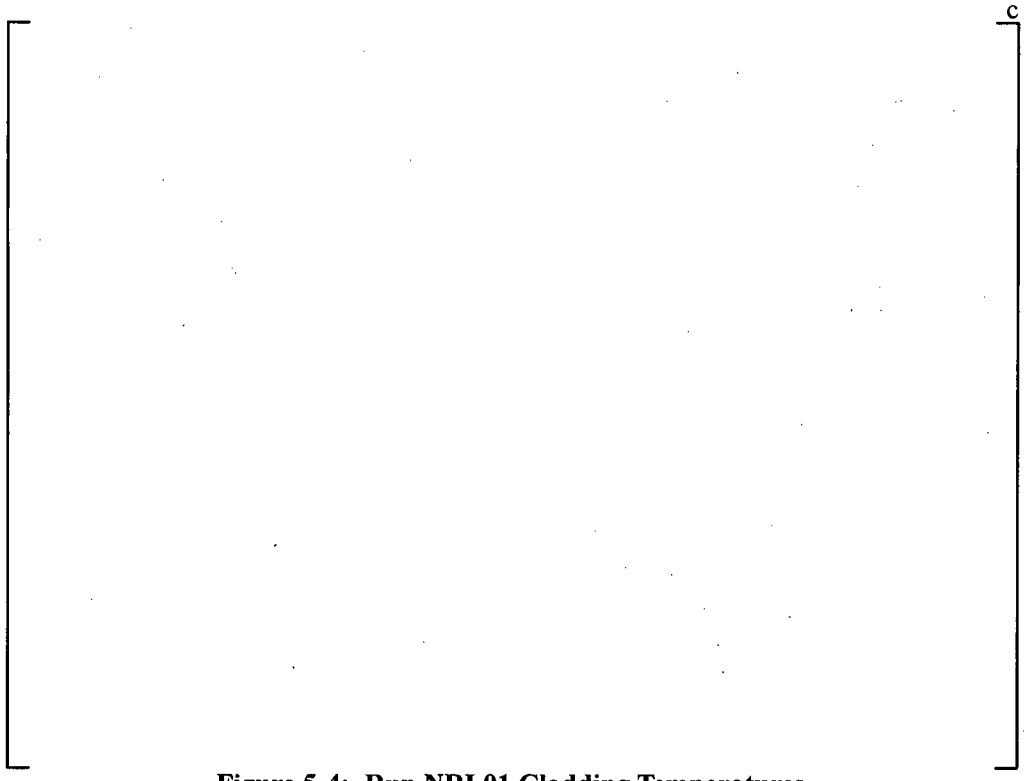

Figure 5-4: Run NRL01 Cladding Temperatures

5.1.5 Two-Phase Flow Visualizations

Two-phase flow visualizations were not recorded during run NRL01.

5.2 RUN NRL02

Run NRL02 is conducted using unbuffered borated water without any debris loading. The purpose of this run is to collect data that can be compared to runs conducted with buffered borated water without debris loading as well as unbuffered borated water with debris loadings. By comparing runs of this nature, it may be possible to observe the effects of buffering agents and debris on the boiling and two-phase flow characteristics.

The boric acid concentration of the solution used in run NRL02 is [ ]^{c} which is equivalent to a boron concentration of [ ]^{c} The temperature of the solution in the sump tank is controlled at a temperature of 149°F and the injection flow rate is set at 1600 ml/min. After a short preheating period, the power controller is set to follow the 10CFR50 Appendix K decay curve as discussed in Section 2.2. The total run time for this experiment is roughly 10.5 hours. Table 5-3 summarizes the test parameters used for run NRL02.

Solution samples drawn from the lower plenum and core were analyzed to determine the boric acid concentration. In addition, temperature measurements were recorded for the heater rod cladding and fluid within the sump, downcomer, lower plenum, and core regions. Still photographs were also taken to show the formation of boric acid precipitate in the lower plenum and core region. One high-speed video was recorded to provide images for flow regime visualization and identification.

Table 5-3: Run NRL02 Test Parameters c

[ ]

Boric acid precipitation was observed in the lower plenum after [ ]^{c} This precipitation was initially observed on and around the walls of the lower plenum. After [ ]^{c} it was observed that the precipitate began to form within the bulk solution contained in the lower plenum. At the [ ]^{c} mark, a small amount of boric acid precipitation was also observed on the vessel walls of the core region near the top of the heated length. No precipitation was observed on the heater rod surfaces.

5.2.1 Power Measurement

The power transient for run NRL02 is shown in Figure 5-5. As the figure shows, the power is held constant at around [ ]^{c} for approximately 5 minutes to allow some preheating of the vessel. After the short preheating period, the power controller is set to simulate the 10CFR50 Appendix K decay heat curve for the remainder of the experiment.

Figure 5-5: Run NRL02 Power Transient

5.2.2 Concentration Measurements

[

]^{c}

[

]c

Table 5-4: Run NRL02 Concentration Measurements c

[

]c

5.2.3 Precipitation and Debris Observations

During run NRL02, boric acid precipitation was observed in the lower plenum and upper portion of the heated section of the core. Figure 5-6 and Figure 5-7 show two photographs of the lower plenum region taken after [ ]c, respectively. Figure 5-8 shows a photograph taken of the upper core region after [ ]c. Based on observations made during the experiment and using the photographs in the figures as evidence, the following remarks can be made regarding the formation of boric acid precipitates within the lower plenum and core regions:

- [
  ]c
- [
  ]c
- [
  ]c
- [
  ]c

- [ ]^{c}
- [ ]^{c}
- [ ]^{c}
- [ ]^{c}

Run NRL02 was conducted without debris loading, therefore no observations regarding the effects of debris are made.

c

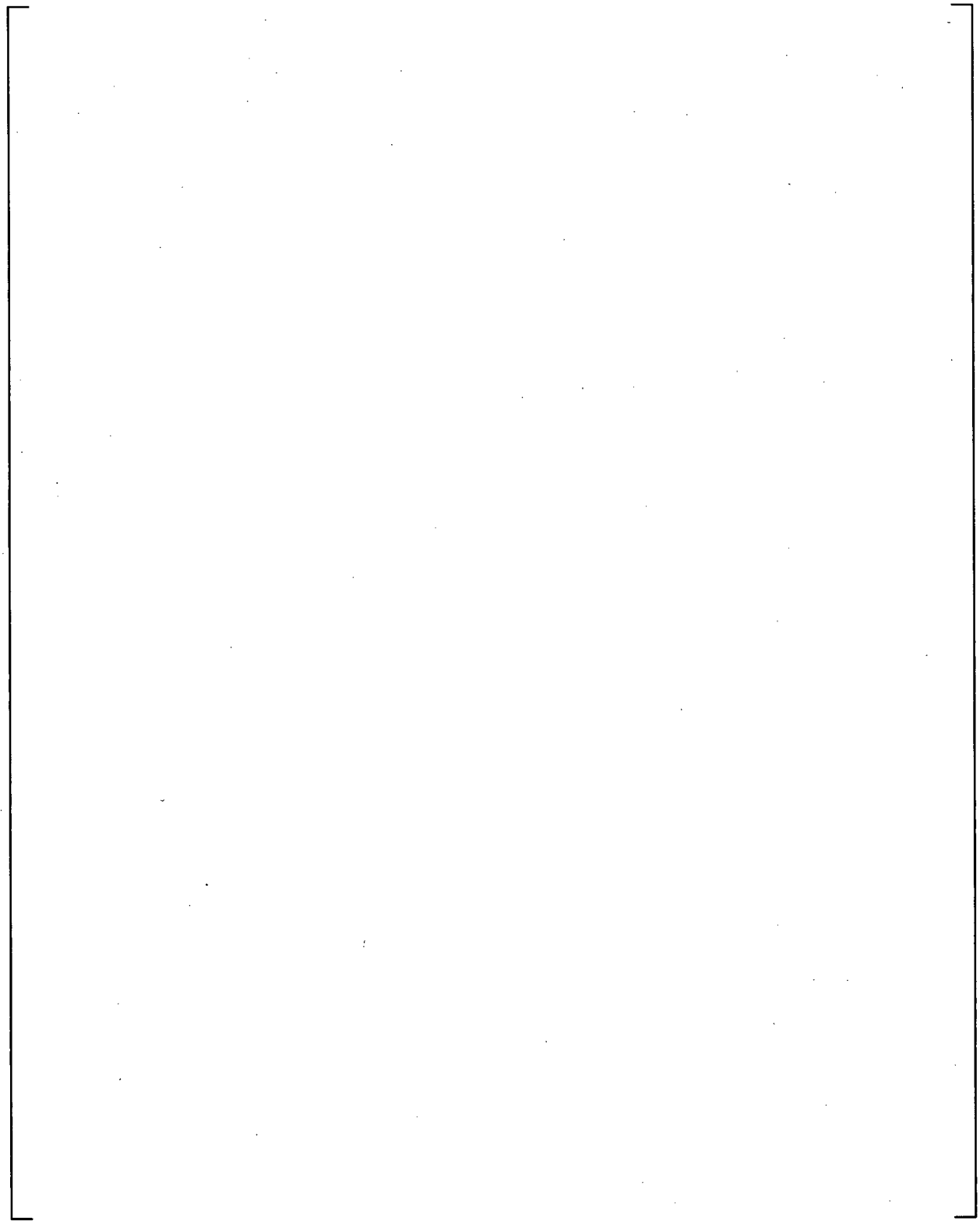

Figure 5-6: Run NRL02 Boric Acid Precipitation Observed on the Lower Plenum Walls after [ ]^{c}

c

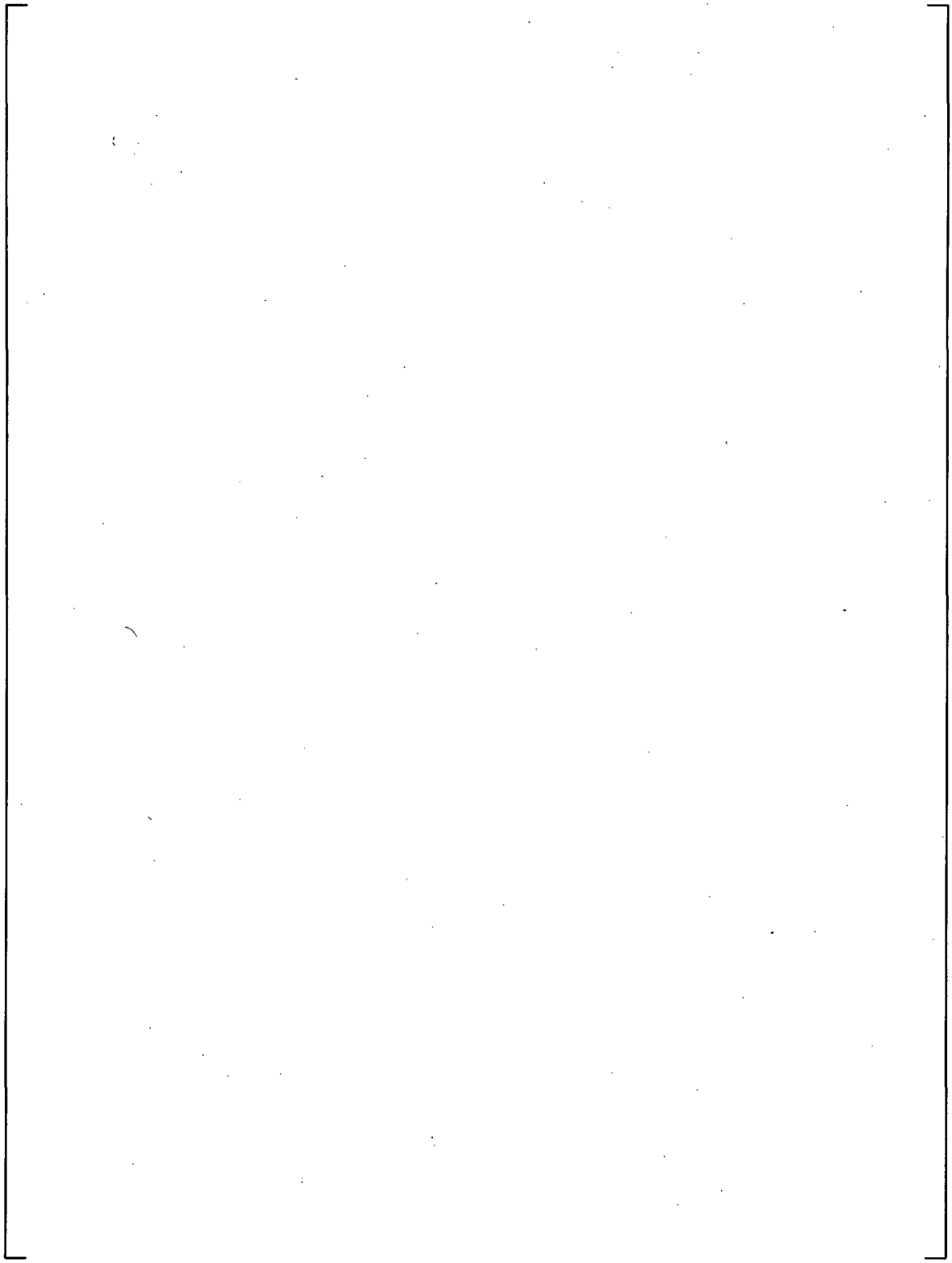

Figure 5-7: Run NRL02 Boric Acid Precipitation Observed on the Lower Plenum Walls and within the Bulk Fluid Contained in the Lower Plenum after [ ]^{c}

c

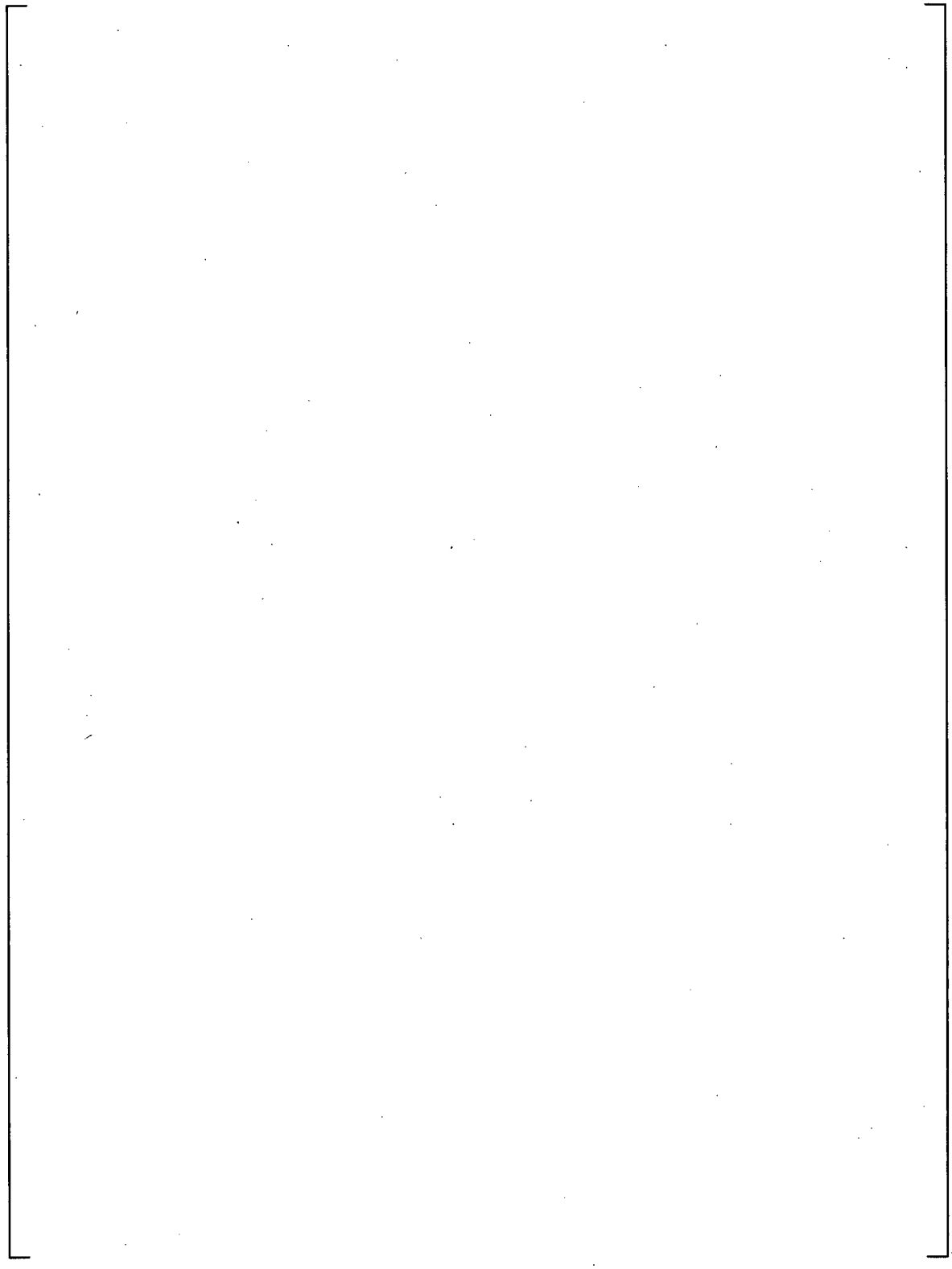

Figure 5-8: Run NRL02 Boric Acid Precipitation Observed on the Walls within the Core Region at the Top of the Heated Length after [ ]^{c}

5.2.4 Temperature Measurements

Fluid temperatures measured in the sump tank, downcomer, and lower plenum are shown in Figure 5-9. Based on this figure, the following observations can be made:

- [ ]^{c}
- [ ]^{c}
- [ ]^{c}
- [ ]^{c}
- [ ]^{c}
- [ ]^{c}

In Figure 5-10, the lower plenum fluid temperatures are compared to fluid temperatures measured in the heated section of the core. Based on this figure, the following observations can be made:

- [ ]^{c}
- [ ]^{c}
- [ ]^{c}

The heater rod cladding temperatures measured during run NRL02 are shown in Figure 5-11. Based on this figure, the following observations can be made:

- [ ]^{c}

- [
  ]^{c}
- [
  ]^{c}

[
c

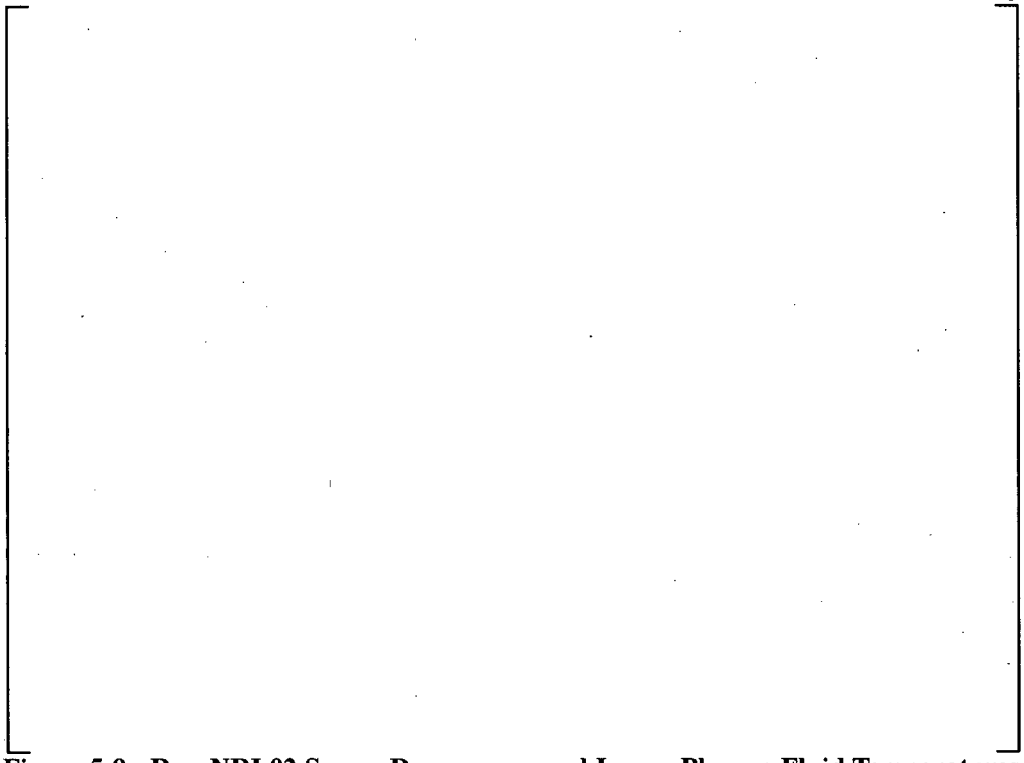

]

Figure 5-9: Run NRL02 Sump, Downcomer and Lower Plenum Fluid Temperatures

[c]

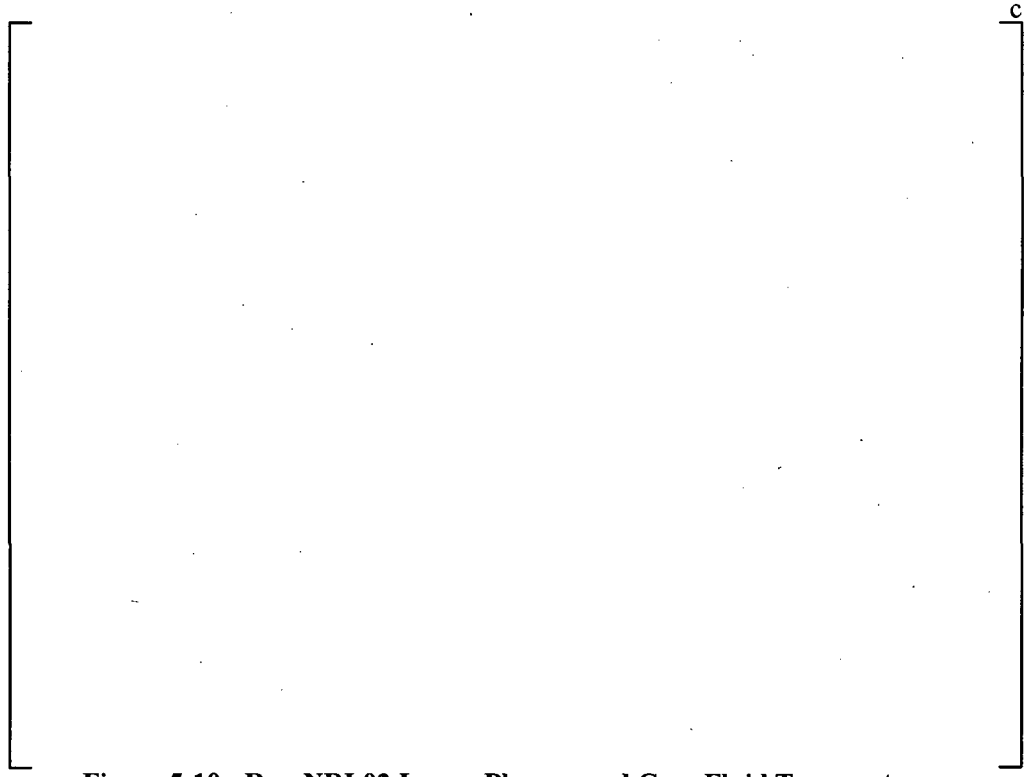

Figure 5-10: Run NRL02 Lower Plenum and Core Fluid Temperatures

[c]

Figure 5-11: Run NRL02 Cladding Temperatures

5.2.5 Two-Phase Flow Visualizations

A two-phase flow visualization was recorded during run NRL02 using the high-speed video camera. The video was collected approximately 3.3 hours into the experiment when the decay power level was around 1700W. Table 5-5 lists the experimental time, bundle elevation, and bundle power at which this video was recorded. Overall, the two-phase flow visualization video showed that the [

]^{c}

When the bulk flow velocity is high, periods of bubbly flow exist as shown in Figure 5-12. Based on this figure, the following observations can be made:

- [ ]^{c}
- [ ]^{c}
- [ ]^{c}
- [ ]^{c}

The chaotic motion observed in the bubbly flow regime is further illustrated in Figure 5-13 which shows a series of images collected 10 ms apart. Based on this figure, the following observations regarding the motion of bubbles can be made:

- [ ]^{c}
- [ ]^{c}
- [ ]^{c}

When the relative velocity of the bulk fluid slows, there are periods where large vapor slugs form. Several of these vapor slugs are shown in Figure 5-14. Based on this figure, the following observations can be made:

- [ ]^{c}
- [ ]^{c}

- [ ]^{c}
- [ ]^{c}
- [ ]^{c}

The observations made regarding the periods of vapor slug formation are further illustrated by Figure 5-15 which shows the formation of a slug in 20 ms intervals.

Table 5-5: Run NRL02 Video Collected for Flow Visualization

Video Title	Collection Speed (fps)	Experimental Time (hr:min:sec)	Video Length (sec)	Bundle Elevation (in.)	Bundle Power (W)
Video#1	200	3:20:00	3.465	22	1718

c

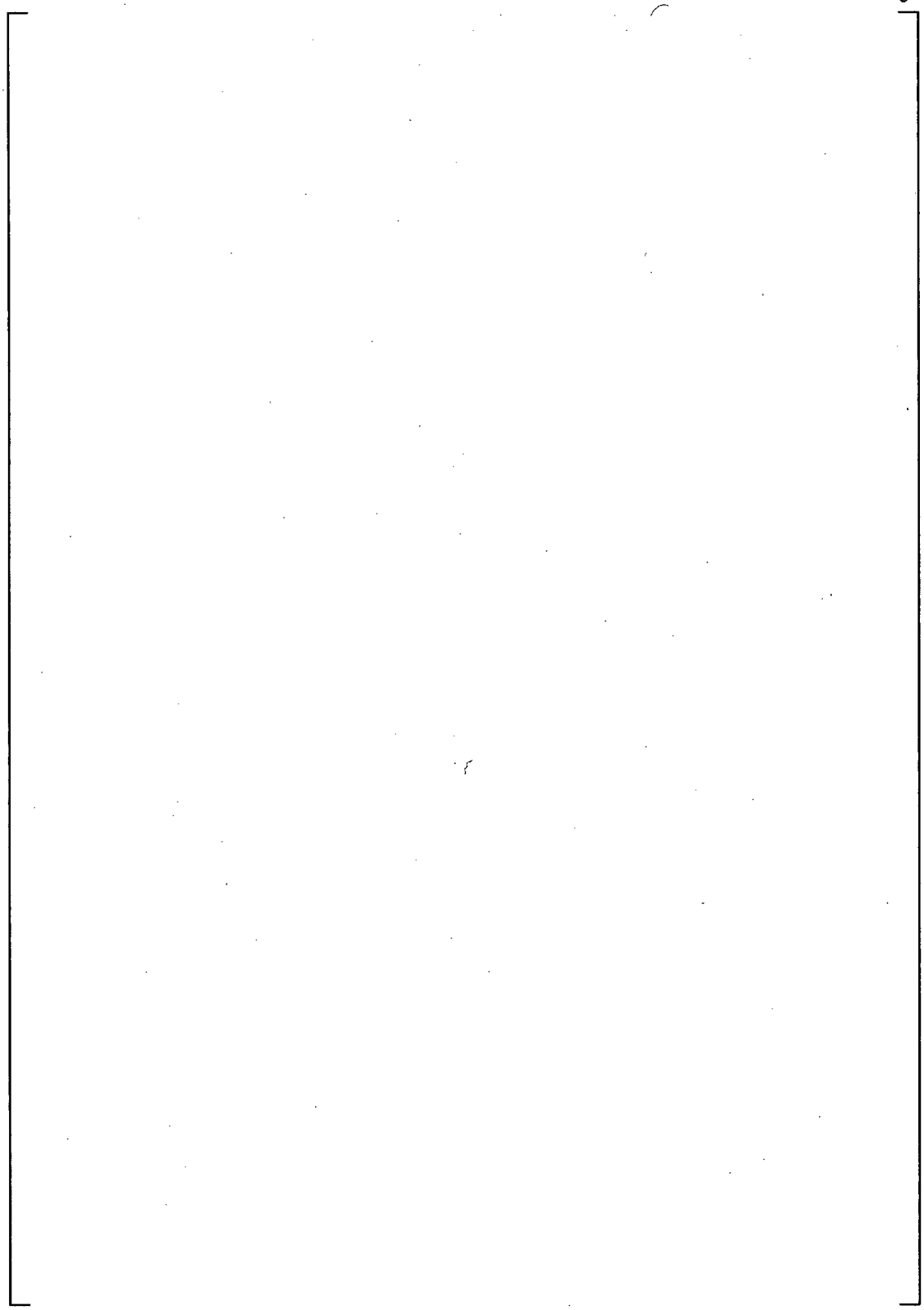

Figure 5-12: Run NRL02 Flow Visualization of Bubbly Flow

c

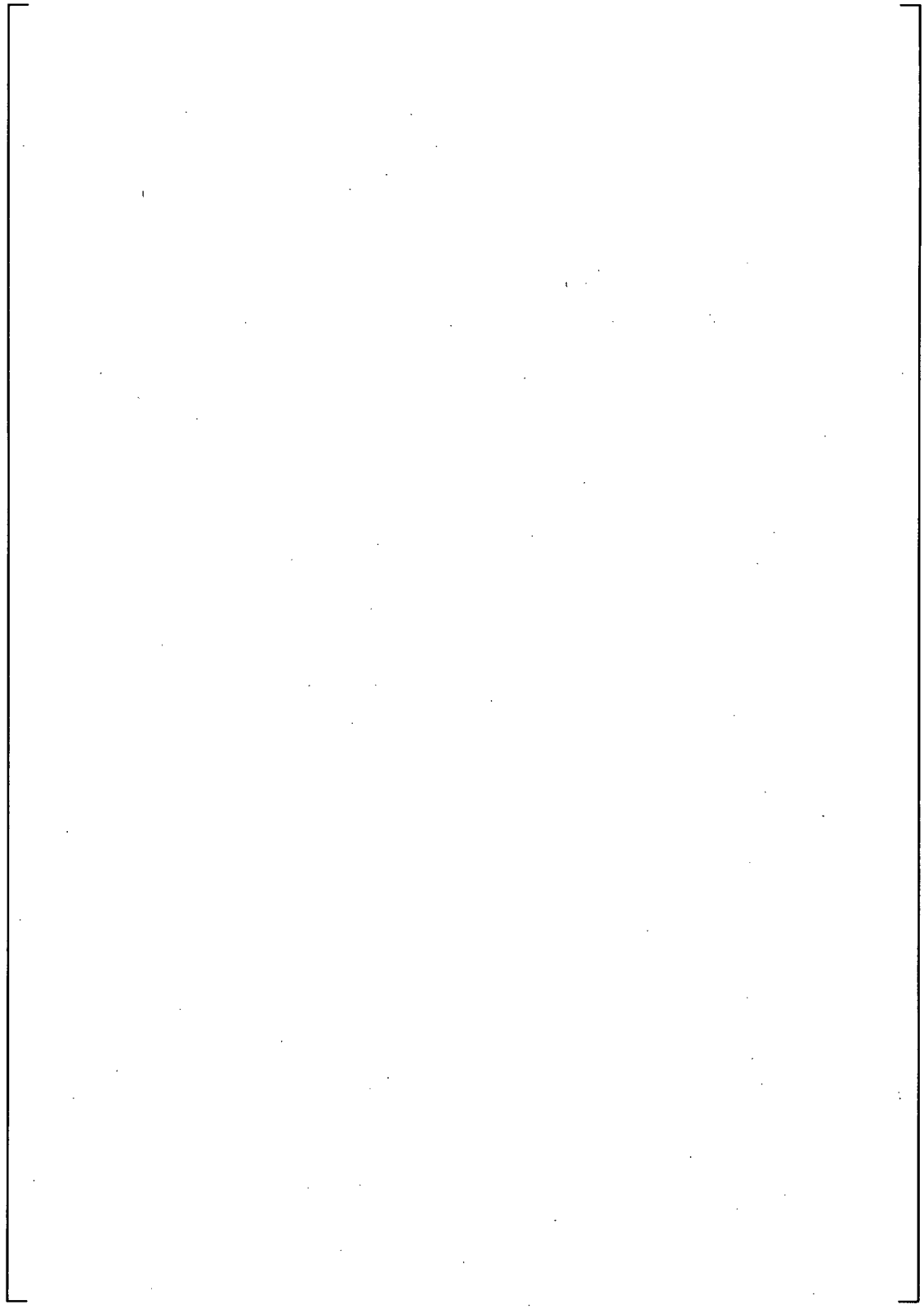

Figure 5-13: Run NRL02 Flow Visualization of Bubble Motion

c

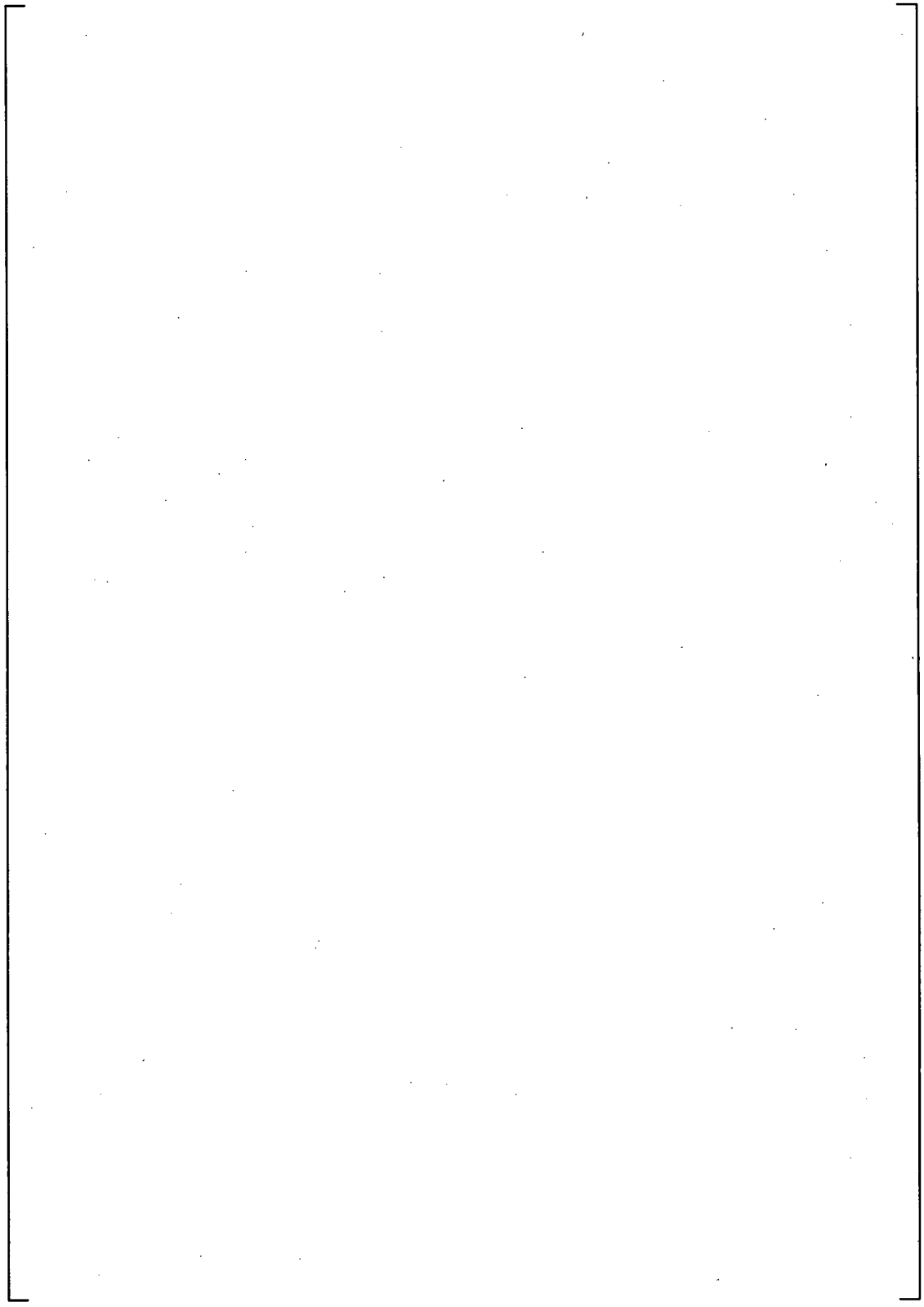

Figure 5-14: Run NRL02 Flow Visualization of Vapor Slugs

c

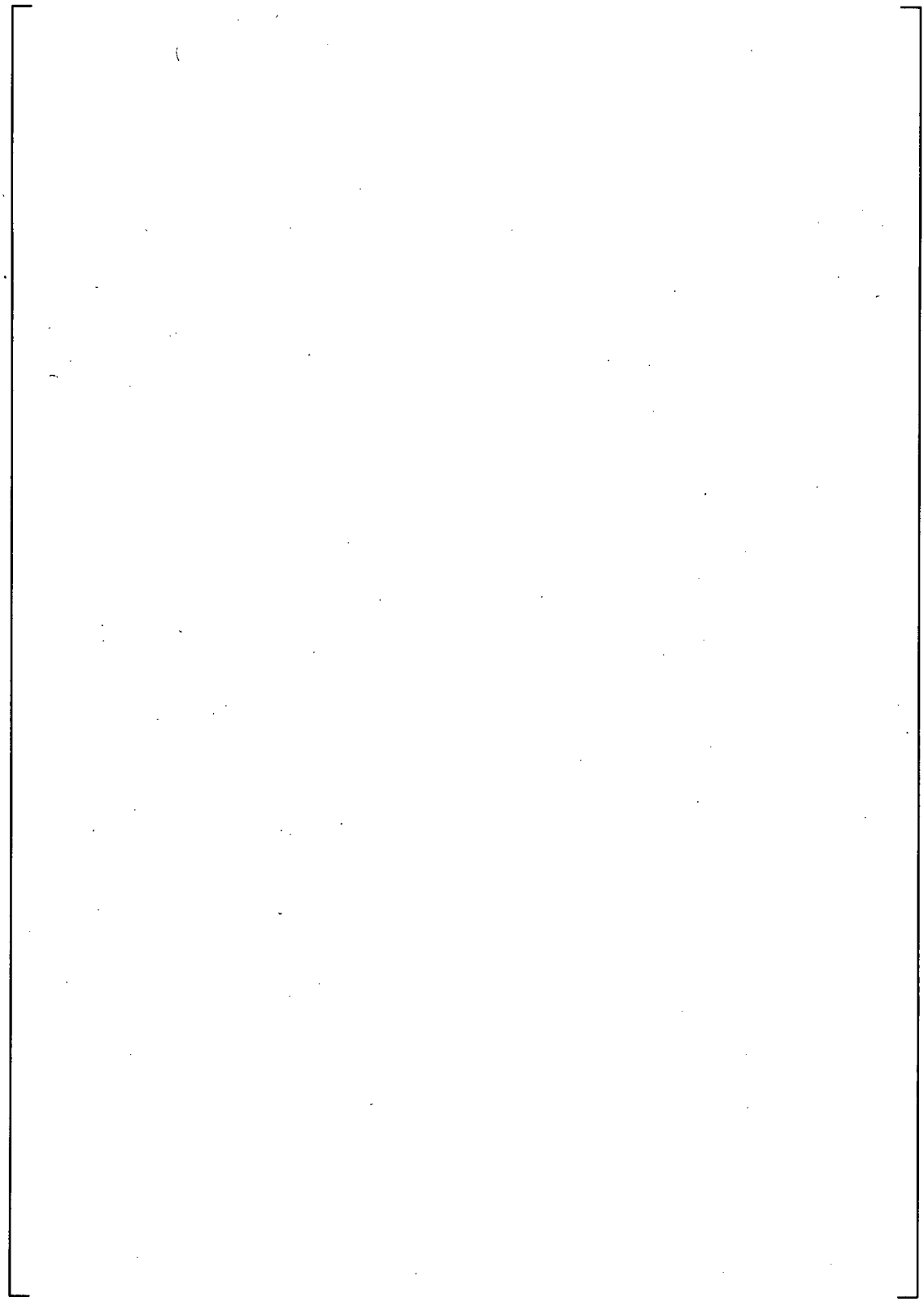

Figure 5-15: Run NRL02 Formation of Vapor Slug

5.3 RUN NRL03

Run NRL03 is conducted using unbuffered borated water with debris loading. The purpose of this run is to collect data that can be compared to run NRL02 which was conducted with unbuffered borated water without debris loading. By comparing these two runs it is possible to determine the effects of debris on the boiling and two-phase flow characteristics of an unbuffered boric acid solution.

The boric acid concentration of the solution used in run NRL03 is [ ]^{c} which corresponds to a boron concentration of [

]^{c} was added to the solution. Table 5-6 summarizes the loading times for the [ ]^{c} debris types. The temperature of the solution in the sump tank is controlled at an average temperature of 147°F and the injection flow rate is set at 1600 ml/min. After a short preheating period, the power controller is set to follow the 10CFR50 Appendix K decay curve as discussed in Section 2.2. Roughly 2 hours into the experiment, the power was lost in heater rod number 9. Although this resulted in an 11% bundle power loss, the run was continued. The total run time for this experiment is roughly 10 hours. Table 5-7 summarizes the test parameters used for run NRL03.

Solution samples drawn from the lower plenum and core region at the first sign of precipitation and at the end of the run were analyzed to determine their boric acid concentrations. In addition, temperature measurements were recorded for the heater rod cladding and fluid within the sump, downcomer, lower plenum, and core regions. Still photographs were also taken to show the accumulation of debris and boric acid precipitate in the lower plenum and core region. Multiple high-speed videos were recorded to provide images for flow regime visualization and identification.

Boric acid precipitation was observed in the lower plenum after [ ]^{c} This precipitation was initially observed on and around the walls of the lower plenum. After [ ]^{c} it was observed that the precipitate began to form within the bulk solution contained in the lower plenum. At the [ ]^{c} mark, a small amount of boric acid precipitation was also observed on the walls of the core region near the top of the heated length. No precipitation was observed on the heater rod surfaces.

Table 5-6: Run NRL03 Summary of Debris Loading Times c

Table 5-7: Run NRL03 Test Parameters

[ ]c

5.3.1 Power Measurement

The power transient for run NRL03 is shown in Figure 5-16. As the figure shows, the power is held constant at around [ ]c for approximately 4 minutes to allow some preheating of the vessel. After the short preheating period, the power controller is set to simulate the 10CFR50 Appendix K decay heat curve for the remainder of the experiment. Just before 2 hours of run time, the power lead to heater rod 9 was damaged and power to the rod was lost. This resulted in an 11% decrease in total bundle power.

[ ]c

Figure 5-16: Run NRL03 Power Transient

5.3.2 Concentration Measurements

[

]c

[

]c

Table 5-8: Run NRL03 Concentration Measurements	c

5.3.3 Precipitation and Debris Observations

Crystalline precipitation was first observed roughly [ ]c into the experiment. The precipitate was observed on the walls of the vessel housing in the lower plenum and near the top of the heated length. The vessel walls are cooler than the heated surfaces which is why it is expected that precipitation would be observed on these surfaces first. As the experiment progressed, the formation of crystalline precipitate continued to propagate down the vessel walls; by the end of the experiment precipitation could be observed from roughly the [ ]c. Figure 5-17 was taken after [ ]c and shows the precipitate that formed on the vessel walls near the two-phase mixture level. During the experiment, no precipitation was observed on any of the heater rod surfaces and no bulk precipitation within the solution could be identified.

The debris components were added to the sump tank in the order shown in Table 5-6. [

]c

[

]^c

c

Figure 5-17: Run NRL03 Crystalline Precipitate on the Vessel Walls near the Two-Phase Mixture Level after [ ]^c

Table 5-9: Run NRL03 Summary of Time Lapse Videos Showing Debris Accumulation in the Lower Plenum			
Video Title	**Collection Speed (fps)**	**Experimental Time (hr:min:sec)**	**Video Length (min)**
24555_8	1	6:49:15	30
26605_8	1	7:23:25	30
30455_8	1	8:27:35	30

c

[

]

Figure 5-18: Run NRL03 Suspension of Fibrous Debris in Downcomer

c

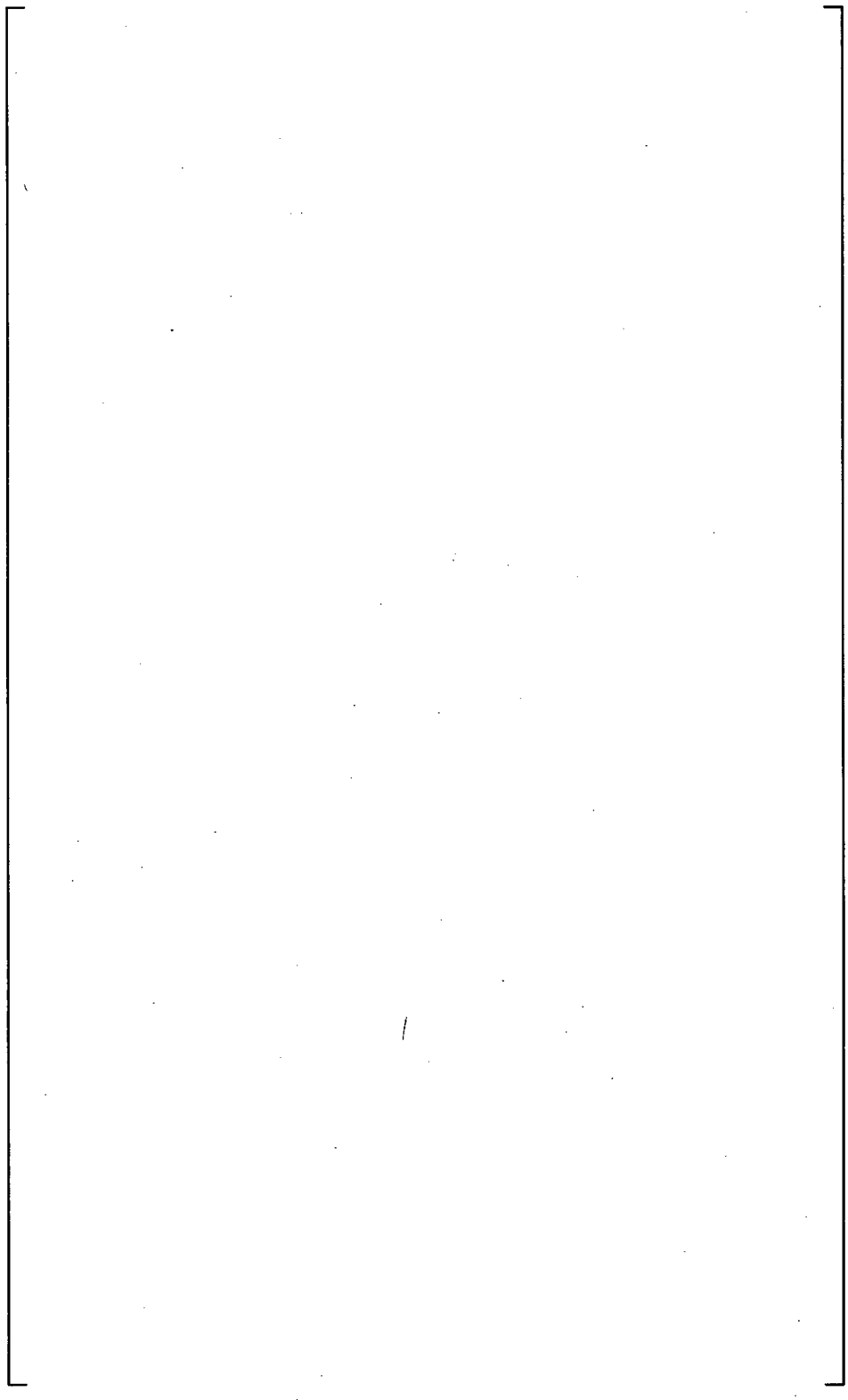

Figure 5-19: Run NRL03 Debris Accumulation in the Lower Plenum after: [ ]^{c}

[c

]c

Figure 5-20: Run NRL03 Fiber Accumulation on the Outer Edge of a Spacer Grid Observed after [ ]c

5.3.4 Temperature Measurements

Fluid temperatures measured in the sump tank, downcomer, and lower plenum are shown in Figure 5-21. Based on this figure, the following observations can be made:

- [ ]c
- [ ]c
- [ ]c
- [ ]c
- [ ]c

[ ]^{c}

- [ ]^{c}
- [ ]^{c}

In Figure 5-22, the lower plenum fluid temperatures are compared to fluid temperatures measured in the heated section of the core. Based on this figure, the following observations can be made:

- [ ]^{c}
- [ ]^{c}
- [ ]^{c}
- [ ]^{c}

The heater rod cladding temperatures measured during run NRL03 are shown in Figure 5-23 through Figure 5-25 for heater rods 7, 8, and 9, respectively. Based on these figures, the following observations can be made:

- [ ]^{c}
- [ ]^{c}
- [ ]^{c}

Figure 5-21: Run NRL03 Sump Tank, Downcomer, and Lower Plenum Fluid Temperatures

Figure 5-22: Run NRL03 Lower Plenum and Core Fluid Temperatures

Figure 5-23: Run NRL03 Cladding Temperatures (Heater Rod 7)

Figure 5-24: Run NRL03 Cladding Temperatures (Heater Rod 8)

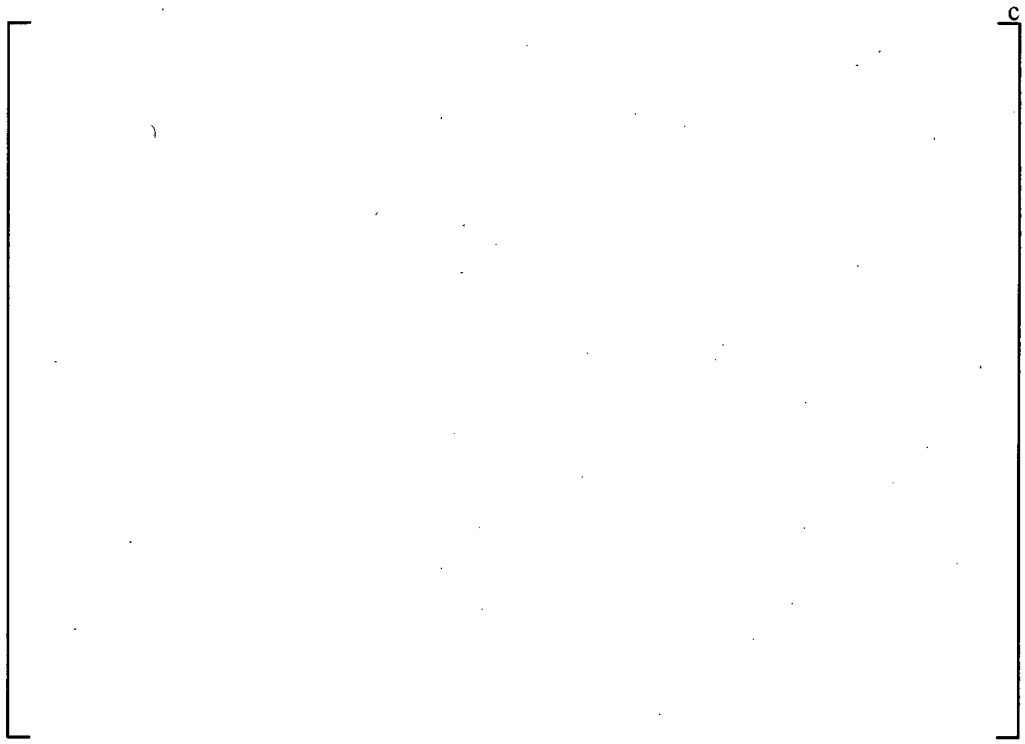

Figure 5-25: Run NRL03 Cladding Temperatures (Heater Rod 9)

5.3.5 Two-Phase Flow Visualizations

Several high-speed videos for flow visualization were collected during run NRL03. Table 5-10 lists the experimental time, bundle elevation, and bundle power at which these videos were recorded. After reviewing the videos, the following observations were made regarding the two-phase flow structure:

- [

  ]^{c}

- [

  ]^{c}

- [

  ]^{c}

- [ ]^{c}

[

]^{c}

Table 5-10: Run NRL03 Video Collected for Flow Visualization					
Video Title	**Collection Speed (fps)**	**Experimental Time (hr:min:sec)**	**Video Length (sec)**	**Bundle Elevation (in.)**	**Bundle Power (W)**
14346_18	200	3:59:06	3.11	18	1441
14525_22	200	4:02:05	3.11	22	1437
16615_34.5	200	4:36:55	3.11	34.5	1396

c

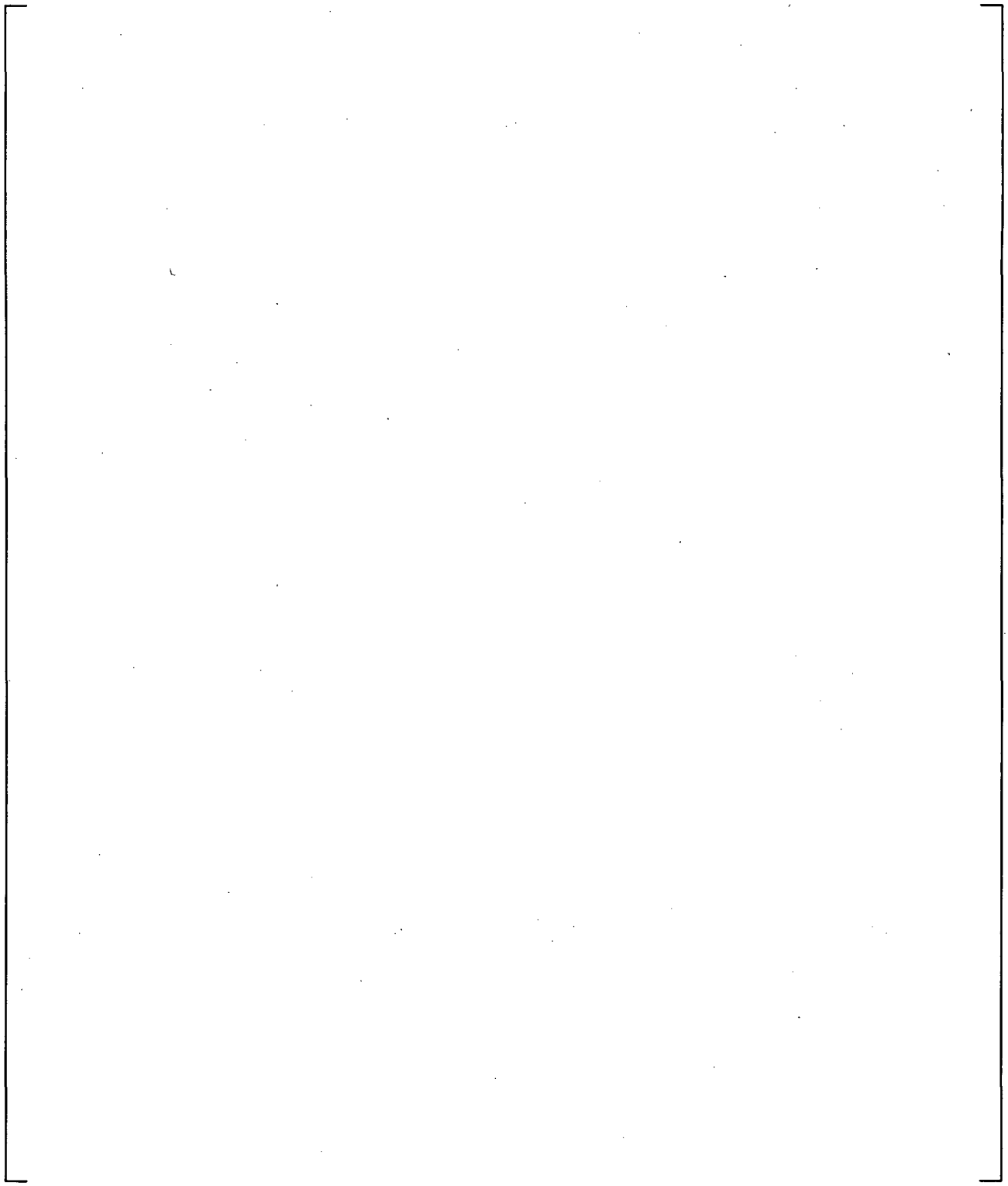

Figure 5-26: Run NRL03 Breakup of a Cap Bubble at 18 Inch Elevation and a Bundle Power of 1441W

c

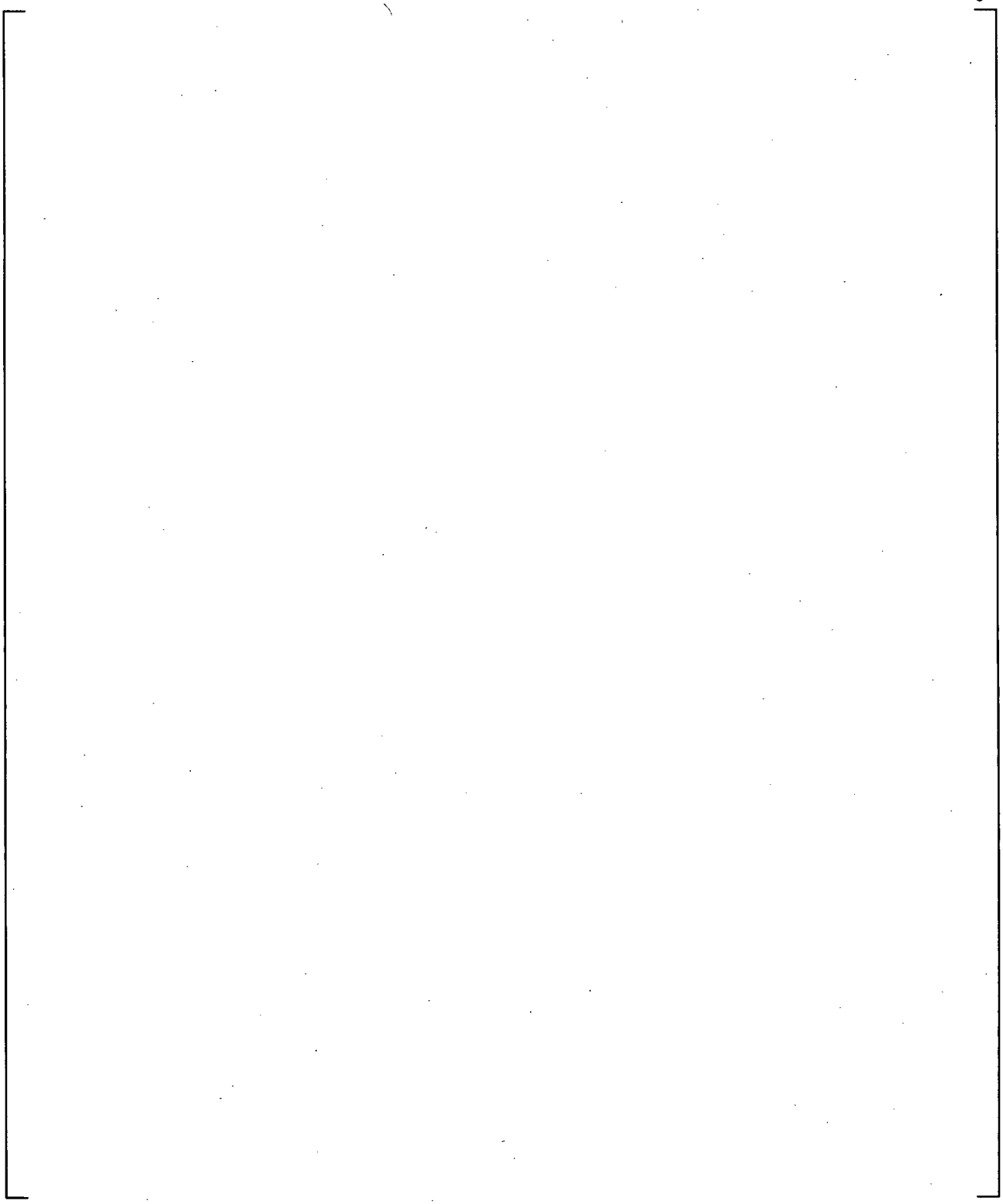

Figure 5-27: Run NRL03 Formation of Distorted Cap Bubbles at the Downstream Edge of a Spacer Grid at 22 Inch Elevation and a Bundle Power of 1437W

c

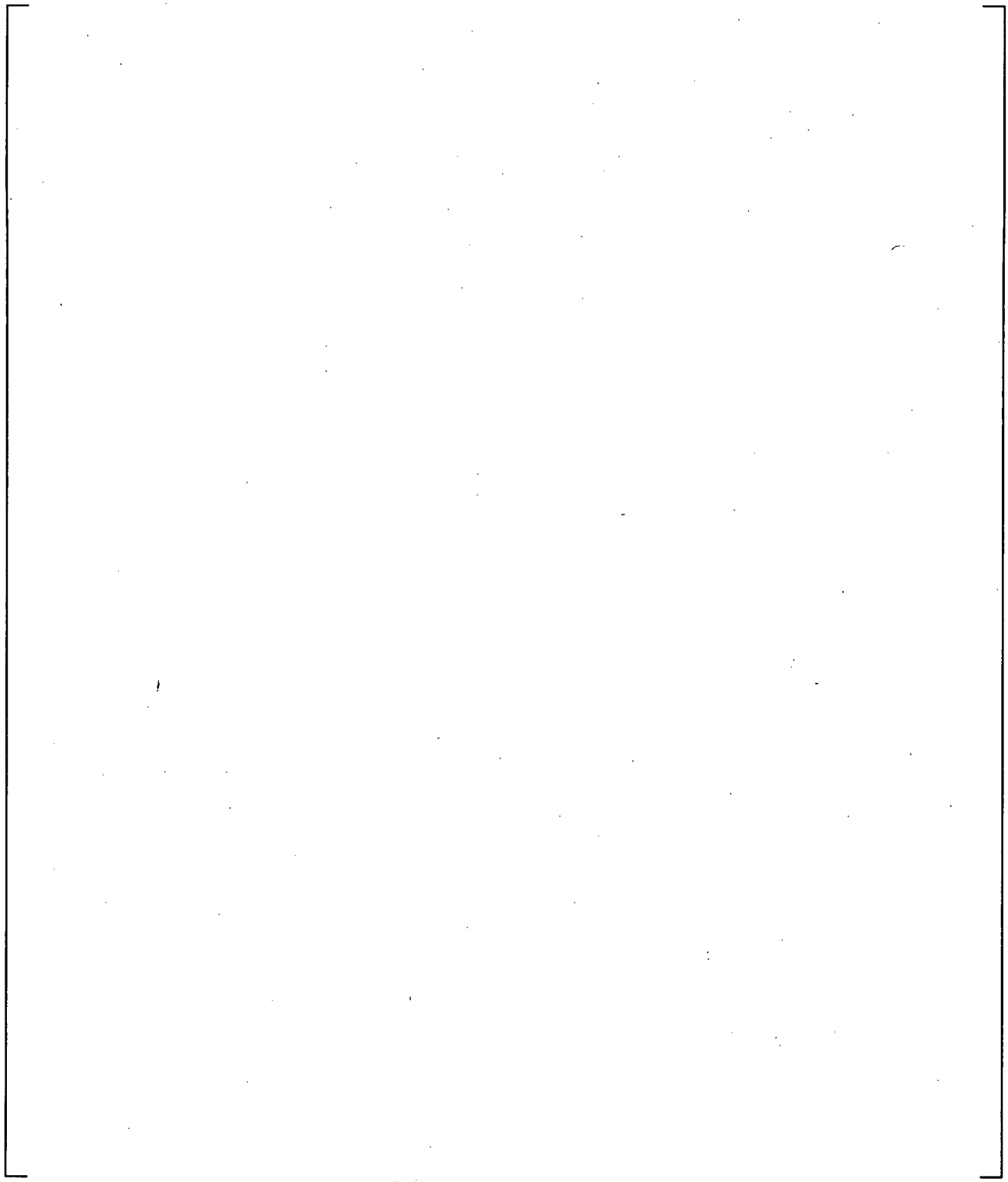

Figure 5-28: Run NRL03 Formation of a Large Vapor Slug at the Downstream Edge of a Spacer Grid at 34.5 Inch Elevation and a Bundle Power of 1396W

5.4 RUN NRL04

Run NRL04 is conducted using de-ionized water without any debris loading. The purpose of this run is to obtain flow visualizations of two-phase flow behavior in the core region at different power levels. These high-speed videos can provide a basis for the study of two-phase flow behavior in cases where unbuffered and buffered boric acid solution with and without debris is injected into the core.

The temperature of the injection water in the sump tank is controlled at an average temperature of 148°F and the injection flow rate is set at 1600 ml/min. Flow visualizations are collected at six elevations along the heated length and at three constant power levels; 2900, 1400 and 1212W. In addition, temperature measurements are recorded for the heater rod cladding and fluid within the sump, downcomer, lower plenum, and core regions. The total run time for this experiment is roughly 2.5 hours. Table 5-11 summarizes the test parameters used for run NRL04.

Table 5-11: Run NRL04 Test Parameters

c

5.4.1 Power Measurement

The power transient for run NRL04 is shown in Figure 5-29. As the figure shows, the power is rapidly increased to a value of 2900W and is held constant for 55 minutes. The power is then reduced and, once steady at 1400W, held constant for 43 minutes. Finally, the power level is reduced to 1212W where it remains for 45 minutes until the experiment is terminated. At each power level, a 30 minute period elapses to allow the vessel to reach a quasi-steady state condition before flow visualization videos were recorded.

[ ]c

Figure 5-29: Run NRL04 Power Transient

5.4.2 Concentration Measurements

Since run NRL04 was conducted with de-ionized water, no samples were taken to measure the solution concentration.

5.4.3 Precipitation and Debris Observations

No precipitation occurred in run NRL04 since it was conducted with de-ionized water. There was no debris loading used in run NRL04 and therefore, no observations related to debris behavior can be made.

5.4.4 Temperature Measurements

Fluid temperatures measured in the sump tank, downcomer, and lower plenum are shown in Figure 5-30. Based on this figure, the following observations can be made:

- [ ]c
- [ ]c

- [
  ]c
- [
  ]c
- [
  ]c

Fluid temperatures measured in the lower plenum and core region are shown in Figure 5-31. Based on this figure, the following observations can be made:

- [
  ]c
- [
  ]c
- [
  ]c

The cladding temperatures measured during run NRL04 are shown in Figure 5-32. Based on this figure, the following observations can be made:

- [
  ]c
- [
  ]c
- [
  ]c

[c]

Figure 5-30: Run NRL04 Sump, Downcomer, and Lower Plenum Fluid Temperatures

[c]

Figure 5-31: Run NRL04 Lower Plenum and Core Fluid Temperatures

[c

]

Figure 5-32: Run NRL04 Cladding Temperatures

5.4.5 Two-Phase Flow Visualizations

Two-phase flow visualizations were recorded during run NRL04 using the high-speed video camera. Table 5-12 lists the experimental time, bundle elevation, and bundle power at which these videos were recorded. [

]^{c}

[

]c

Based on the high-speed videos collected during this run and using the images presented in the three figures, the following remarks can be made regarding the two-phase flow structure at the three different power levels:

- [
  ]c
- [
  ]c
- [
  ]c
- [ ]c
- [
  ]c

Table 5-12: Run NRL04 Video Collected for Flow Visualization					
Video Title	**Collection Speed (fps)**	**Experimental Time (hr:min:sec)**	**Video Length (sec)**	**Bundle Elevation (in.)**	**Bundle Power (W)**
2900_13.0	200	0:47:15	3.465	13	2900
2900_18.0	200	0:46:05	3.465	18	2900
2900_20.5	200	0:44:45	3.465	20.5	2900
2900_22.0	200	0:43:45	3.465	22	2900
2900_32.0	200	0:42:55	3.465	32	2900
2900_34.5	200	0:41:25	3.465	34.5	2900
1400_13.0	200	1:37:45	3.465	13	1400
1400_18.0	200	1:38:35	3.465	18	1400
1400_20.5	200	1:39:25	3.465	20.5	1400
1400_22.0	200	1:40:35	3.465	22	1400
1400_32.0	200	1:41:25	3.465	32	1400
1400_34.5	200	1:42:15	3.465	34.5	1400
1212_13.0	200	2:28:55	3.465	13	1212
1212_18.0	200	2:27:55	3.465	18	1212
1212_20.5	200	2:26:45	3.465	20.5	1212
1212_22.0	200	2:25:55	3.465	22	1212
1212_32.0	200	2:25:05	3.465	32	1212
1212_34.5	200	2:24:05	3.465	34.5	1212

c

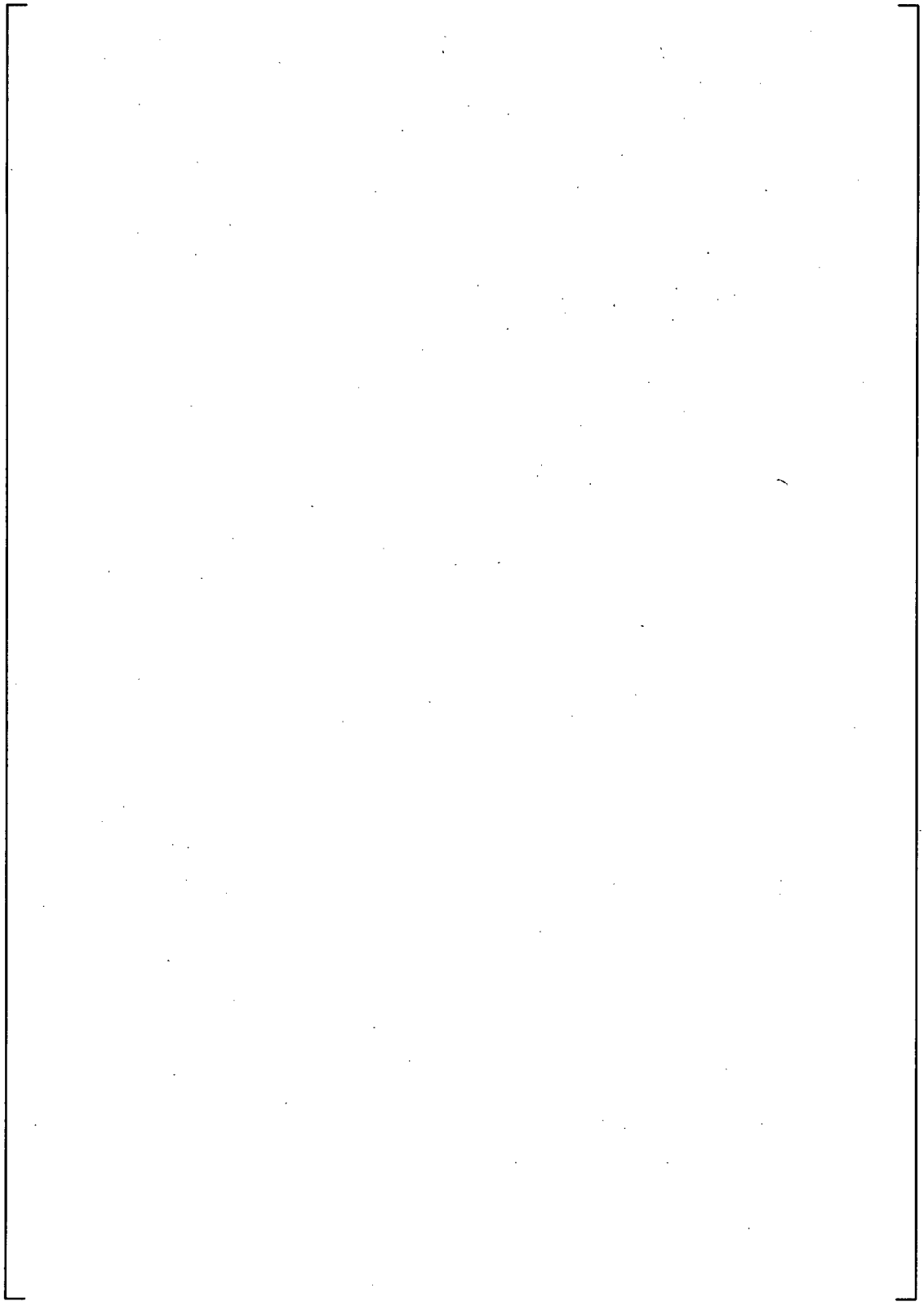

Figure 5-33: Run NRL04 Flow Visualizations at 2900W Power

c

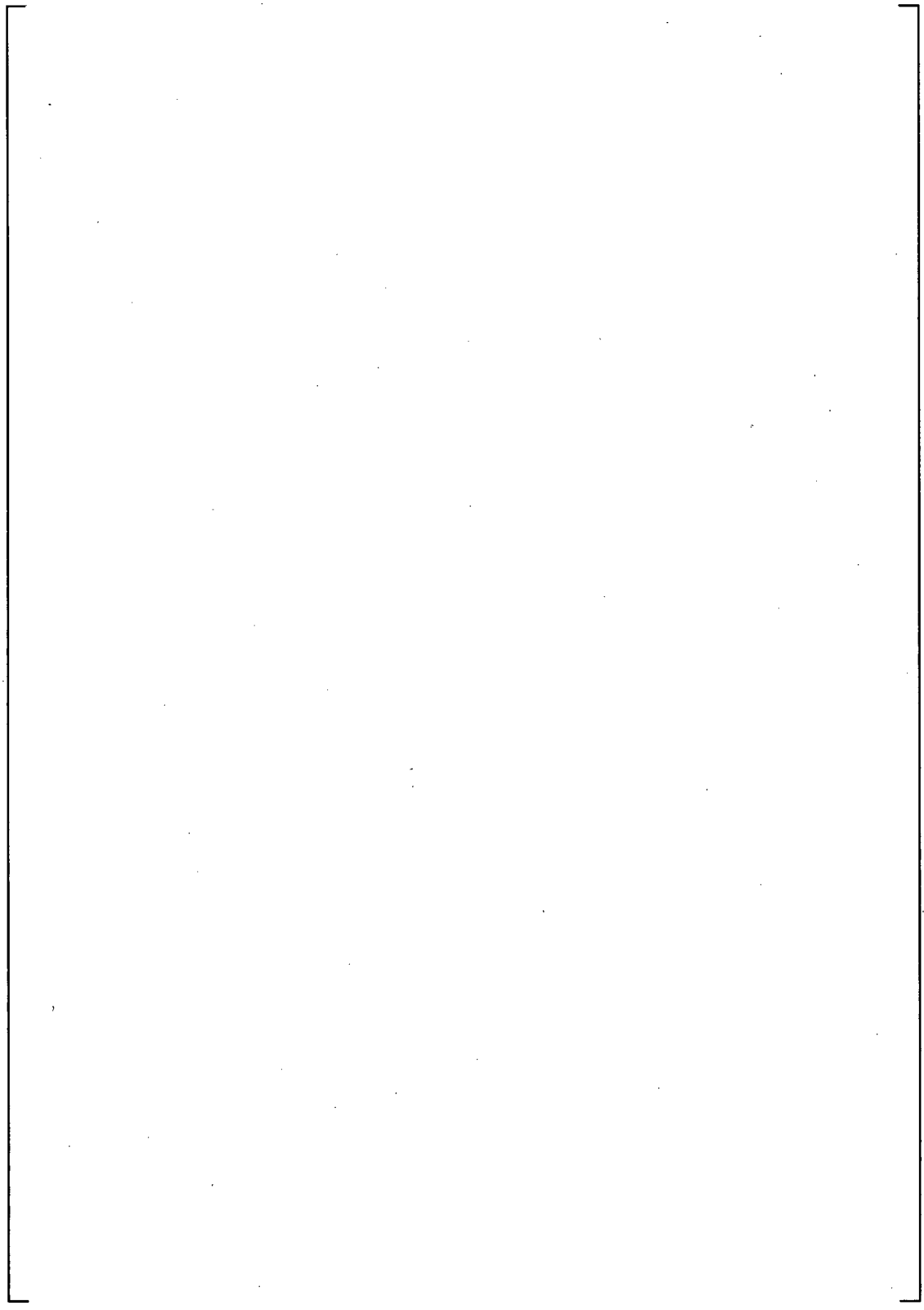

Figure 5-34: Run NRL04 Flow Visualizations at 1400W Power

c

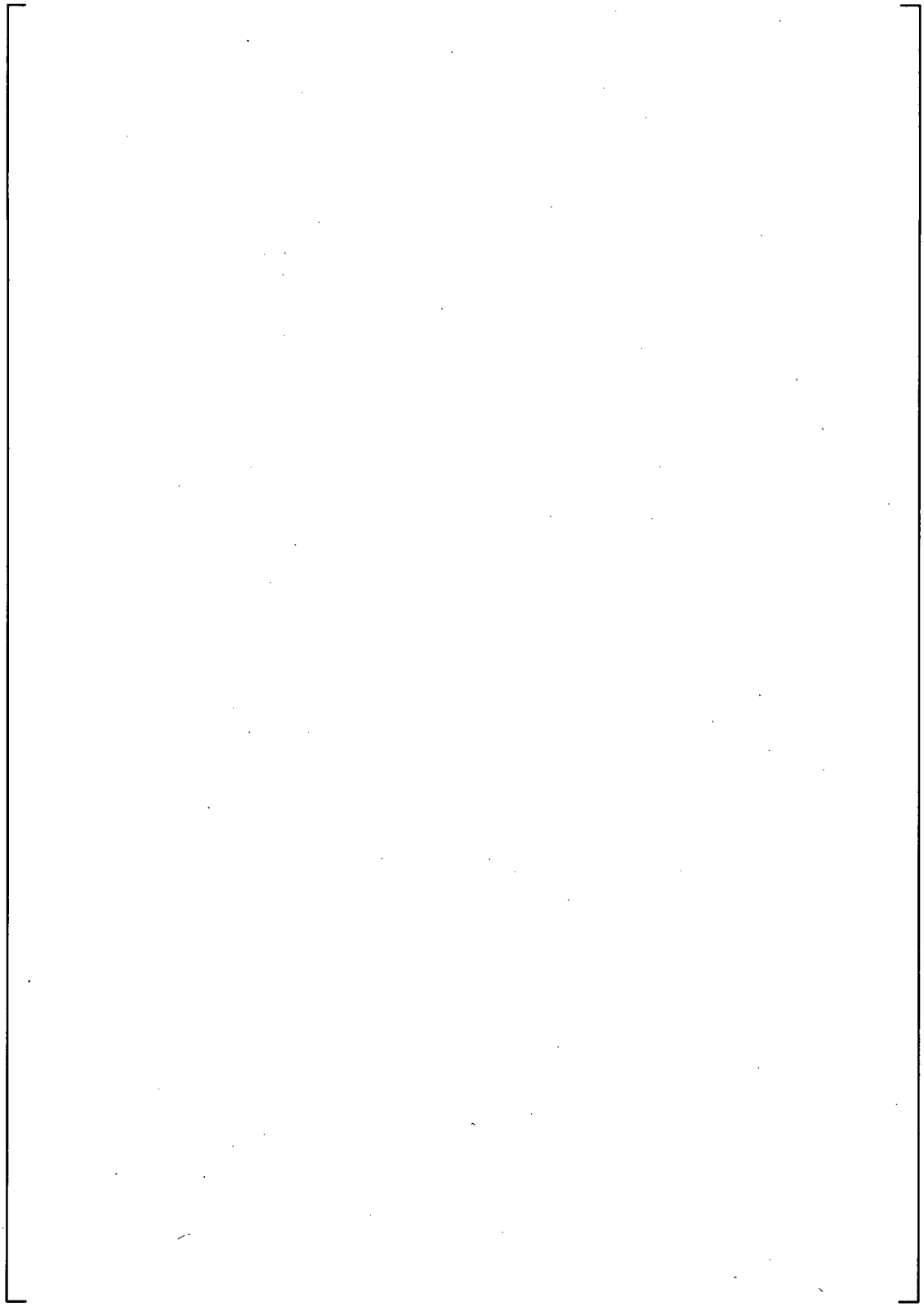

Figure 5-35: Run NRL04 Flow Visualizations at 1212W Power

5.5 RUN NRL05

Run NRL05 is conducted using a buffered borated water solution with debris loading. The purpose of this run is to collect data that can be compared to run NRL03 which was conducted with unbuffered borated water with the same boric acid concentration and debris loading. By comparing the results of these two runs, the effects of the sodium hydroxide (NaOH) buffering agent on the precipitation and boiling characteristics in the presence of debris can be determined.

The buffered solution used in run NRL05 has a boric acid concentration of [ ]^{c} which corresponds to a boron concentration of [ ]^{c} The NaOH buffering agent has a concentration of [ ]^{c} which is equivalent to a sodium concentration of [

]^{c} The temperature of the solution in the sump tank is controlled at an average temperature of 148°F and the injection flow rate is set at 1600 ml/min. After a short preheating period, the power controller is set to follow the 10CFR50 Appendix K decay curve as discussed in Section 2.2. The total run time for this experiment is roughly 10 hours. Table 5-14 summarizes the test parameters used for run NRL05.

Solution samples drawn from the lower plenum and core region midway through the test and at the end of the run were analyzed to determine their boric acid concentrations. In addition, temperature measurements were recorded for the heater rod cladding and fluid within the sump, downcomer, lower plenum, and core regions. Still photographs were also taken to show the accumulation of debris and boric acid precipitate in the lower plenum and core region. Multiple high-speed videos were recorded to provide images for flow regime visualization and identification.

Boric acid precipitation was not observed anywhere in the vessel during run NRL05. This is most likely due to the fact that boric acid buffered with NaOH increases the solubility limit of the solution.

A pH of 8.5 was measured from the downcomer return just before the power was applied.

Table 5-13: Run NRL05 Summary of Debris Loading Times c

Table 5-14: Run NRL05 Test Parameters

[ ]c

5.5.1 Power Measurement

The power transient for run NRL05 is shown in Figure 5-36. As the figure shows, the power is initially raised to a value of approximately [ ]c to preheat the bundle and allow the fluid in the bundle to reach saturation temperature. After 8 minutes of preheating, the power controller is set to simulate the 10CFR50 Appendix K decay heat curve for the remainder of the experiment.

[c

]c

Figure 5-36: Run NRL05 Power Transient

5.5.2 Concentration Measurements

[

]c

Table 5-15: Run NRL05 Concentration Measurements [c

5.5.3 Precipitation and Debris Observations

Precipitation was not observed anywhere in the vessel during run NRL05. This is most likely due to the fact that boric acid buffered with NaOH has a higher solubility limit at the tested pH compared to unbuffered boric acid solutions. Figure 5-37 shows an image of the two-phase mixture level taken at the end of the experiment indicating that no precipitation is visible on any of the surfaces. Since no precipitation formed near the two-phase mixture level, it is likely that precipitation did not occur anywhere in the heated length of the test section.

The debris components were added to the sump tank in the order shown in Table 5-13. [

]c

[

]^{c}

[c

]

Figure 5-37: Run NRL05 Two-Phase Mixture Level at the End of the Experiment Indicating No Visible Precipitation

[ ]c

Figure 5-38: Run NRL05 Debris Accumulation in the Lower Plenum Roughly [ ]c into the Experiment

[ ]c

Figure 5-39: Run NRL05 Debris Clumps Swept into the Core Region after Breaking from the Debris Bed Formed in the Lower Plenum

Figure 5-40: Run NRL05 Debris Accumulation on Outer Edge of a Spacer Grid Observed at the End of the Experiment

Figure 5-41: Run NRL05 Debris that Settled in the Lower Plenum after Termination of the Experiment which Indicates that Debris was Present in the Core Region

Figure 5-42: Run NRL05 Debris that Settled at the Core Inlet after Termination of the Experiment which Indicates that Debris was Present in the Core Region

5.5.4 Temperature Measurements

Fluid temperatures measured in the sump tank, downcomer, and lower plenum are shown in Figure 5-43. Based on this figure, the following observations can be made:

- [ ]
- [ ]
- [ ]
- [ ]
- [ ]
- [ ]

[

]^c

- [

]^c

In Figure 5-44, the lower plenum fluid temperatures are compared to fluid temperatures measured in the heated section of the core. Based on this figure the following observations can be made:

- [

]^c

- [

]^c

- [

]^c

- [

]^c

The heater rod cladding temperatures measured during run NRL05 are shown in Figure 5-45. Based on this figure, the following observations can be made:

- [

]^c

- [

]^c

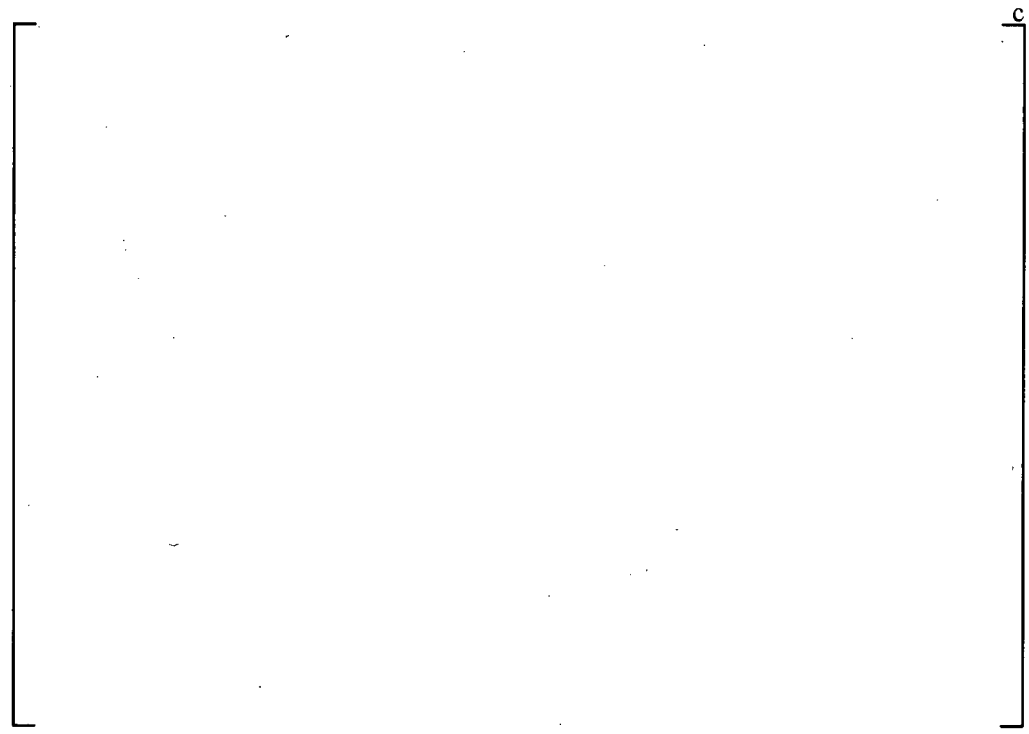

Figure 5-43: Run NRL05 Sump Tank, Downcomer, and Lower Plenum Fluid Temperatures

Figure 5-44: Run NRL05 Lower Plenum and Core Fluid Temperatures

[ ]c

Figure 5-45: Run NRL05 Cladding Temperatures

5.5.5 Two-Phase Flow Visualizations

Several high-speed videos for flow visualization were collected during run NRL05. Table 5-16 lists the experimental time, bundle elevation, and bundle power at which these videos were recorded. After reviewing the videos, the following observations were made regarding the two-phase flow structure:

- [ ]c
- [ ]c
- [ ]c

[

]^{c}

Table 5-16: Run NRL05 Video Collected for Flow Visualization

Video Title	Collection Speed (fps)	Experimental Time (hr:min:sec)	Video Length (sec)	Bundle Elevation (in.)	Bundle Power (W)
1964_18	200	0:32:44	3.465	18	2632
2494_32	200	0:41:34	3.465	32	2480
2559_22	200	0:42:34	3.465	22	2465
2595_20pt5	200	0:43:14	3.465	20.5	2451
23063_34pt5	200	6:24:23	3.465	34.5	1395
23223_32	200	6:27:03	3.465	32	1393
23483_22	200	6:31:23	3.465	22	1390
23713_20pt5	200	6:35:13	3.465	20.5	1386
23763_18	200	6:36:03	3.465	18	1386
33154_18	200	9:12:34	3.465	18	1288
33434_20pt5	200	9:17:14	3.465	20.5	1284
33604_22	200	9:20:04	3.465	22	1283
33863_32	200	9:24:23	3.465	32	1282
33954_34	200	9:25:54	3.465	34	1280

c

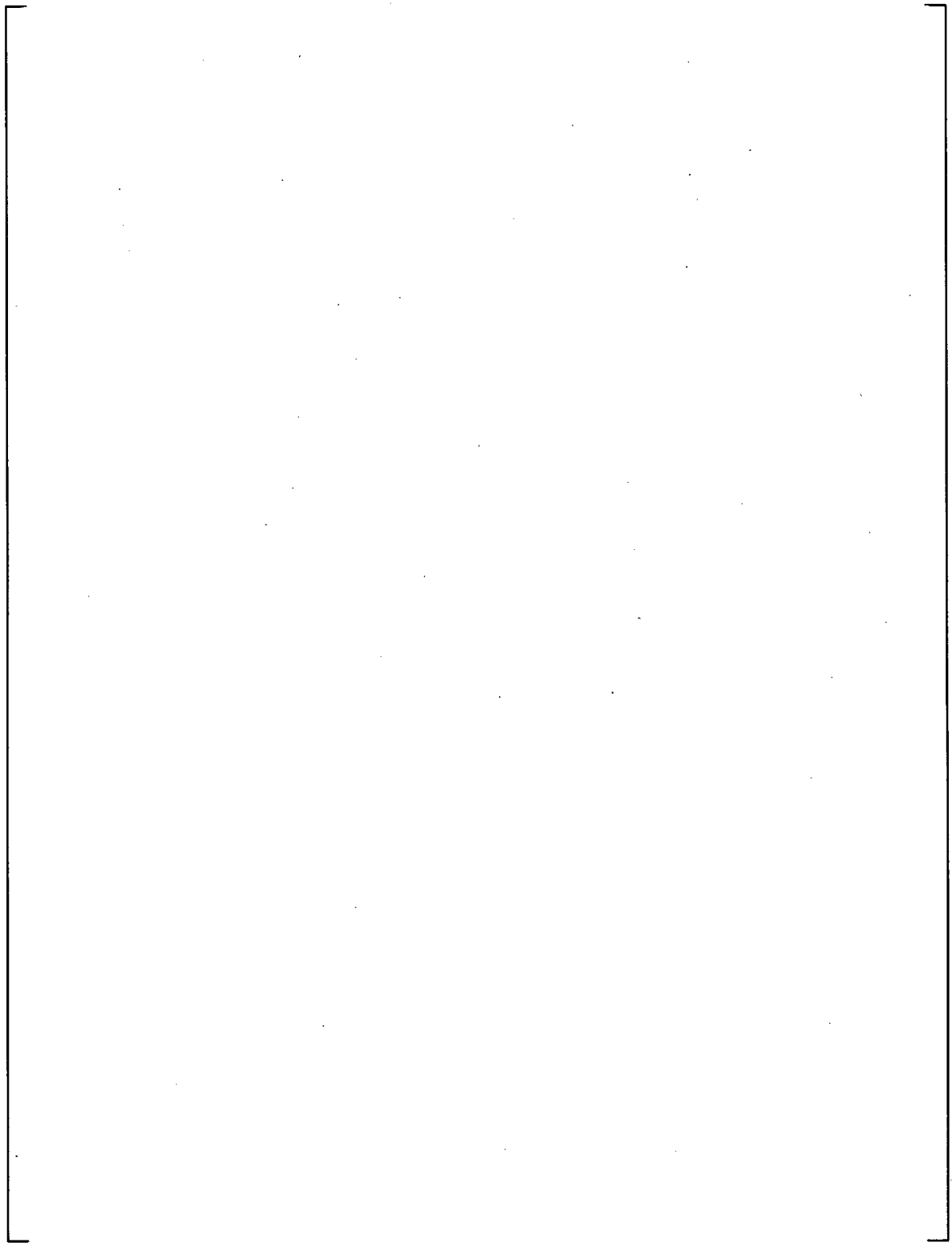

Figure 5-46: Run NRL05 Two-Phase Flow Regimes at Three Elevations and Powers Early in the Experiment

c

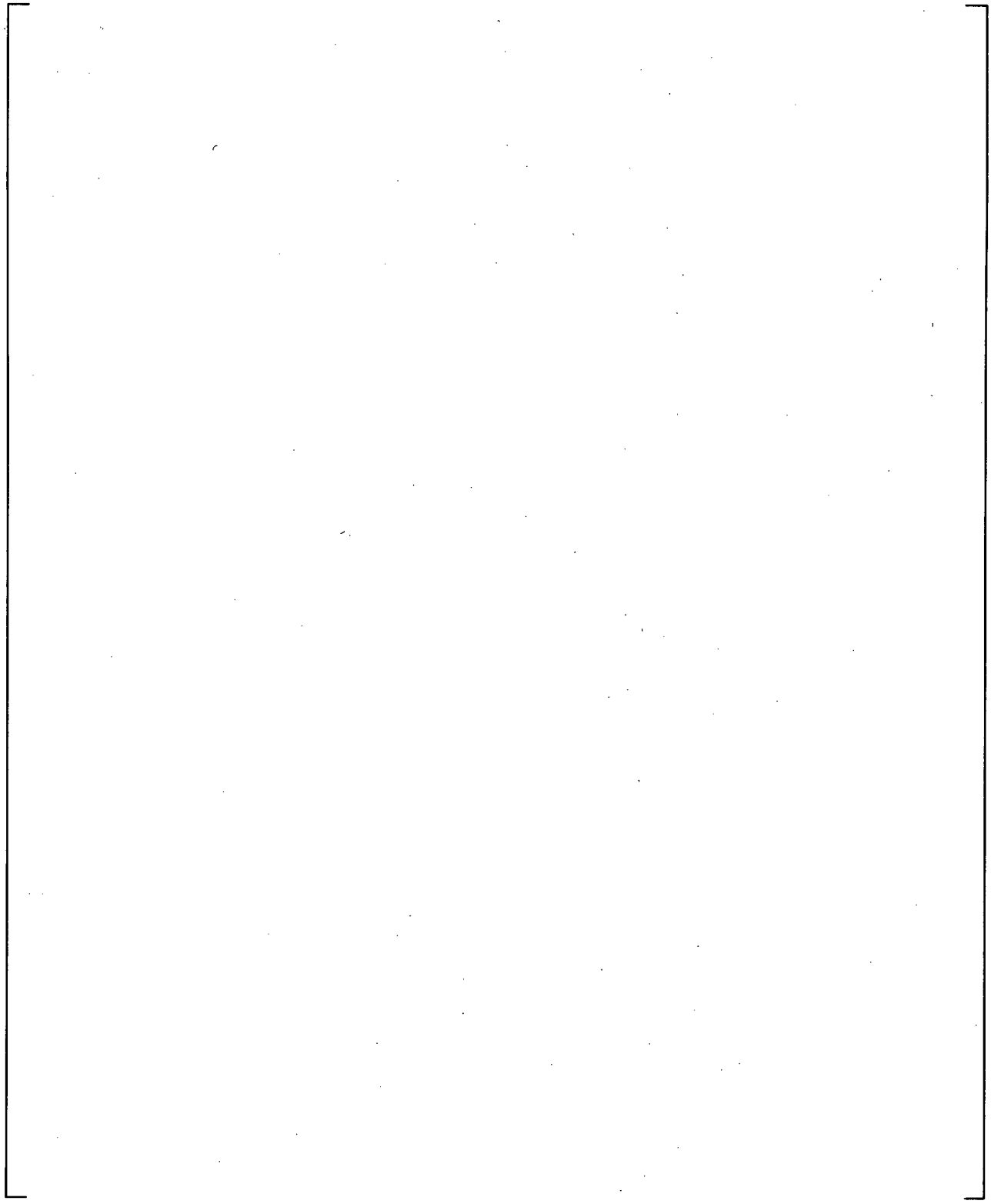

Figure 5-47: Run NRL05 Two-Phase Flow Regimes at Three Elevations and an Average Power of 1390W

c

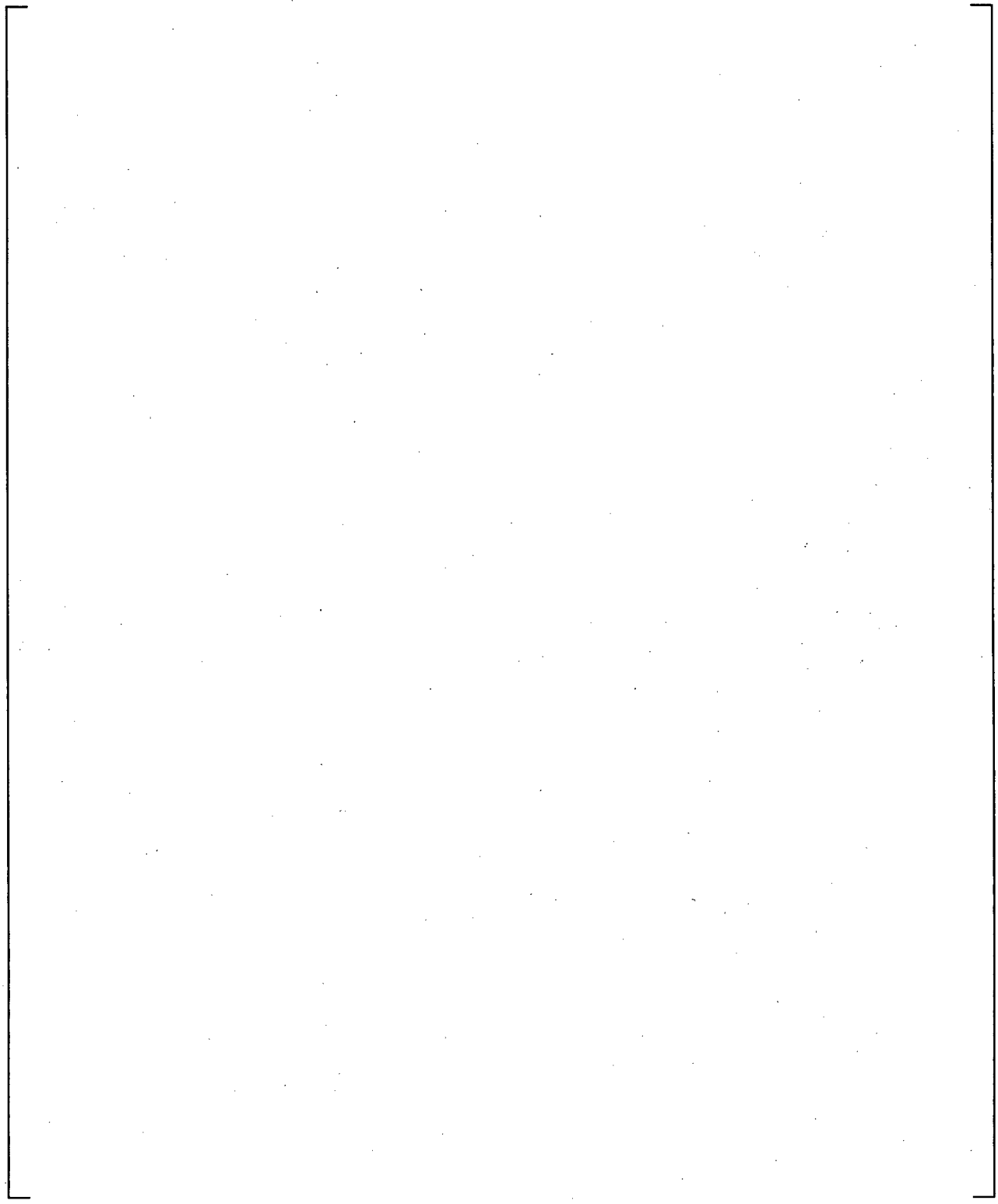

Figure 5-48: Run NRL05 Two-Phase Flow Regimes at Three Elevations and an Average Power of 1284W

5.6 RUN NRL06

Run NRL06 is conducted using borated water buffered with trisodium phosphate (TSP) and debris loading. The objective of this run is to obtain data that highlights the effect of debris loading in a borated water solution buffered with TSP. This run is conducted using a smaller volume lower plenum to see if this would allow more debris to enter the core region by limiting the space in which debris could settle and accumulate within the lower plenum. Near the end of the run, several uncovery and recovery cycles were performed to study boron precipitation and dissolution under high boron concentration and low heat flux conditions.

The solution used in run NRL06 is buffered borated water with a boric acid concentration of [ ]^{c} which corresponds to a boron concentration of [ ]^{c} The buffering agent is TSP with a concentration of [ ]^{c} which is equivalent to a sodium concentration of [

]^{c} The temperature of the solution in the sump tank is controlled at an average temperature of 152°F and the injection flow rate is set at 1600 ml/min. After a short preheating period, the power controller is set to follow the 10CFR50 Appendix K decay curve as discussed in Section 2.2. The total run time for this experiment is roughly 7 hours. Table 5-18 summarizes the test parameters used for run NRL06.

Solution samples drawn from the lower plenum and core region midway through the test and at the end of the run were analyzed to determine the boric acid concentration. In addition, temperature measurements were recorded for the heater rod cladding and fluid within the sump, downcomer, lower plenum, and core regions. Still photographs were also taken to show the accumulation of debris and boric acid precipitate in the lower plenum and core region. Multiple high-speed videos were recorded to provide images for flow regime visualization and identification as well as precipitation and dissolution during the core uncovery and recovery cycles.

Table 5-17: Run NRL06 Summary of Debris Loading Times c

Table 5-18: Run NRL06 Test Parameters [c]

5.6.1 Power Measurement

The power transient for run NRL06 is shown in Figure 5-49. As the figure shows, the power is initially raised to a value of approximately [ ]^{c} to preheat the bundle and allow the fluid in the bundle to reach saturation temperature. After 6 minutes of preheating, the power controller is set to simulate the 10CFR50 Appendix K decay heat curve for the remainder of the experiment.

Figure 5-49: Run NRL06 Power Transient

5.6.2 Concentration Measurements

The samples taken during run NRL06 are listed in Table 5-19 along with the measured concentrations.

[

]

Table 5-19: Run NRL06 Concentration Measurements [c

5.6.3 Precipitation and Debris Observations

Precipitation was not observed anywhere in the vessel during normal operation of the test facility. This indicates that boric acid buffered with TSP has a higher solubility limit compared to unbuffered boric acid solutions. Two uncovery and recovery cycles were performed during run NRL06 and precipitation was observed to occur on the heater rods and unheated vessel walls above the two-phase mixture level during core uncovery. The results of these uncovery and recovery cycles are presented in Section 5.6.6 and include images of the precipitation observed during core uncovery as well as images of the dissolution process during core recovery.

[

]^{c}

[

]^{c}

Figure 5-50: Run NRL06 Debris Accumulation in the Lower Plenum, Downcomer, and Core Inlet Region after [ ]^{c}

Figure 5-51: Run NRL06 Rod Bundle after Experiment and Disassembly; (a) Debris Accumulation on Outer Edge of a Spacer Grid, (b) White Haze on Heater Rod Surfaces where Precipitation Formed During Core Uncovery

5.6.4 Temperature Measurements

Fluid temperatures measured in the sump tank, downcomer, and lower plenum are shown in Figure 5-52. Based on this figure, the following observations can be made:

- [ ]^{c}
- [ ]^{c}
- [ ]^{c}
- [ ]^{c}

In Figure 5-53, the lower plenum fluid temperatures are compared to fluid temperatures measured in the heated section of the core. Based on this figure the following observations can be made:

- [ ]^{c}
- [ ]^{c}
- [ ]^{c}
- [ ]^{c}

The heater rod cladding temperatures measured during run NRL06 are shown in Figure 5-54. Based on this figure, the following observations can be made:

- [ ]^{c}
- [ ]^{c}
- [ ]^{c}

Figure 5-52: Run NRL06 Sump Tank, Downcomer, and Lower Plenum Fluid Temperatures

Figure 5-53: Run NRL06 Lower Plenum and Core Fluid Temperatures

[ ]c

Figure 5-54: Run NRL06 Cladding Temperatures

5.6.5 Two-Phase Flow Visualizations

Several high-speed videos for flow visualization were collected during run NRL06. Table 5-20 lists the experimental time, bundle elevation, and bundle power at which these videos were recorded. After reviewing the videos, the following observations were made regarding the two-phase flow structure:

- [

  ]c

- [

  ]c

- [

  ]c

Table 5-20: Run NRL06 Video Collected for Flow Visualization					
Video Title	**Collection Speed (fps)**	**Experimental Time (hr:min:sec)**	**Video Length (sec)**	**Bundle Elevation (in.)**	**Bundle Power (W)**
NRL06_01	200	0:45:12	3.465	13	2410
NRL06_02	200	0:46:42	3.465	18	2383
NRL06_03	200	0:48:12	3.085	20.5	2371
NRL06_04	200	0:49:42	3.465	22	2347
NRL06_05	200	0:53:12	3.465	32	2301
NRL06_06	200	0:54:42	3.465	34.5	2289
NRL06_07	200	2:44:12	3.465	34.5	1696
NRL06_08	200	2:45:42	3.465	32	1695
NRL06_09	200	2:47:12	3.465	22	1689
NRL06_10	200	2:48:42	4.815	18	1685
NRL06_11	200	2:50:42	4.815	20.5	1680
NRL06_12	200	2:54:12	17.255	13	1670
NRL06_13	200	5:16:45	13.620	13	1432
NRL06_14	200	5:17:44	5.310	18	1431
NRL06_15	200	5:18:44	5.310	20.5	1429
NRL06_16	200	5:19:44	5.310	22	1429
NRL06_17	200	5:23:44	5.310	32	1425
NRL06_18	200	5:25:44	5.310	34.5	1424

c

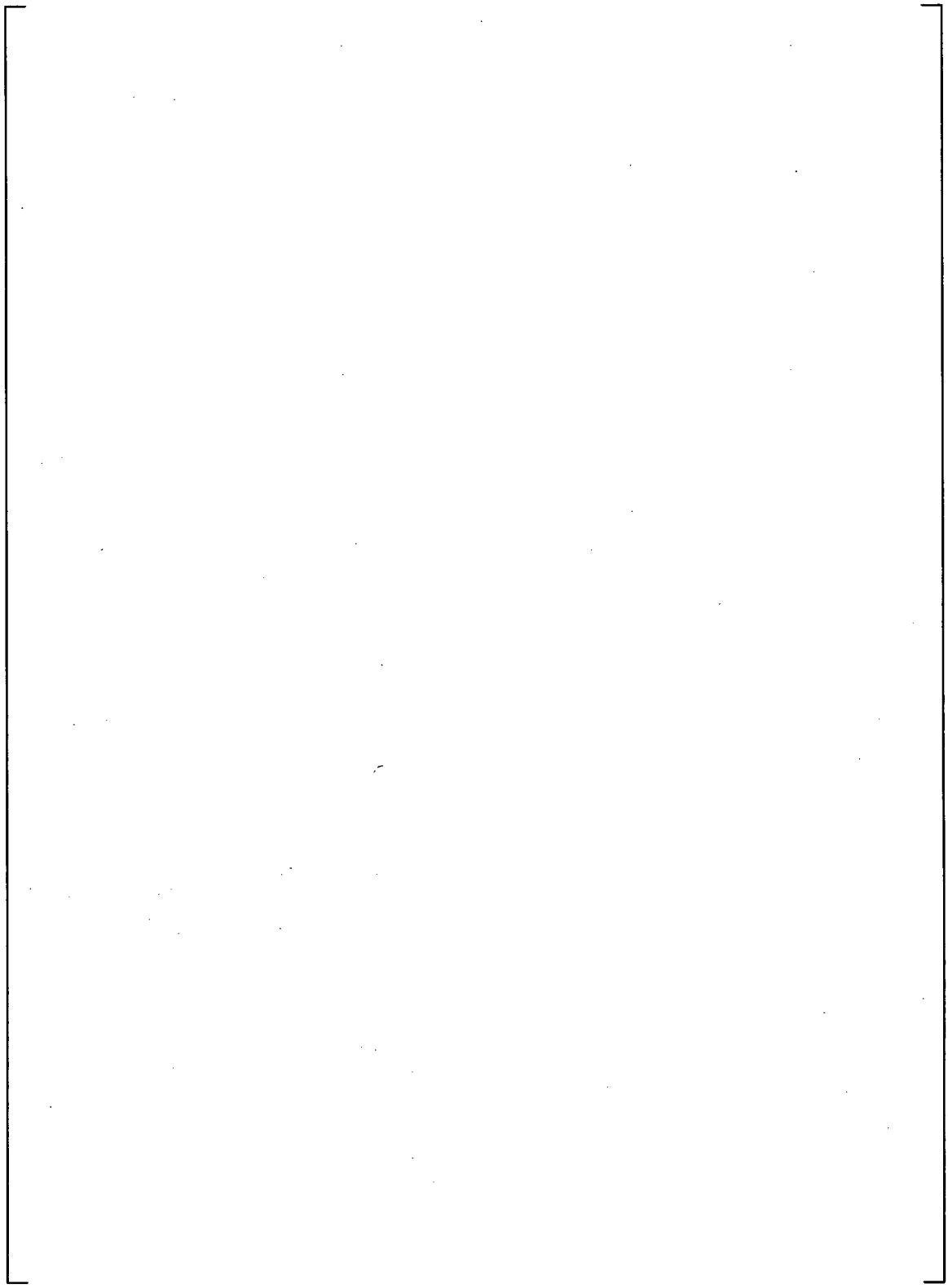

Figure 5-55: Run NRL06 Two-Phase Flow Regimes at Three Elevations and Powers Early in the Experiment

c

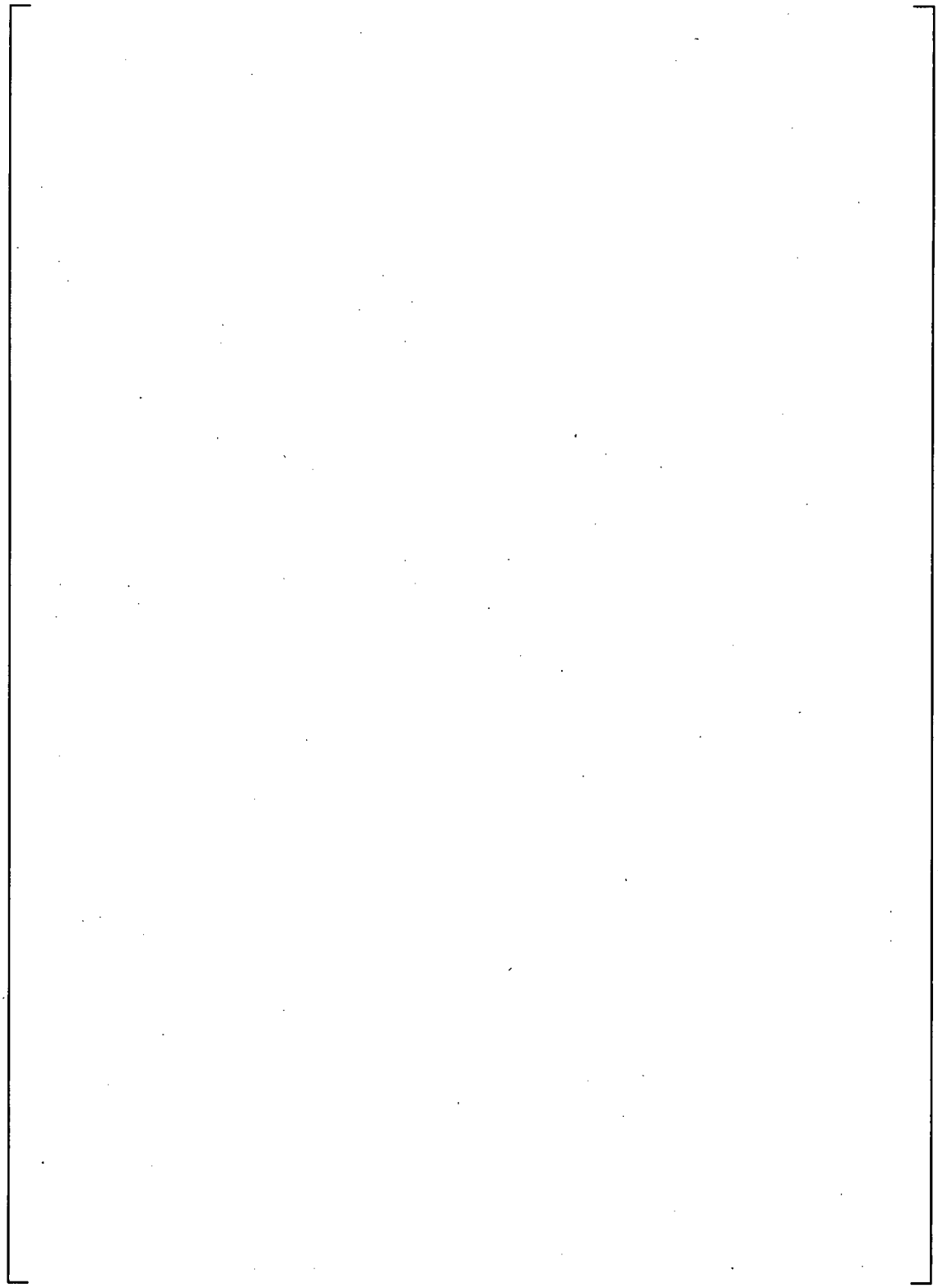

Figure 5-56: Run NRL06 Two-Phase Flow Regimes at Three Elevations and Powers Later in the Experiment

c

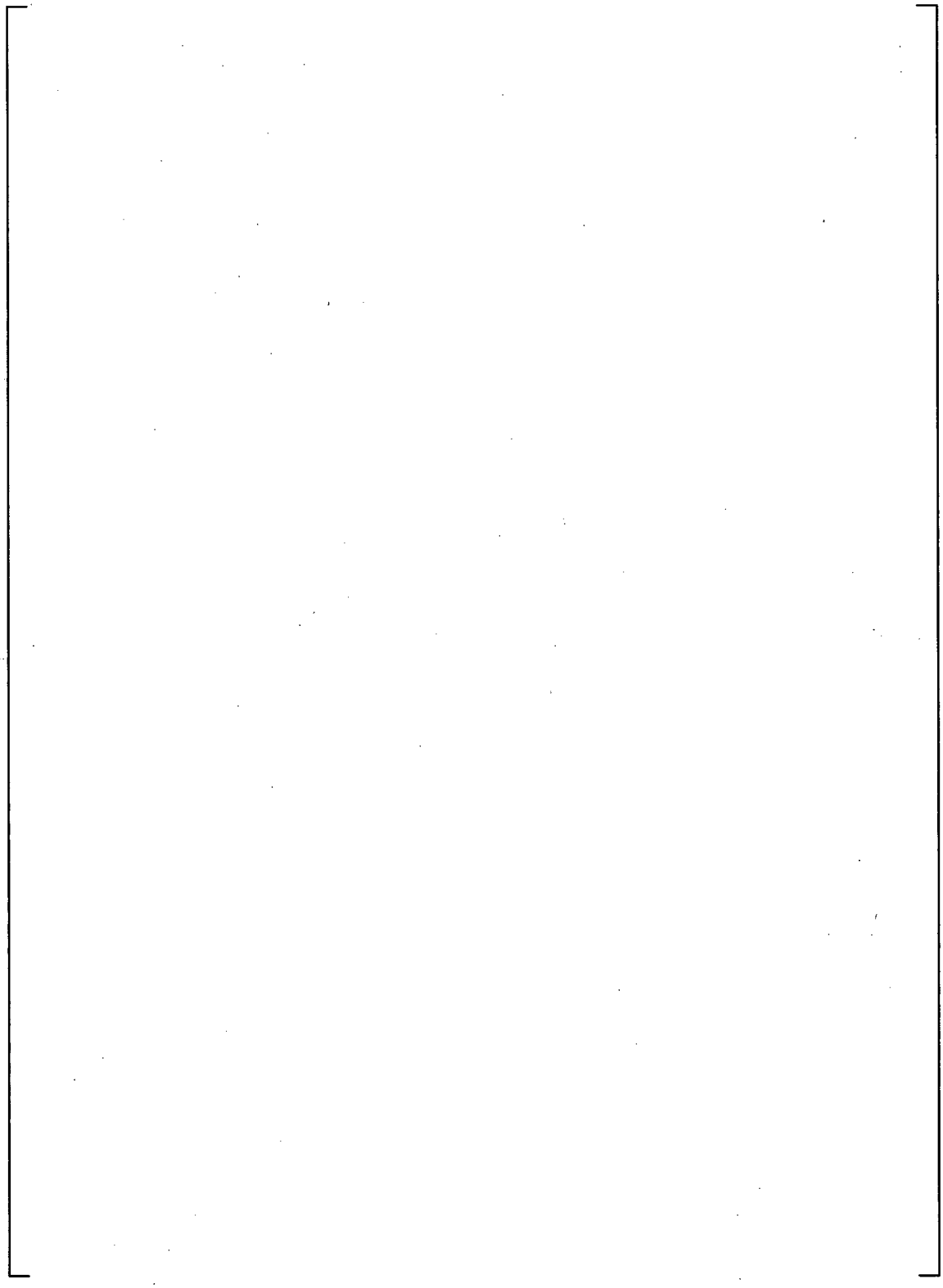

Figure 5-57: Run NRL06 Two-Phase Flow Regimes at Three Elevations and a Power of Approximately 1427W

5.6.6 Core Uncovery and Recovery Cycles

Two core uncovery and recovery cycles were performed at the end of run NRL06. [

]^{c}

Table 5-21: Run NRL06 Cladding Temperatures, Turnaround and Recovery Times during Uncovery and Recovery Cycles

[ ]^{c}

Figure 5-58: Run NRL06 Cladding Temperature Measured at the Top of the Bundle during the Two Uncovery and Recovery Cycles

Figure 5-59: Run NRL06 Core Fluid Temperature Measured at the Top of the Bundle during the Two Uncovery and Recovery Cycles

High-speed videos were collected during the uncovery and recovery cycles performed at the end of run NRL06. Table 5-22 lists the video titles, collection speed, and experimental times at which these videos were recorded. Note that the cycle times listed in Table 5-22 are referenced from the beginning of core uncovery; negative time values indicate that video collection begins prior to core uncovery.

[

]^{c}

Table 5-22: Run NRL06 Video Collected during Uncovery and Recovery Cycles

Cycle 1: Average Power = 1406W				
Video Title	**Collection Speed (fps)**	**Experimental Time (hr:min:sec)**	**Cycle Time (sec)**	**Bundle Elevation (in.)**
NRL06_19	30	5:32:24 – 5:34:15	(-10) – 100	34
NRL06_20	30	5:34:45 – 5:36:34	130 – 240	34
NRL06_21	200	5:38:35 – 5:38:40	360 – 365	34
NRL06_22	200	5:41:45 – 5:41:50	550 – 555	34
NRL06_23	30	5:45:15 – 5:47:05	760 – 870	34
NRL06_24	30	5:47:55 – 5:49:45	920 – 1030	34
NRL06_25	30	5:51:05 – 5:52:55	1110 – 1220	34
Cycle 2: Average Power = 1390W				
Video Title	**Collection Speed (fps)**	**Experimental Time (hr:min:sec)**	**Cycle Time (sec)**	**Bundle Elevation (in.)**
NRL06_26	30	5:53:25 – 5:55:15	(-20) – 90	33
NRL06_27	60	5:58:05 – 5:59:05	260 – 320	33
NRL06_28	60	6:03:05 – 6:04:05	560 – 620	33

c

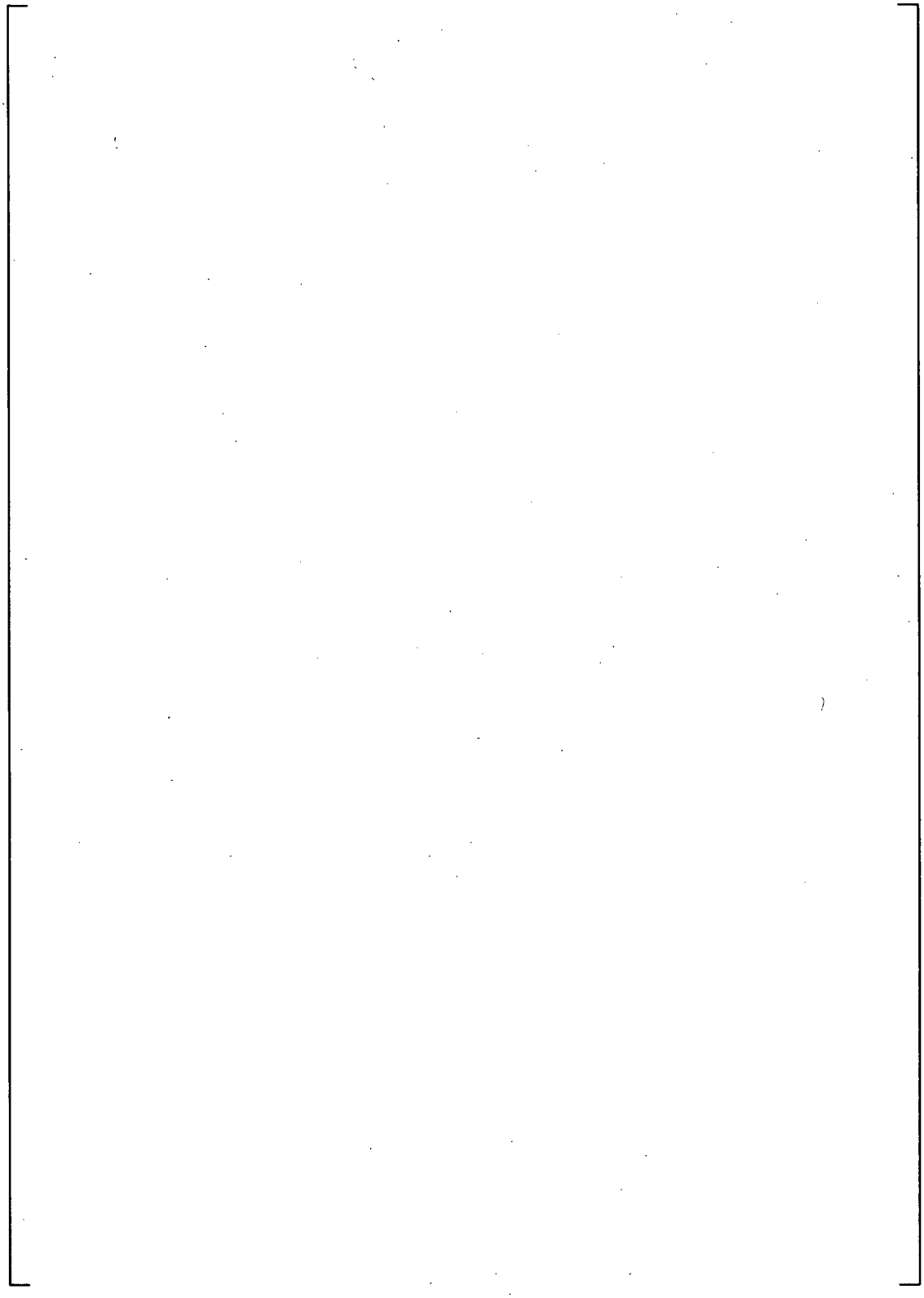

Figure 5-60: Run NRL06 Core Uncovery with High Boric Acid Concentration (Cycle 1)

c

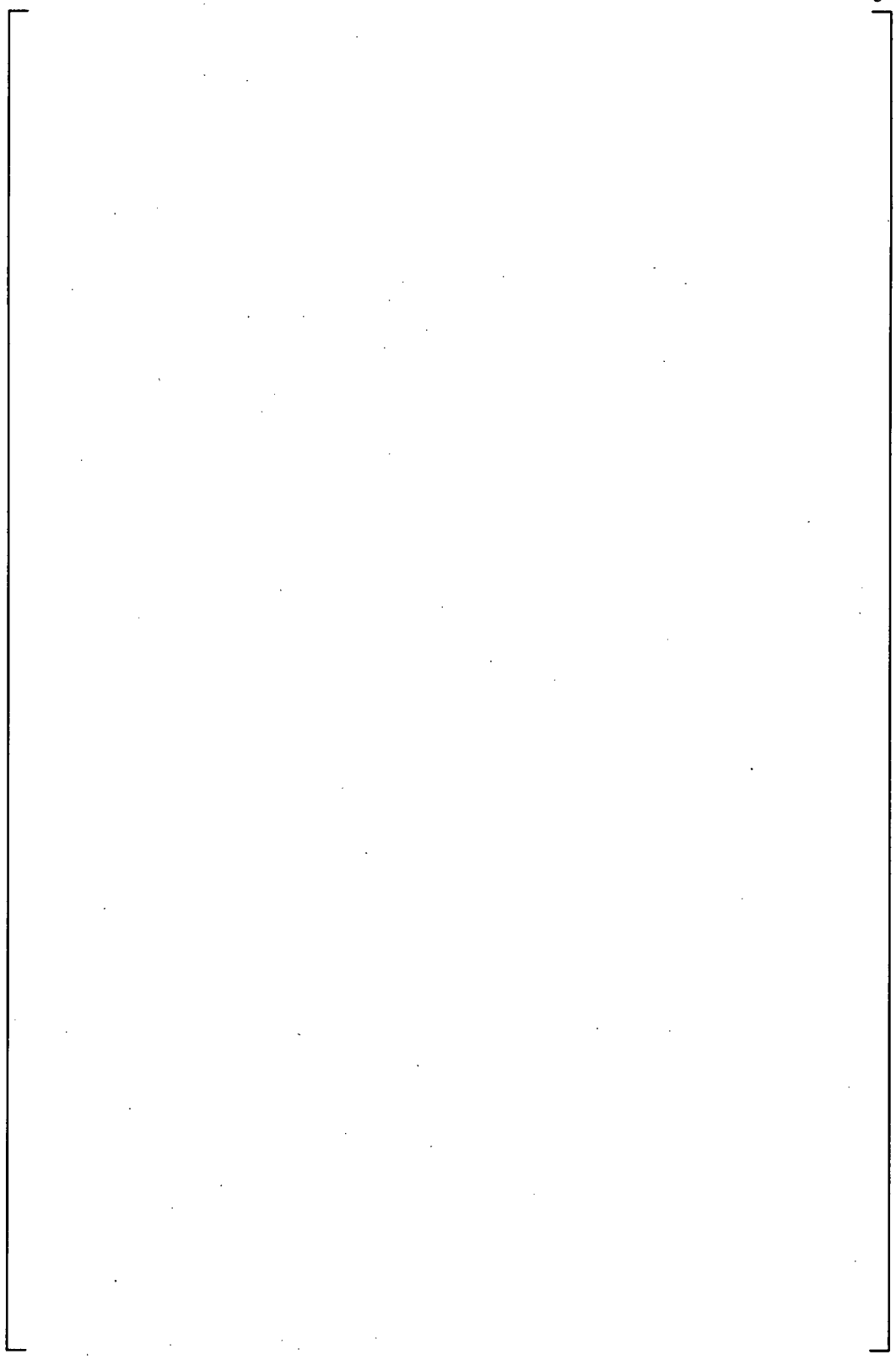

Figure 5-61: Run NRL06 Core Uncovery with High Boric Acid Concentration (Cycle 2)

c

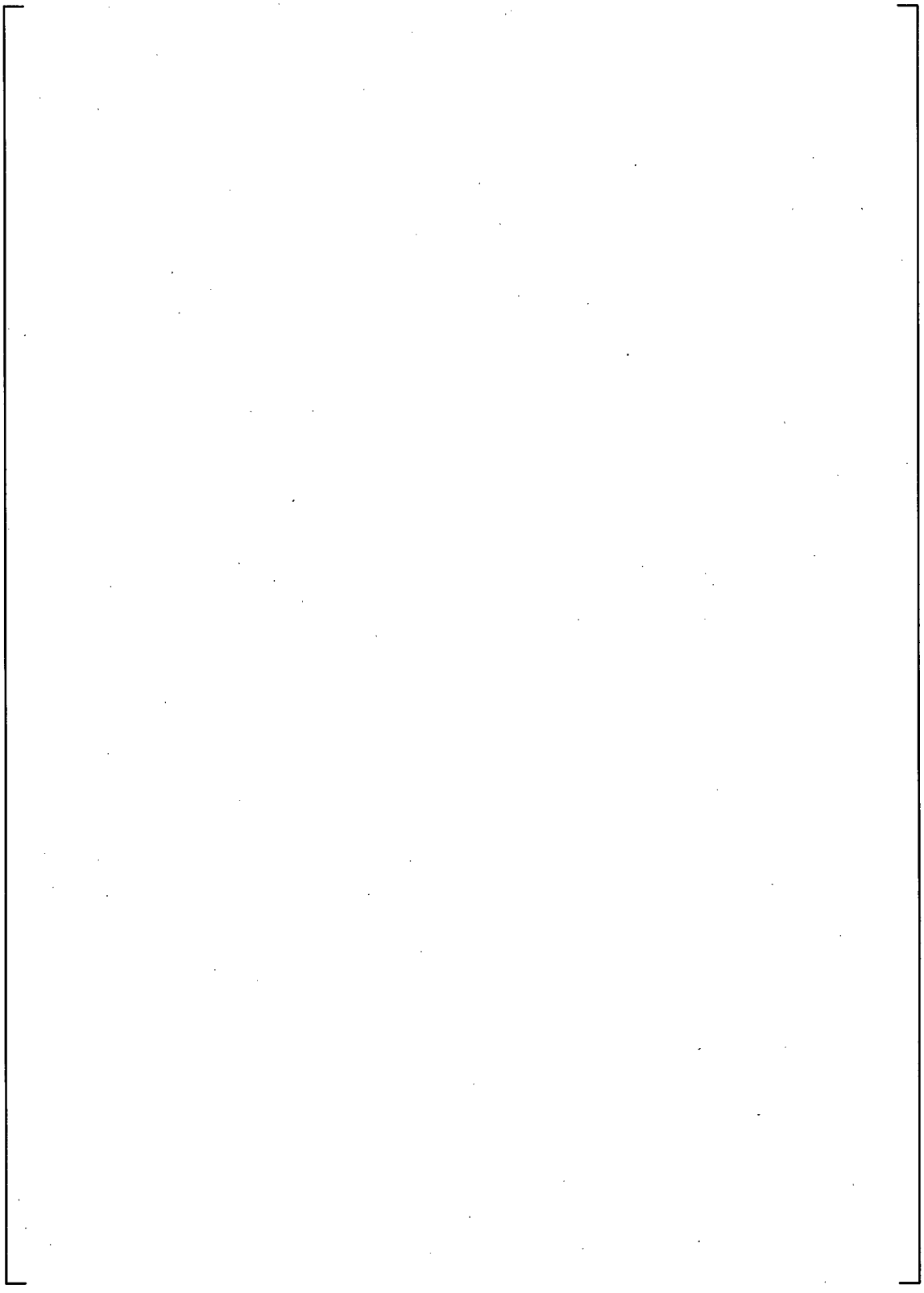

Figure 5-62: Run NRL06 Core Recovery with High Boric Acid Concentration (Cycle 1)

5.7 RUN NRL07

Run NRL07 is conducted using a buffered borated water solution with debris loading and coolant added to the top of the core rather than the downcomer side. The objective of this run is to collect data that can be compared to run NRL05 which was run with the same solution and debris loading but with the typical injection method through the downcomer. By comparing the results of these two runs, the effects of debris concentration within the core region can be studied since the coolant injection at the top of the core is expected to create a condition in which the debris concentration in the core is higher compared to runs in which coolant injection was to the downcomer.

The solution used in run NRL07 is buffered borated water with a boric acid concentration of [ ]^{c} which corresponds to a boron concentration of [ ]^{c} The buffering agent is sodium hydroxide (NaOH) with a concentration of [ ]^{c} which is equivalent to a sodium concentration of [

]^{c} The temperature of the solution in the sump tank is controlled at an average temperature of 149°F and the injection flow rate is set at 2000 ml/min. After a short preheating period, the power controller is set to follow the 10CFR50 Appendix K decay curve as discussed in Section 2.2. The total run time for this experiment is roughly 3 hours. Table 5-24 summarizes the test parameters used for run NRL07.

The power and injection flow were terminated during run NRL07 after roughly 1.75 hours due to a leak at the injection pump. The data acquisition system continued to record the cooldown following the termination of power and flow. During this time, it was observed that debris began to settle within the lower plenum. Since the test was terminated prematurely, no solution samples were collected during the run. Power and temperature measurements were collected and several high-speed videos for flow visualization were recorded early in the run.

Table 5-23: Run NRL07 Summary of Debris Loading Times c

Table 5-24: Run NRL07 Test Parameters c

[ ]

5.7.1 Power Measurement

The power transient for run NRL07 is shown in Figure 5-63. As the figure shows, the power is initially raised to a value of [ ]^{c} to preheat the bundle and allow the fluid in the bundle to reach saturation temperature. After 4 minutes of preheating, the power controller is set to follow the 10CFR50 Appendix K decay curve. The power is terminated roughly 1.75 hours into the run due to a leak in the injection system.

Figure 5-63: Run NRL07 Power Transient

5.7.2 Concentration Measurements

Since the test was terminated prematurely, concentration measurements were not collected during run NRL07.

5.7.3 Precipitation and Debris Observations

Since the test was terminated prematurely, precipitation was not observed during run NRL07.

[

]^{c}

c

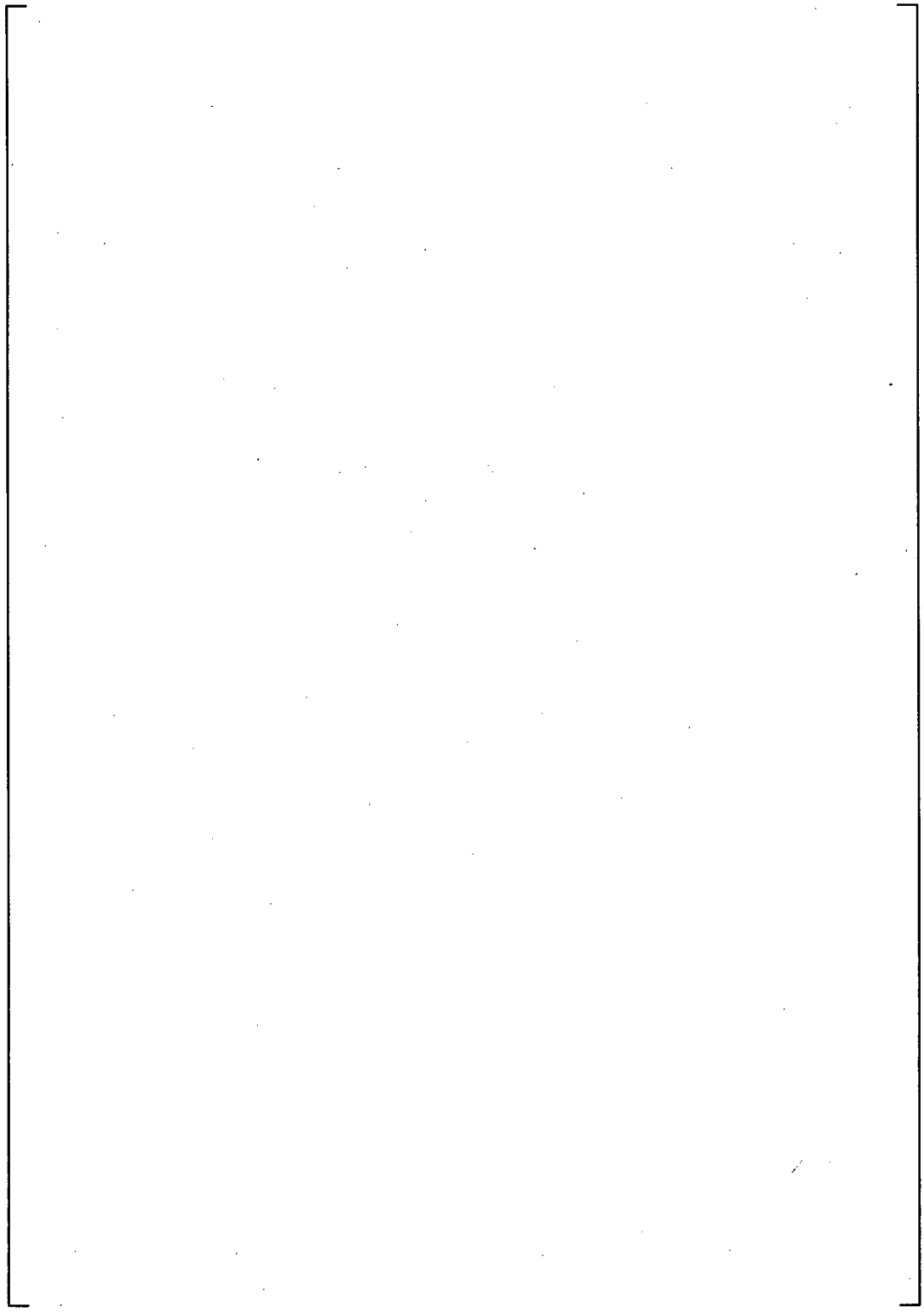

Figure 5-64: Run NRL07 Debris Accumulation in the Lower Plenum at Experiment Termination Following Debris Injection at the Top of the Core

5.7.4 Temperature Measurements

Fluid temperatures measured in the sump tank, downcomer, and lower plenum are shown in Figure 5-65. Based on this figure, the following observations can be made:

- [ ]^{c}
- [ ]^{c}
- [ ]^{c}
- [ ]^{c}
- [ ]^{c}
- [ ]^{c}

In Figure 5-66, the lower plenum fluid temperatures are compared to fluid temperatures measured in the heated section of the core. Based on this figure the following observations can be made:

- [ ]^{c}
- [ ]^{c}
- [ ]^{c}
- [ ]^{c}

The heater rod cladding temperatures measured during run NRL07 are shown in Figure 5-67. Based on this figure, the following observations can be made:

- [ ]^{c}

- [
  ]c

c

Figure 5-65: Run NRL07 Sump, Downcomer, and Lower Plenum Fluid Temperatures

c

Figure 5-66: Run NRL07 Lower Plenum and Core Fluid Temperatures

[ ]c

Figure 5-67: Run NRL07 Cladding Temperatures

5.7.5 Two-Phase Flow Visualizations

Three high-speed videos for flow visualization were collected during run NRL07. Table 5-25 lists the experimental time, bundle elevation, and bundle power at which these videos were recorded. These videos were collected after adding the [ ]c. After reviewing the videos, the following observations were made regarding the two-phase flow structure:

- [ ]c
- [ ]c
- [ ]c

Table 5-25: Run NRL07 Video Collected for Flow Visualization

Video Title	Collection Speed (fps)	Experimental Time (hr:min:sec)	Video Length (sec)	Bundle Elevation (in.)	Bundle Power (W)
NRL07-1	200	0:31:25	3.465	34.5	2610
NRL07-2	200	0:34:25	3.465	22	2557
NRL07-3	200	0:36:55	3.465	18	2509

c

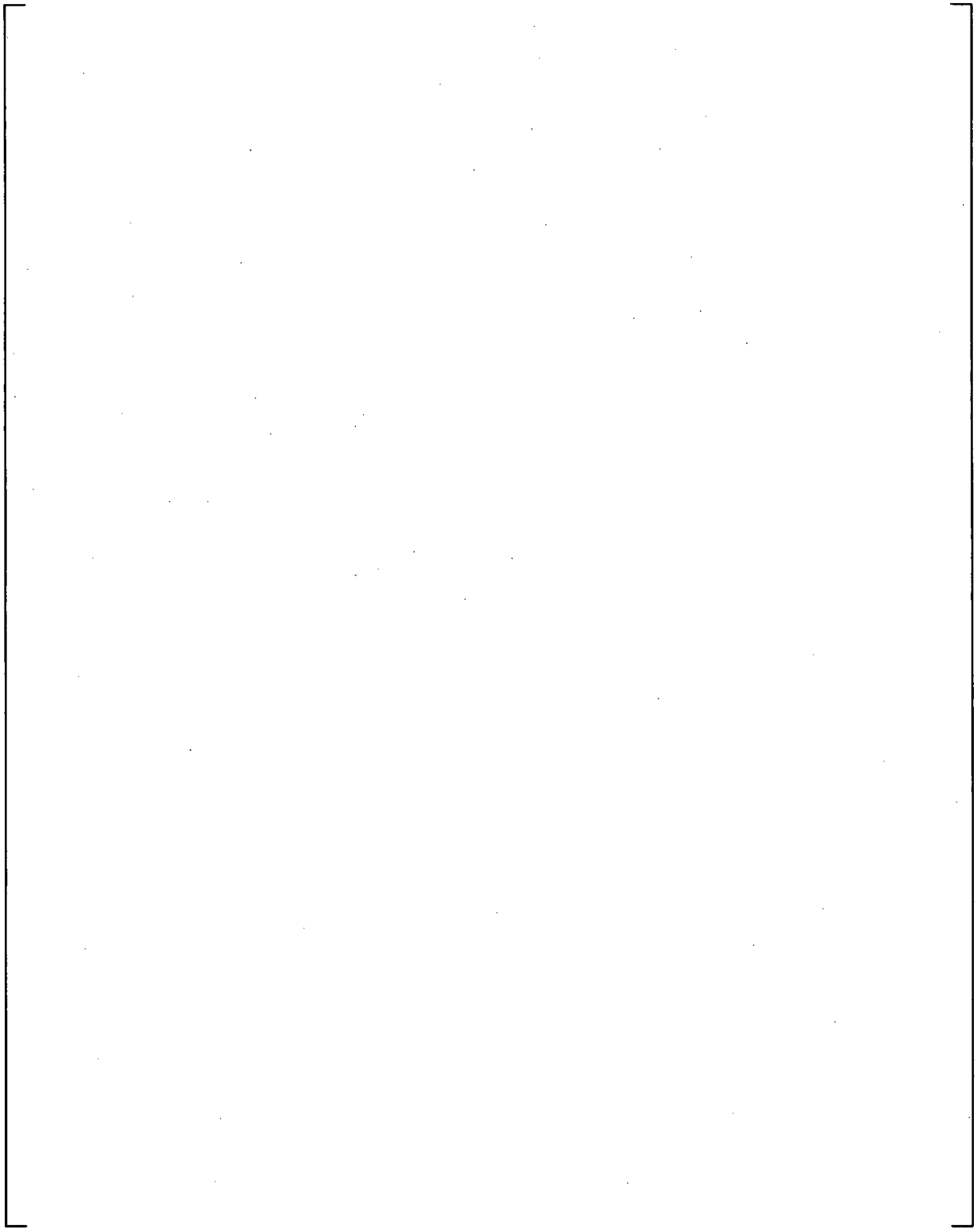

Figure 5-68: Run NRL07 Two-Phase Flow Regimes at Three Elevations and Powers Early in the Experiment

5.8 RUN NRL08

Run NRL08 is conducted using a buffered borated water solution with debris loading. [

]^{c} The purpose of this run is to collect data that can be compared to run NRL05 which was run with the same solution and debris loading but with the large lower plenum. [

]^{c}

The buffered solution used in run NRL08 has a boric acid concentration of [ ]^{c} which corresponds to a boron concentration of [ ]^{c} The buffering agent is sodium hydroxide (NaOH) and has a concentration of [ ]^{c} which corresponds to a sodium concentration of [

]^{c} The temperature of the solution in the sump tank is controlled at an average temperature of 152°F and the injection flow rate is set at 1600 ml/min. After a short preheating period, the power controller is set to follow the 10CFR50 Appendix K decay curve as discussed in Section 2.2. The total run time for this experiment is roughly 7 hours. Table 5-27 summarizes the test parameters used for run NRL08.

Solution samples drawn from the lower plenum and core region at the end of the run will be analyzed to determine the boric acid concentration. In addition, temperature measurements were recorded for the heater rod cladding and fluid within the sump, downcomer, lower plenum, and core regions. Still photographs were also taken to show the accumulation of debris and boric acid precipitate in the lower plenum and core region. Multiple high-speed videos were recorded to provide images for flow regime visualization and identification as well as precipitation and dissolution during the core uncovery and recovery phase.

Table 5-26: Run NRL08 Summary of Debris Loading Times c

Table 5-27: Run NRL08 Test Parameters c

5.8.1 Power Measurement

The power transient for run NRL08 is shown in Figure 5-69. As the figure shows, the power is initially raised to a value of [ ]^{c} to preheat the bundle and allow the fluid in the bundle to reach saturation temperature. After 10 minutes of preheating, the power controller is set to follow the 10CFR50 Appendix K decay curve. The power is terminated roughly 6.25 hours into the experiment.

[ ]c

Figure 5-69: Run NRL08 Power Transient

5.8.2 Concentration Measurements

[

]c

Table 5-28: Run NRL08 Concentration Measurements c

[ ]c

[

]c

[

]^{c}

5.8.3 Precipitation and Debris Observations

Precipitation was not observed anywhere in the vessel during normal operation of the test facility. This could indicate that boric acid buffered with NaOH has a higher solubility limit compared to unbuffered boric acid solutions. One uncovery and recovery cycle was performed during run NRL08 and precipitation was observed to occur on the heater rods and unheated vessel walls above the two-phase mixture level during core uncovery. The results of this uncovery and recovery cycle are presented in Section 5.8.6 and include images of the precipitation observed during core uncovery as well as images of the dissolution process during core recovery.

[

]^{c}

[

]c

Figure 5-70: Run NRL08 Debris Accumulation in the Lower Plenum, Downcomer, and Core Inlet Region after [ ]c

[c]

Figure 5-71: Run NRL08 Debris Accumulation on the Bottom of the Lower Plenum after the Experiment and Disassembly

[c]

Figure 5-72: Run NRL08 Debris Buildup on the Outer Edges of a Spacer Grid after the Experiment and Disassembly

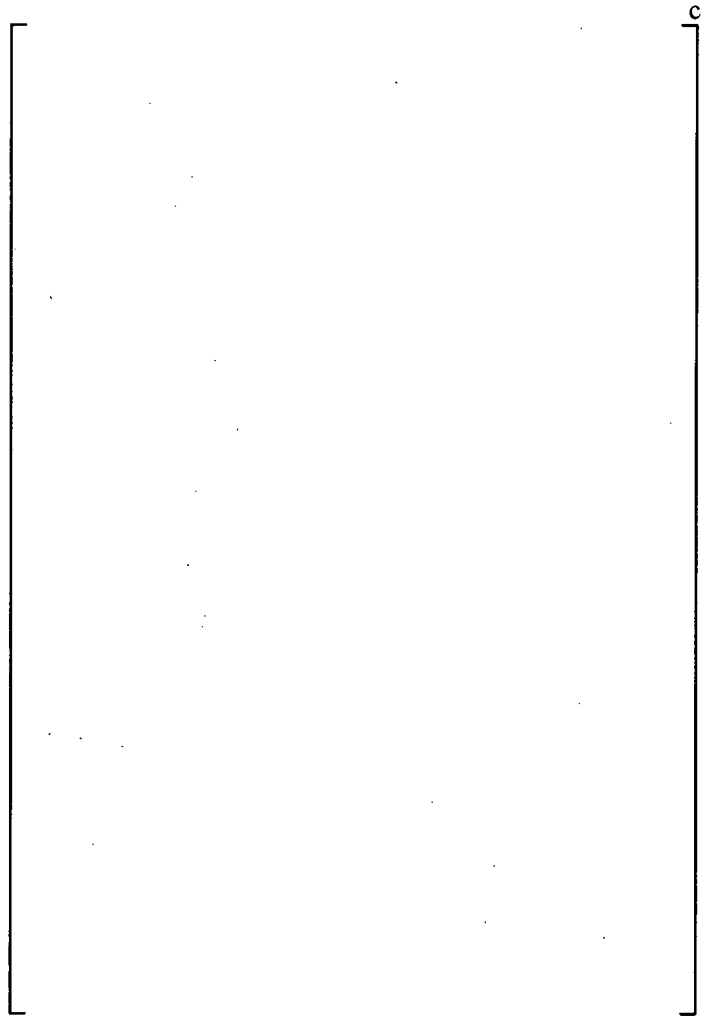

Figure 5-73: Run NRL08 Lower Plenum, Downcomer, and Core Inlet Region: (a) Initial Injection of [ ]^{c}, (b) [ ]^{c} into the Experiment

5.8.4 Temperature Measurements

Fluid temperatures measured in the sump tank, downcomer, and lower plenum are shown in Figure 5-74. Based on this figure, the following observations can be made:

- [ ]^{c}
- [ ]^{c}
- [ ]^{c}
- [ ]^{c}

[

]^{c}

In Figure 5-75, the lower plenum fluid temperatures are compared to fluid temperatures measured in the heated section of the core. Based on this figure the following observations can be made:

- [

  ]^{c}

- [

  ]^{c}

- [

  ]^{c}

- [

  ]^{c}

The heater rod cladding temperatures measured during run NRL08 are shown in Figure 5-76. Based on this figure, the following observations can be made:

- [

  ]^{c}

- [

  ]^{c}

Figure 5-74: Run NRL08 Sump, Downcomer, and Lower Plenum Fluid Temperatures

Figure 5-75: Run NRL08 Lower Plenum and Core Fluid Temperatures

Figure 5-76: Run NRL08 Cladding Temperatures

5.8.5 Two-Phase Flow Visualizations

Several high-speed videos for flow visualization were collected during run NRL08. Table 5-29 lists the experimental time, bundle elevation, and bundle power at which these videos were recorded. After reviewing the videos, the following observations were made regarding the two-phase flow structure:

- [

  ]^{c}

- [

  ]^{c}

- [

  ]^{c}

Table 5-29: Run NRL08 Video Collected for Flow Visualization

Video Title	Collection Speed (fps)	Experimental Time (hr:min:sec)	Video Length (sec)	Bundle Elevation (in.)	Bundle Power (W)
NRL08_01	200	0:46:35	3.465	13	2501
NRL08_02	200	0:48:05	3.465	18	2470
NRL08_03	200	0:49:35	3.465	22	2457
NRL08_04	200	0:51:05	3.465	32	2429
NRL08_05	200	0:52:35	3.465	34.5	2402
NRL08_07	200	2:00:05	6.760	13	1879
NRL08_08	200	2:01:35	4.935	18	1871
NRL08_09	200	2:03:05	4.935	20.5	1866
NRL08_10	200	2:04:35	4.935	22	1859
NRL08_11	200	2:06:05	4.935	32	1851
NRL08_12	200	2:07:35	4.935	34.5	1848

c

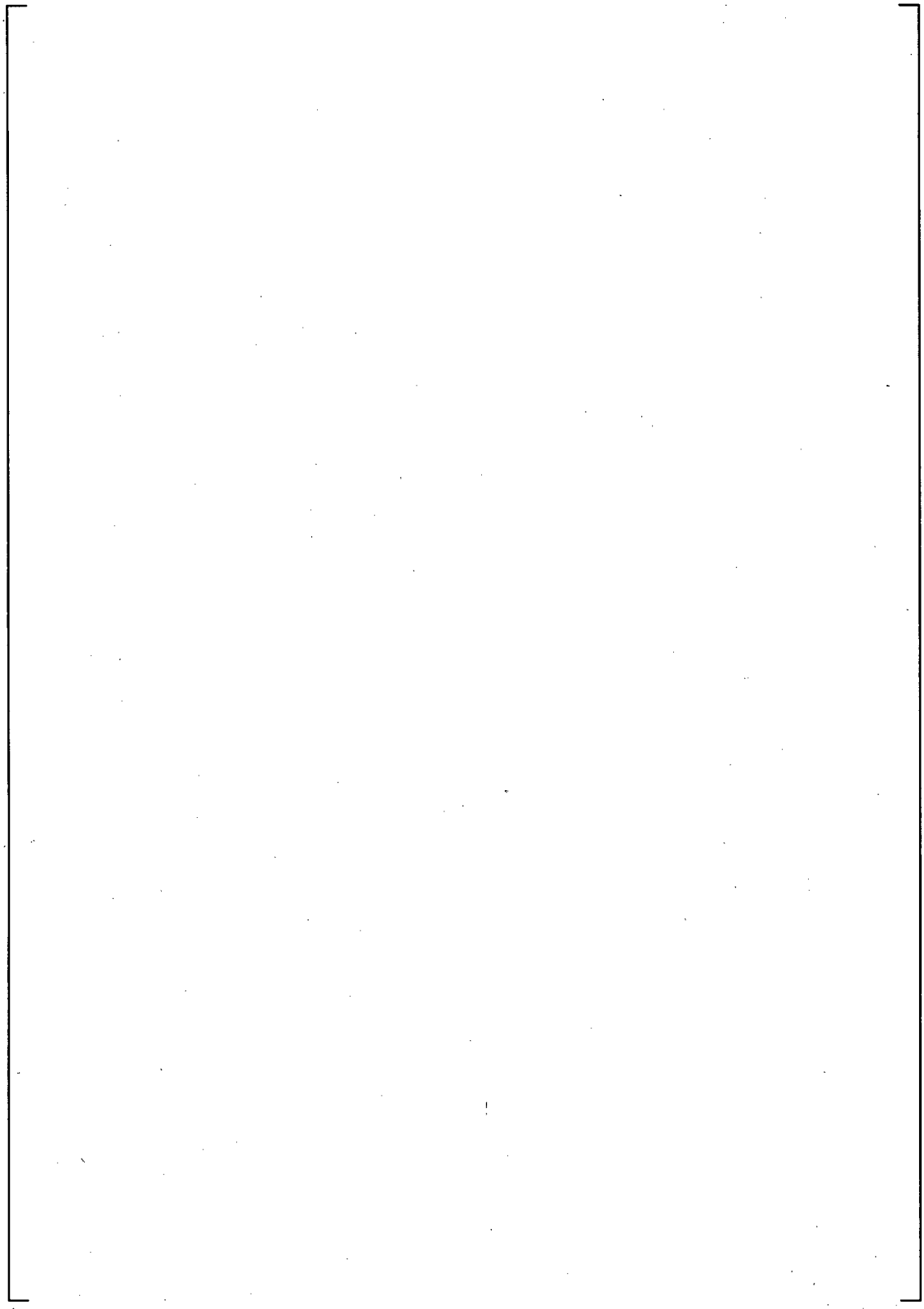

Figure 5-77: Run NRL08 Two-Phase Flow Regimes at Three Elevations and Powers Early in the Experiment

c

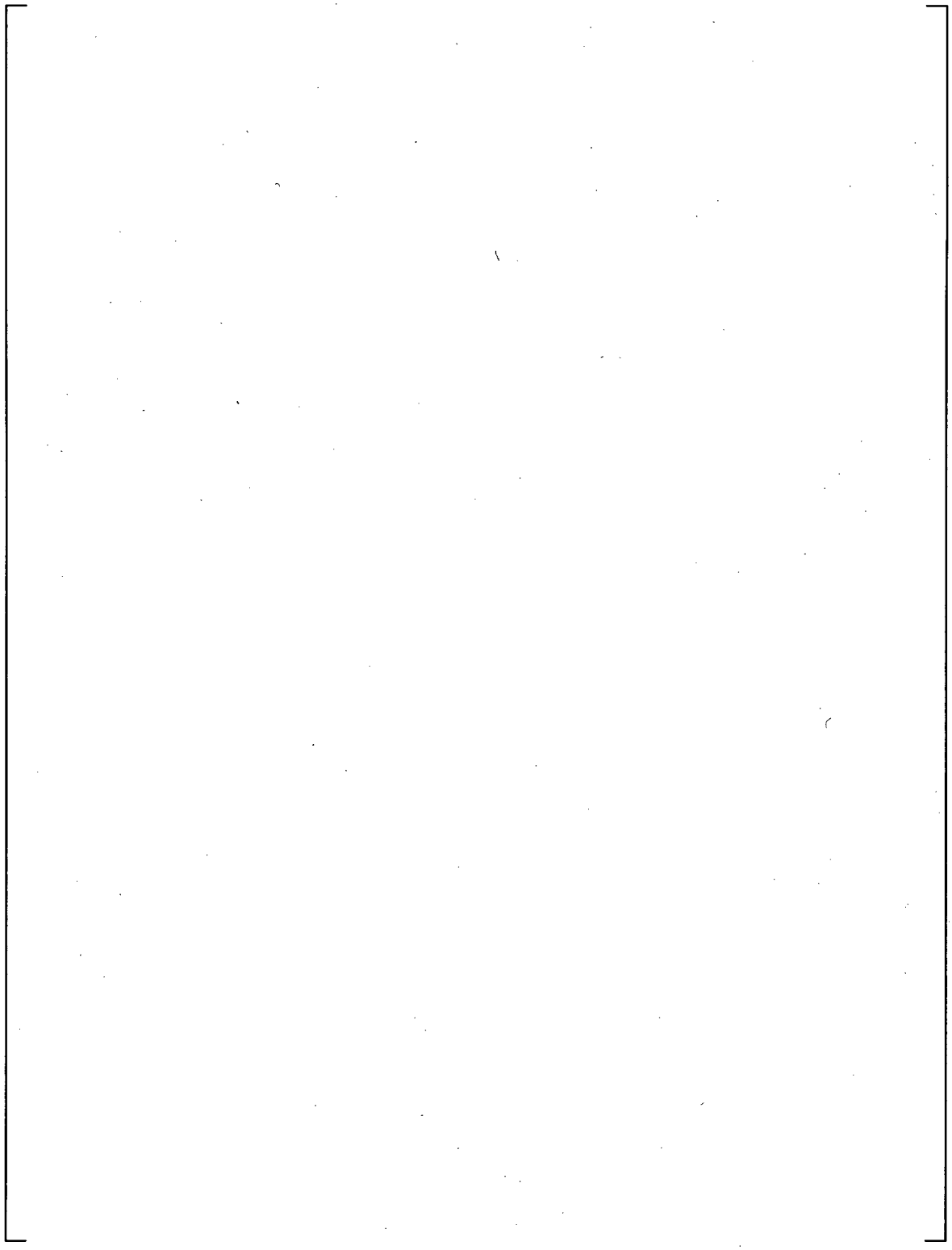

Figure 5-78: Run NRL08 Two-Phase Flow Regimes at Three Elevations and Powers Later in the Experiment

c

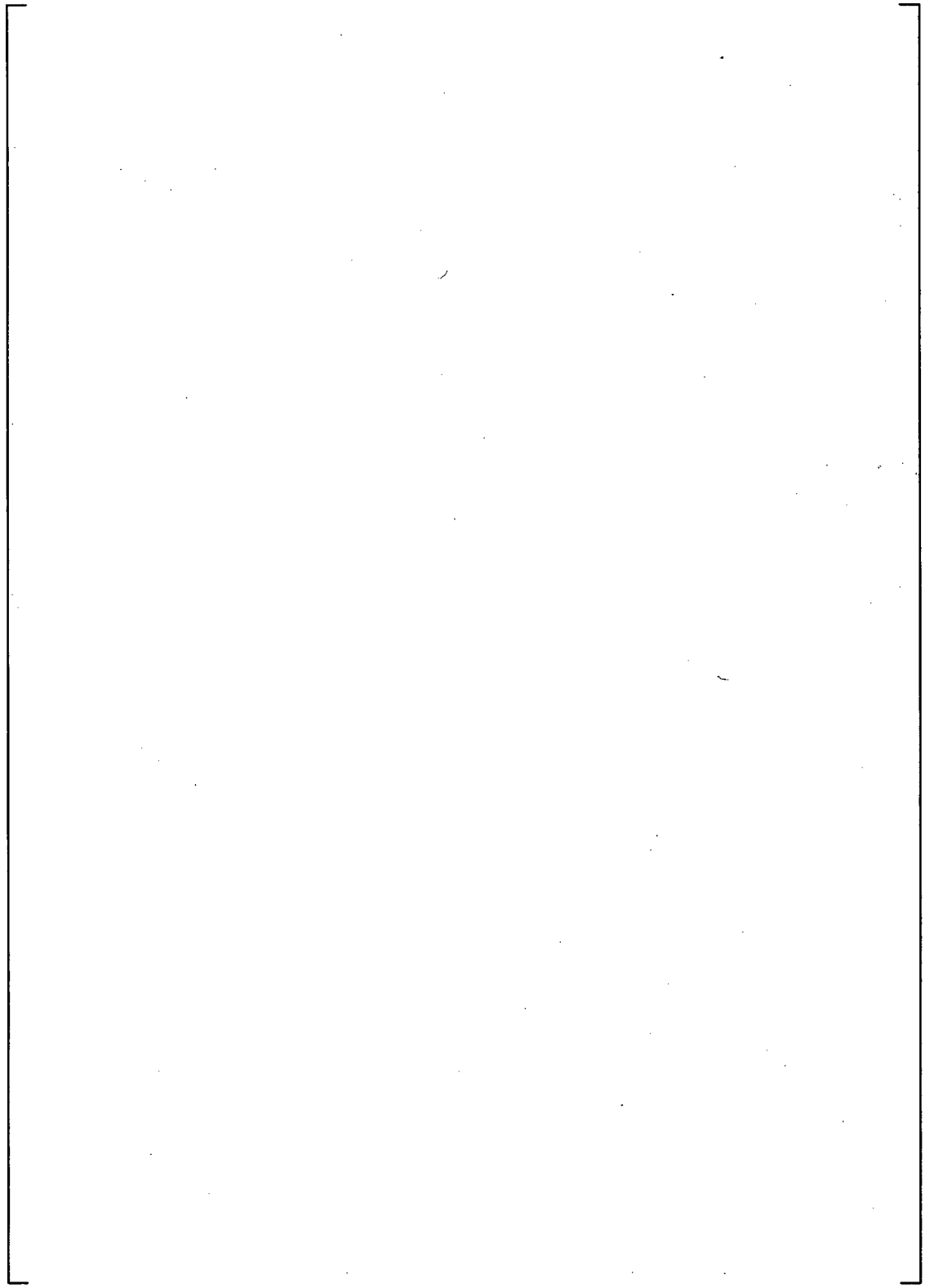

Figure 5-79: Run NRL08 Formation of a Small Vapor Slug by the Coalescence of Several Distorted Bubbles at a Power of 1848W

5.8.6 Core Uncovery and Recovery

One core uncovery and recovery cycle was performed at the end of run NRL08. [

]^{c}

Table 5-30: Run NRL08 Cladding Temperatures, Turnaround and Recovery Times during Uncovery and Recovery Cycle

[ ]^{c}

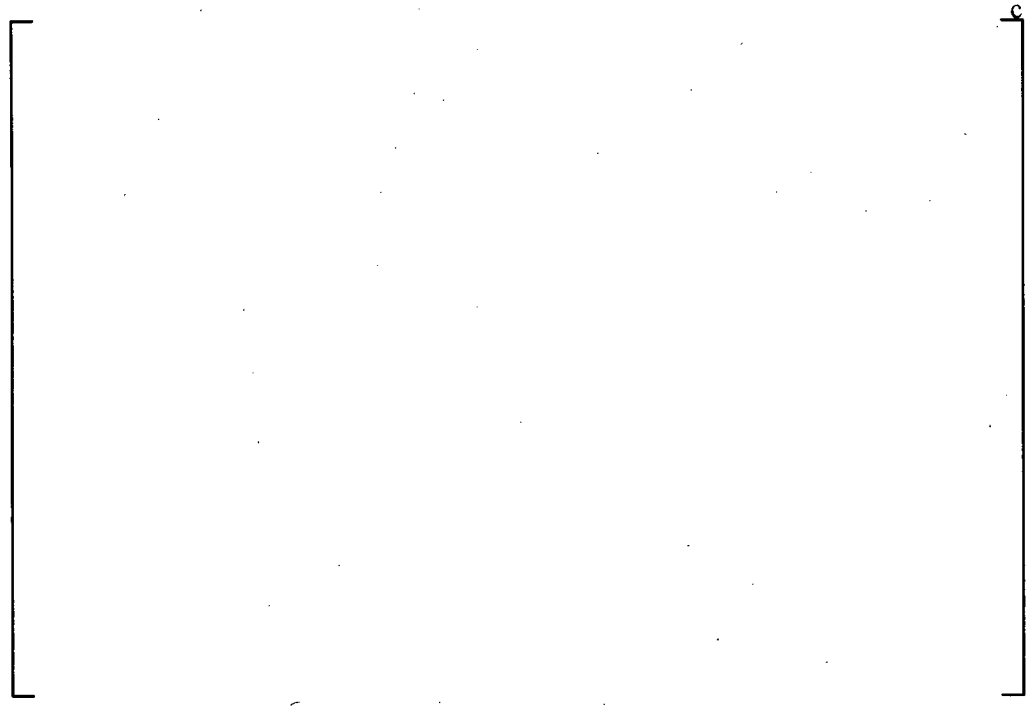

Figure 5-80: Run NRL08 Cladding Temperature Measured at the Top of the Bundle during the Uncovery and Recovery Cycle

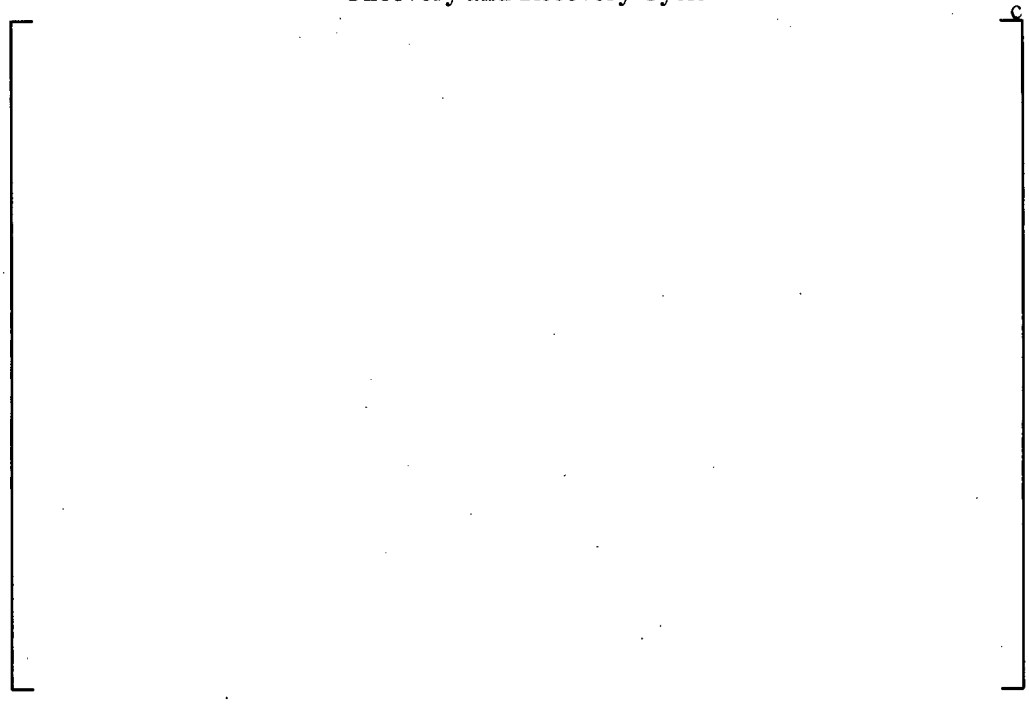

Figure 5-81: Run NRL08 Fluid Temperature Measured at the Top of the Bundle during the Uncovery and Recovery Cycle

During the uncovery and recovery cycle a series of high-speed videos were recorded. Table 5-31 lists the video titles and identifies the collection speed and experimental times that the videos were collected for the cycle. Cycle time in the table refers to the time referenced from the beginning of core uncovery. Video collection begins prior to core uncovery, as indicated by a negative time.

[

]^{c}

Table 5-31: Run NRL08 Video Collected during Uncovery and Recovery Cycle

Cycle 1: Average Power = 1406W				
Video Title	**Collection Speed (fps)**	**Experimental Time (hr:min:sec)**	**Cycle Time (sec)**	**Bundle Elevation (in.)**
NRL08_16	10	6:03:15 – 6:04:30	(-60) – 20	34.5
NRL08_17	200	6:04:55 – 6:05:00	40 – 45	34.5
NRL08_18	200	6:07:25 – 6:07:30	190 – 195	32.5
NRL08_19	200	6:10:05 – 6:10:10	350 – 355	34.5
NRL08_20	200	6:12:45 – 6:12:50	510 – 515	34.5
NRL08_21	200	6:15:25 – 6:15:30	670 – 675	34.5
NRL08_22	10	6:17:45 – 6:19:25	810 – 910	34.5

c

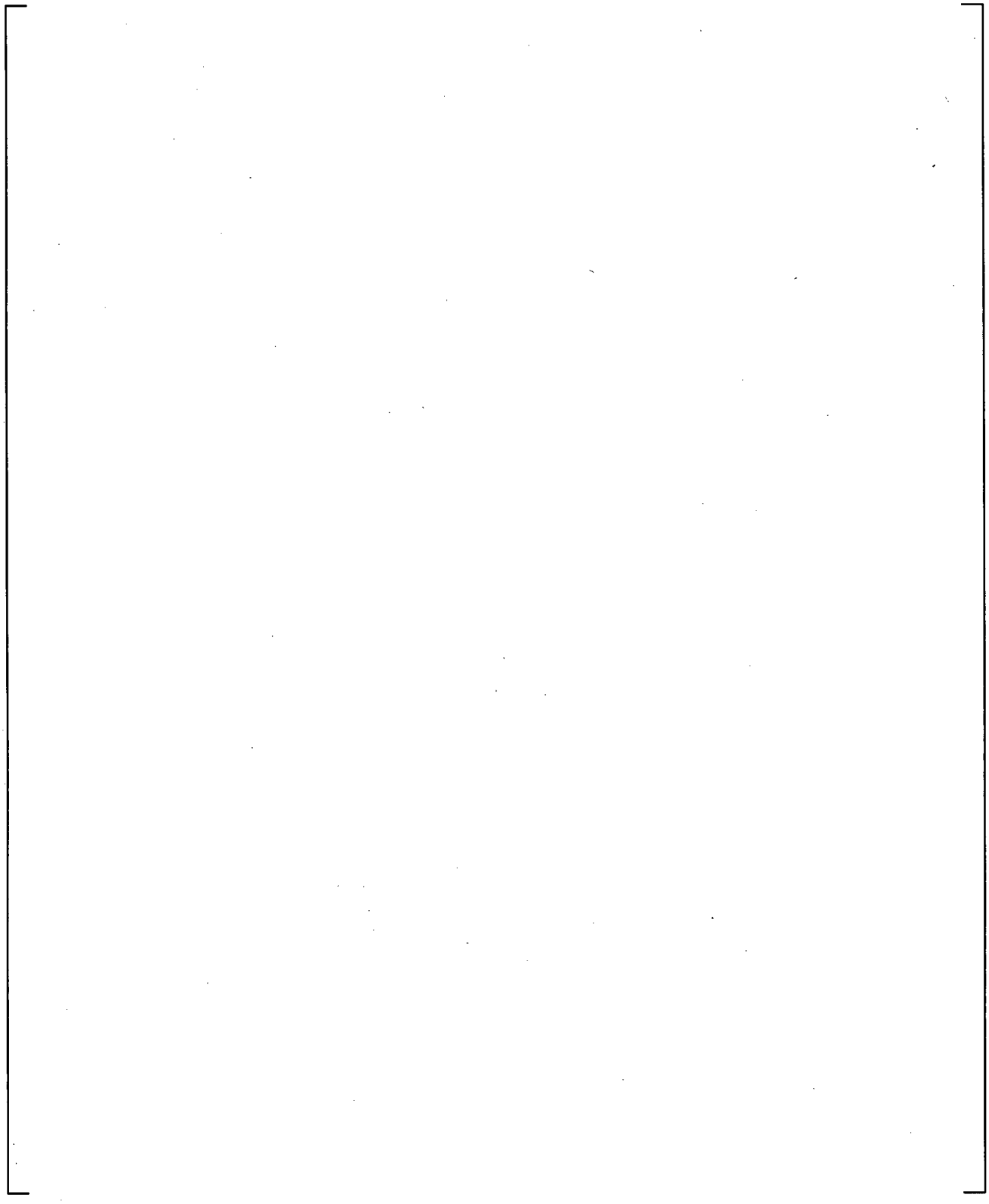

Figure 5-82: Run NRL08 Core Uncovery with High Boric Acid Concentration

c

Figure 5-83: Run NRL08 Top of the Heated Length Roughly [ ]^{c} Minutes after Core Recovery Indicating that all Precipitate Formed during Core Uncovery has Dissolved Back into Solution

5.9 RUN NRL09

Run NRL09 is conducted using the same solution as run NRL06 but does not have a debris loading. By comparing the results from these two tests, the effects of debris on the boiling characteristics and boron precipitation can be investigated. In addition, several core uncovery and recovery cycles are performed to study boron precipitation and dissolution under varying heat fluxes and boron concentrations. The effect of boron concentration on mixture level is also investigated during run NRL09 by comparing the mixture level at the beginning of the test (low boron concentration) to the mixture level near the end of the test (high boron concentration). This comparison can be made at the same power level since data was collected at the beginning of the experiment at low power before the decay heat curve simulation began.

The solution used in run NRL09 is buffered borated water with a boric acid concentration of [ ]^{c} which corresponds to a boron concentration of [ ]^{c} The buffering agent is trisodium phosphate (TSP) with a concentration [ ]^{c} which corresponds to a sodium concentration of [ ]^{c} The temperature of the solution in the sump tank is controlled at a temperature of 152°F and the injection flow rate is set at 1600 ml/min. At the beginning of this test the power level is held constant at several low power levels before being increased and following the 10CFR50 Appendix K decay curve as discussed in Section 2.2.

The total test time is approximately 7.5 hours with the decay heat curve simulation beginning about 40 minutes into the experiment. [ ]^{c} is also added approximately 7 hours into the experiment just prior to the last core uncovery and recovery cycle. A summary of the test parameters used for run NRL09 is listed in Table 5-32.

Table 5-32: Run NRL09 Test Parameters c

5.9.1 Power Measurement

The power transient for run NRL09 is shown in Figure 5-84. As the figure shows, the power is initially raised to a value of [ ]^{c} to preheat the bundle and allow the fluid in the bundle to reach saturation temperature. It is then reduced to a value of approximately 1400W to perform the first uncovery and recovery cycle. After completing the recovery phase, about 40 minutes into the test, the power is again increased to [ ]^{c} and the power controller is set to simulate the 10CFR50 Appendix K decay heat curve for the remainder of the experiment. The power level is adjusted and held constant at the beginning of the experiment so that data collected during this time period, when the boron concentration is low, can be compared to data collected later on in the experiment when the power has decayed to a comparable value and the boron concentration is higher.

Figure 5-84: Run NRL09 Power Transient

5.9.2 Concentration Measurements

Five samples from run NRL09 were analyzed. [

]^{c}

[

]^{c}

Table 5-33: Run NRL09 Concentration Measurements c

[

[

]^{c}

5.9.3 Precipitation and Debris Observations

Precipitation was only observed to occur during run NRL09 when the core uncovery and recovery cycles were performed. The crystalline precipitate was observed when the two-phase mixture level in the core was lowered below the heated length. The precipitate formed just above the mixture level on both the flow housing and heater rod surfaces. When the mixture level was returned to its original location, the precipitate readily dissolved back into the solution. Images collected during the core uncovery and recovery cycles showing the formation and dissolution of the precipitate can be found in Section 5.9.6.

Run NRL09 was conducted without any debris loading, therefore, no observations regarding debris can be made.

5.9.4 Temperature Measurements

Fluid temperatures measured in the sump tank, downcomer, and lower plenum are shown in Figure 5-85. Based on this figure the following observations can be made:

- [
  ]^{c}
- [
  ]^{c}
- [
  ]^{c}
- [
  ]^{c}

Fluid temperatures measured in the lower plenum and core region are shown in Figure 5-86. Based on this figure the following observations can be made:

- [
  ]^{c}
- [
  ]^{c}
- [
  ]^{c}
- [
  ]^{c}

The cladding temperatures measured during run NRL09 are shown in Figure 5-87. Based on this figure the following observations can be made:

- [
  ]^{c}
- [
  ]^{c}

[ ]c

- [ ]c

- [ ]c

[c

]c

Figure 5-85: Run NRL09 Sump, Downcomer, and Lower Plenum Fluid Temperatures

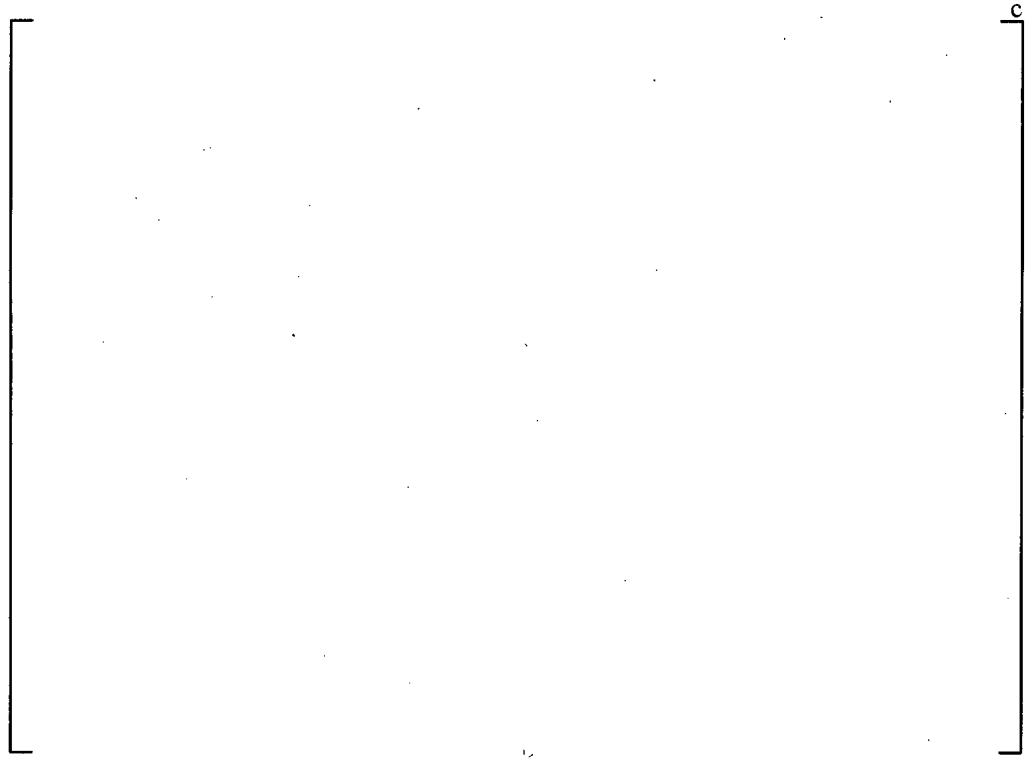

Figure 5-86: Run NRL09 Lower Plenum and Core Fluid Temperatures

Figure 5-87: Run NRL09 Cladding Temperatures

5.9.5 Two-Phase Flow Visualizations

Two-phase flow visualizations were recorded during run NRL09 using the high-speed video camera. [

]^{c} Table 5-34 summarizes the conditions in which the high-speed videos were collected including the experimental times, bundle location and power. Overall, the two-phase flow visualization videos show that the [

]^{c}

Table 5-34: Run NRL09 Video Collected for Flow Visualization (Images Presented)

Video Title	Collection Speed (fps)	Experimental Time (hr:min:sec)	Video Length (sec)	Bundle Elevation (in.)	Bundle Power (W)
NRL09_09	200	4:05:11	5.43	34	1616
NRL09_10_02	200	4:07:11	5.43	32	1612
NRL09_11_02	200	4:10:11	5.43	22	1607
NRL09_13_02	200	4:14:51	5.43	18	1599
NRL09_14_02	200	4:20:41	5.43	13	1587

[

]^{c}

[

]^{c}

Table 5-35: Run NRL09 Additional Video Collected for Flow Visualization (No Images Presented)

Video Title	Collection Speed (fps)	Experimental Time (hr:min:sec)	Video Length (sec)	Bundle Elevation (in.)	Bundle Power (W)
NRL09_15	200	5:51:51	5.43	13	1464
NRL09_16	200	5:52:51	5.43	18	1463
NRL09_18	200	5:56:01	5.43	22	1459
NRL09_19	200	5:59:21	5.43	32	1456
NRL09_20	200	6:01:41	5.43	34	1452

c

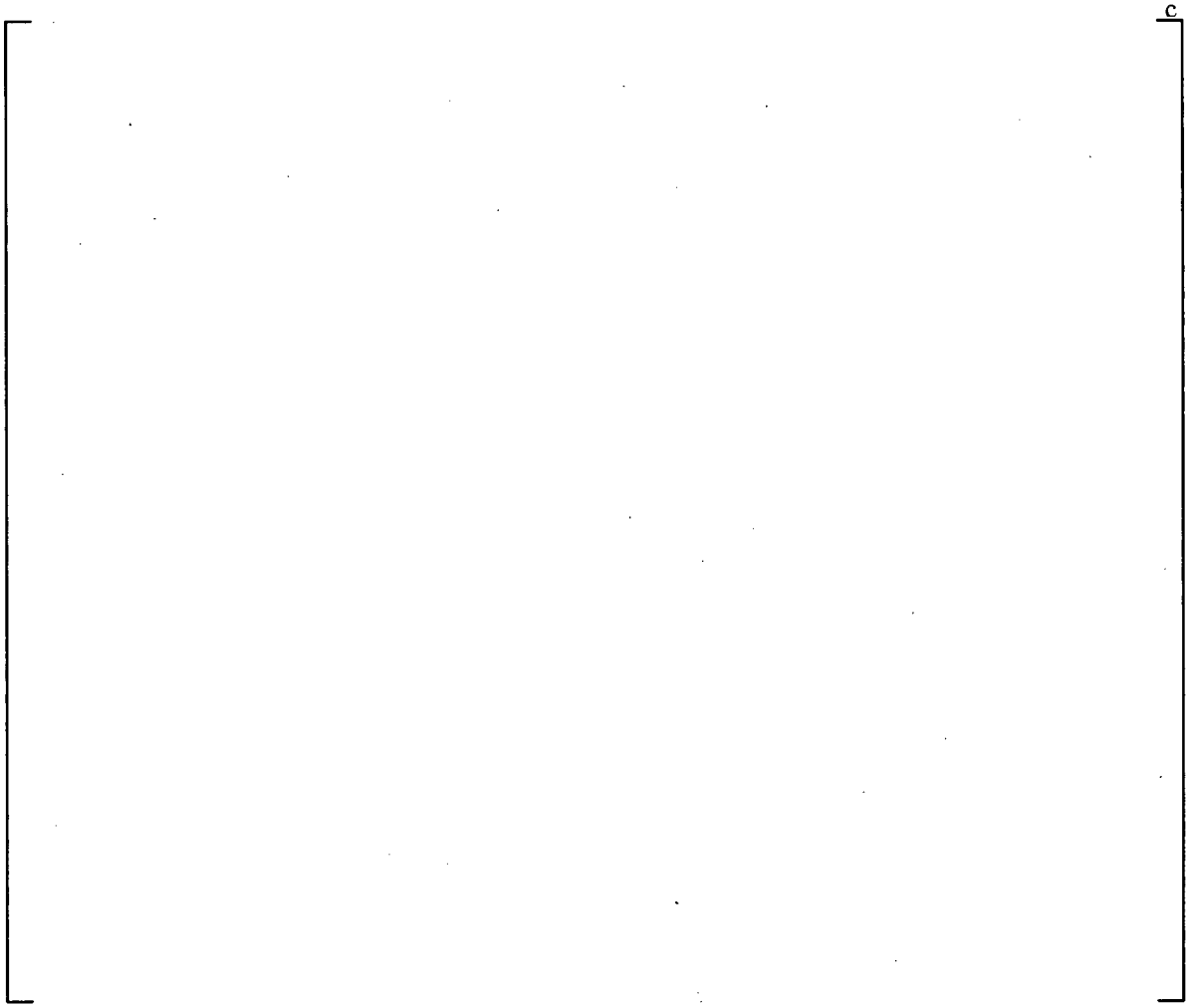

Figure 5-88: Run NRL09 Flow Visualization of Lower Plenum and Flow Stratification in the Bottom of Downcomer

Figure 5-89: Run NRL09 Flow Visualization of a Vapor Slug at 34 Inch Elevation

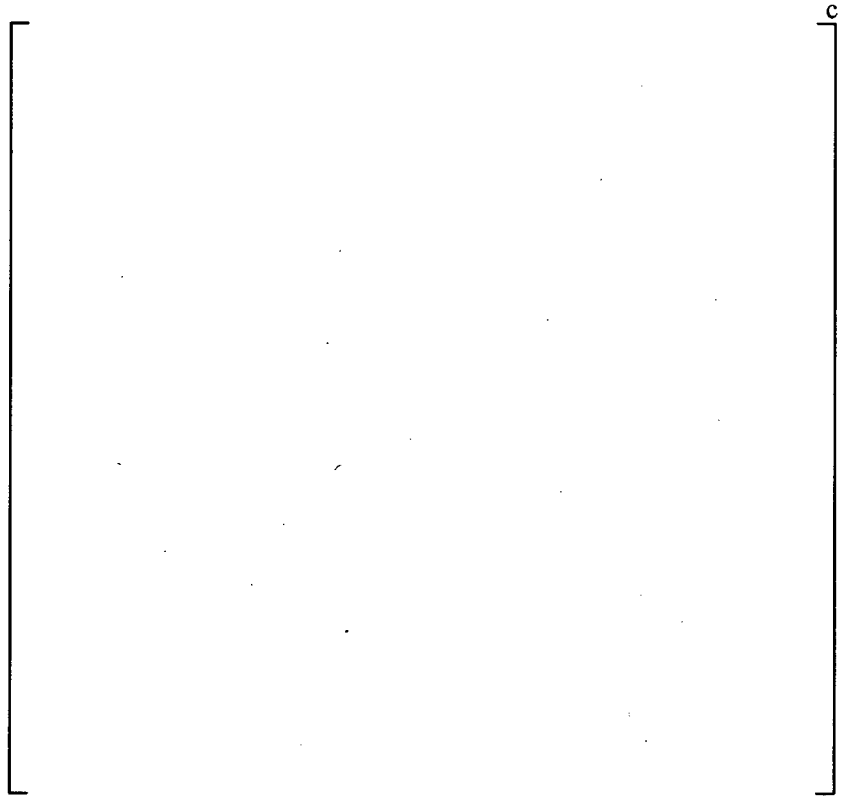

Figure 5-90: Run NRL09 Flow Visualization of Dispersed Bubbly Flow at 34 Inch Elevation

[c]

Figure 5-91: Run NRL09 Flow Visualization of a Vapor Slug at 32 Inch Elevation

[c]

Figure 5-92: Run NRL09 Flow Visualization of Dispersed Bubbly Flow at 32 Inch Elevation

[c]

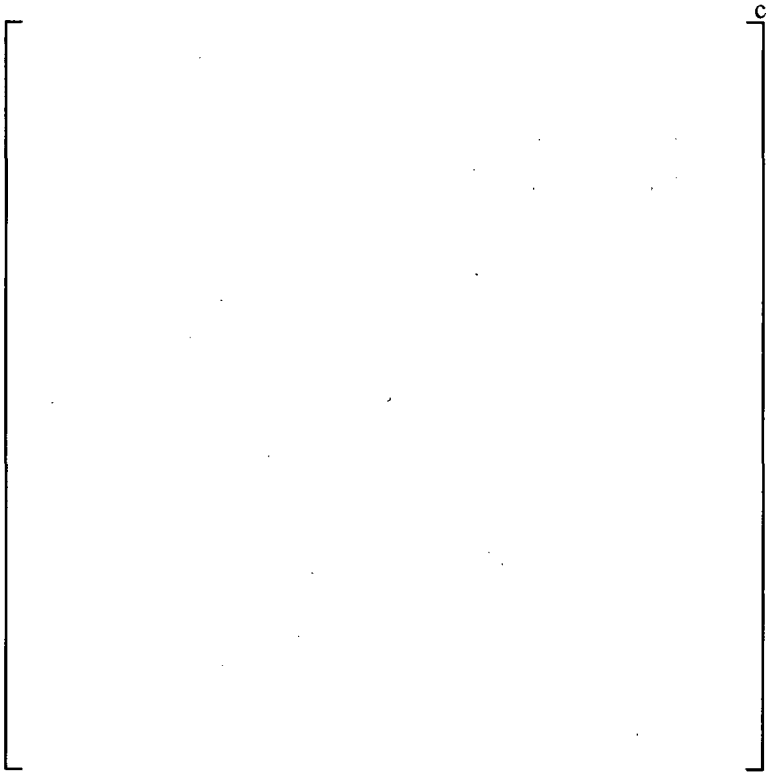

Figure 5-93: Run NRL09 Flow Visualization of Bubbly Flow (Large Bubble Generation) at 22 Inch Elevation

[c]

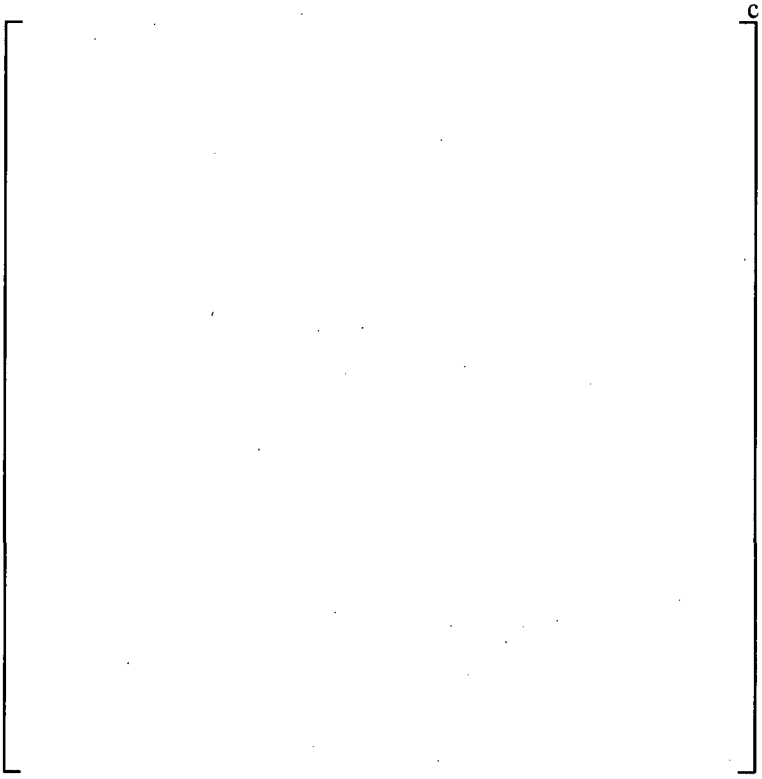

Figure 5-94: Run NRL09 Flow Visualization of Dispersed Bubbly Flow (after Large Bubble Breakup) at 22 Inch Elevation

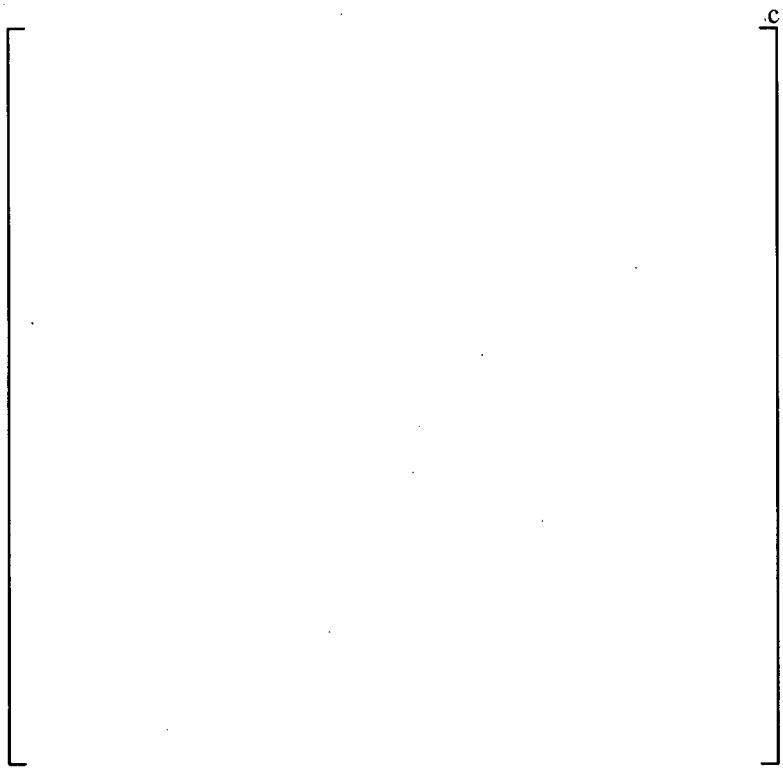

Figure 5-95: Run NRL09 Flow Visualization of Bubbly Flow (Large Distorted Bubble) at 18 Inch Elevation

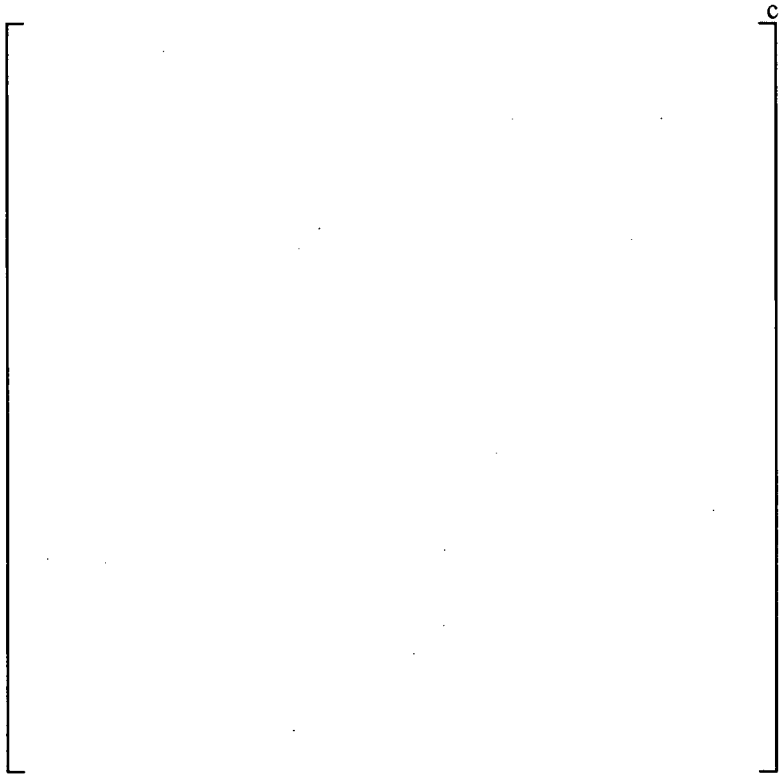

Figure 5-96: Run NRL09 Flow Visualization of Dispersed Bubbly Flow at 18 Inch Elevation

[

]^{c}

c

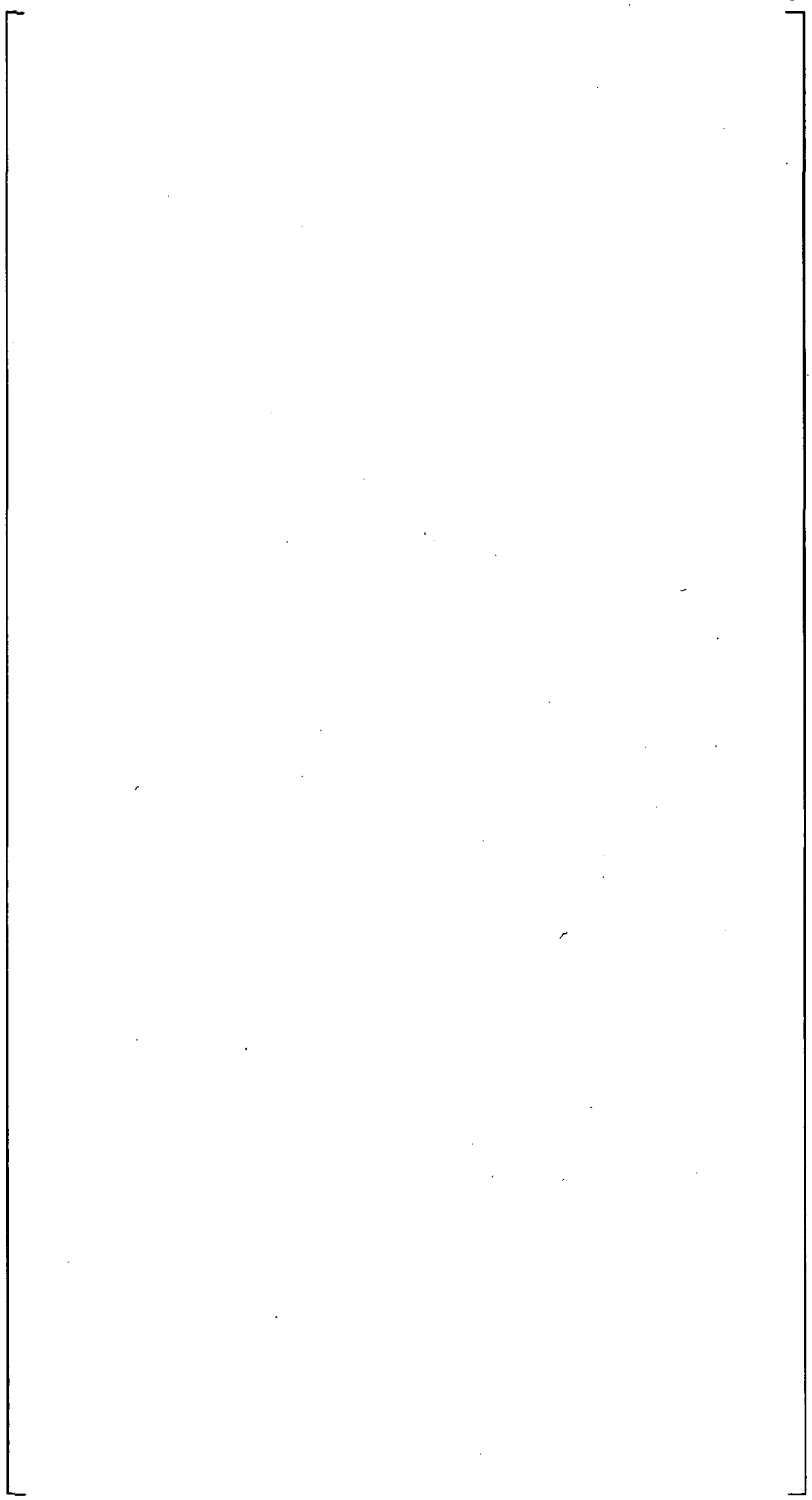

Figure 5-97: Run NRL09 Estimated Rise Velocity of a Small Spherical Bubble

5.9.6 Core Uncovery and Recovery Tests

Four core uncovery and recovery cycles are performed in Run NRL09. [

]^{c}

Table 5-36: Run NRL09 Cladding Temperatures, Turnaround and Recovery Times during Uncovery and Recovery Cycles

c

[ ]

c

[ ]

Figure 5-98: Run NRL09 Cladding Temperature Measured at the Top of the Bundle during the Four Uncovery and Recovery Cycles

Figure 5-99: Run NRL09 Core Fluid Temperature Measured at the Top of the Bundle during the Four Uncovery and Recovery Cycles

During the uncovery and recovery cycles a series of high-speed and real-time videos were recorded. Table 5-37 lists the video titles and identifies the collection speed and experimental times that the videos were collected for each cycle. Cycle time in the table refers to the time referenced from the beginning of core uncovery. For all cycles, video collection begins prior to core uncovery, as indicated by a negative time.

[

]^{c}

[

]c

Table 5-37: Run NRL09 Video Collected during Uncovery and Recovery Cycles				
Cycle 1: Average Power = 1378W				
Video Title	**Collection Speed (fps)**	**Experimental Time (hr:min:sec)**	**Cycle Time (sec)**	**Bundle Elevation**
NRL09_05	60	0:29:41 – 0:30:41	(-20) – 40	34 in.
NRL09_06	30	0:31:01 – 0:32:21	60 – 140	34 in.
NRL09_07	30	0:33:01 – 0:35:01	180 – 300	34 in.
M2U00552 (Sony)	Real Time	0:35:21 – 0:36:21	320 – 380	Entire Bundle
NRL09_08	30	0:37:21 – 0:39:11	440 – 550	34 in.
Cycle 2: Average Power = 1444W				
Video Title	**Collection Speed (fps)**	**Experimental Time (hr:min:sec)**	**Cycle Time (sec)**	**Bundle Elevation**
NRL09_21	30	6:04:01 – 6:06:01	(-50) – 70	34 in.
M2U00555 (Sony)	Real Time	6:04:41 – 6:10:25	(-10) – 334	Top of Bundle
NRL09_22	30	6:06:21 – 6:08:11	90 – 200	34 in.
NRL09_23	30	6:08:31 – 6:10:21	220 – 330	34 in.
NRL09_24	30	6:11:21 – 6:13:11	390 – 500	34 in.
Cycle 3: Average Power = 1433W				
Video Title	**Collection Speed (fps)**	**Experimental Time (hr:min:sec)**	**Cycle Time (sec)**	**Bundle Elevation**
NRL09_25	30	6:15:41 – 6:17:31	(-10) – 100	34 in.
NRL09_26	30	6:18:11 – 6:20:11	140 – 250	34 in.
NRL09_27	30	6:20:31 – 6:21:46	280 – 345	34 in.
Cycle 4: Average Power = 1385W				
Video Title	**Collection Speed (fps)**	**Experimental Time (hr:min:sec)**	**Cycle Time (sec)**	**Bundle Elevation**
NRL09_28	30	7:10:31 – 7:12:31	(-10) – 110	34 in.
NRL09_29	30	7:13:01 – 7:15:01	140 – 260	34 in.
NRL09_30	30	7:15:31 – 7:17:31	290 – 410	34 in.

c

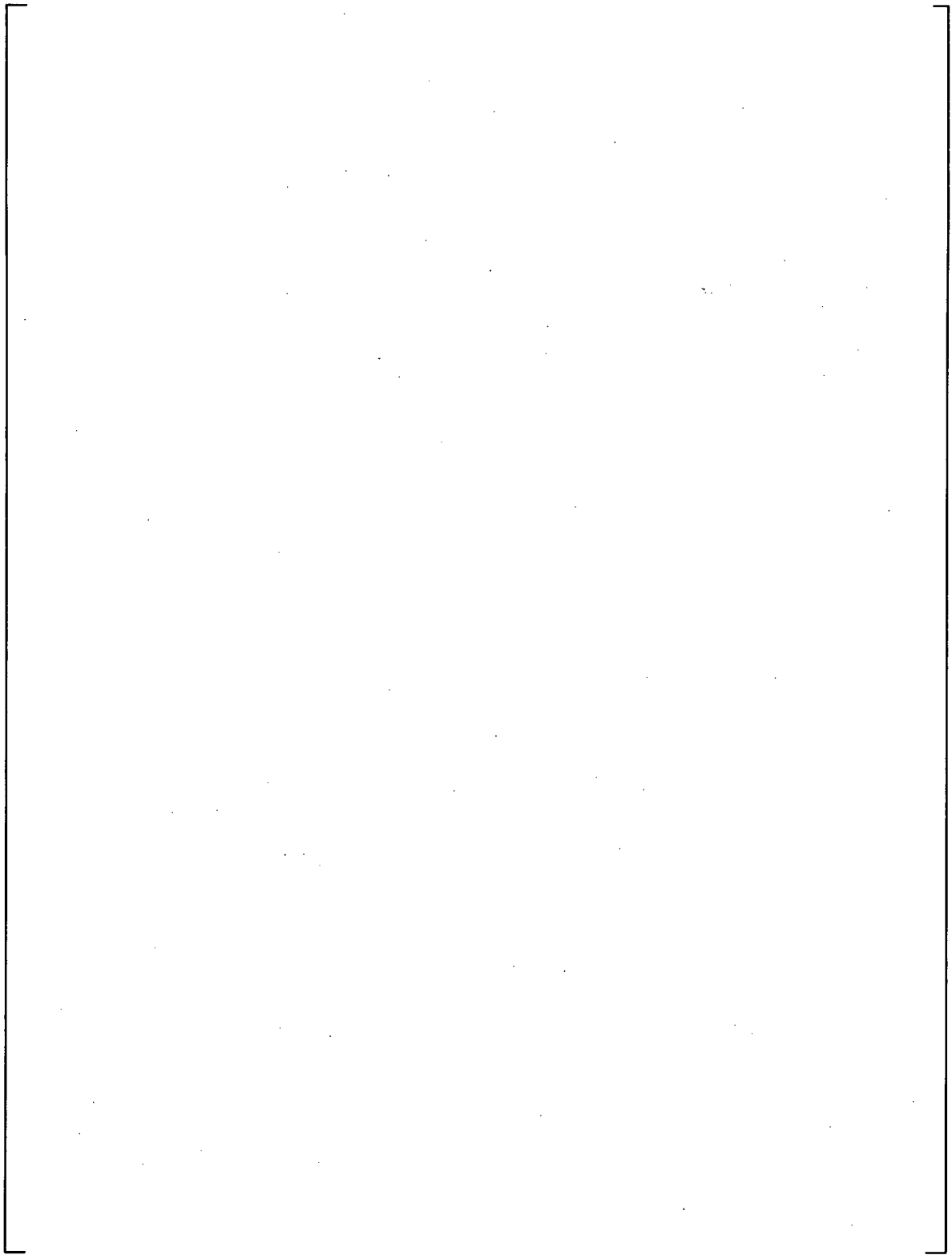

Figure 5-100: Run NRL09 Two-Phase Mixture Level during Core Uncovery

c

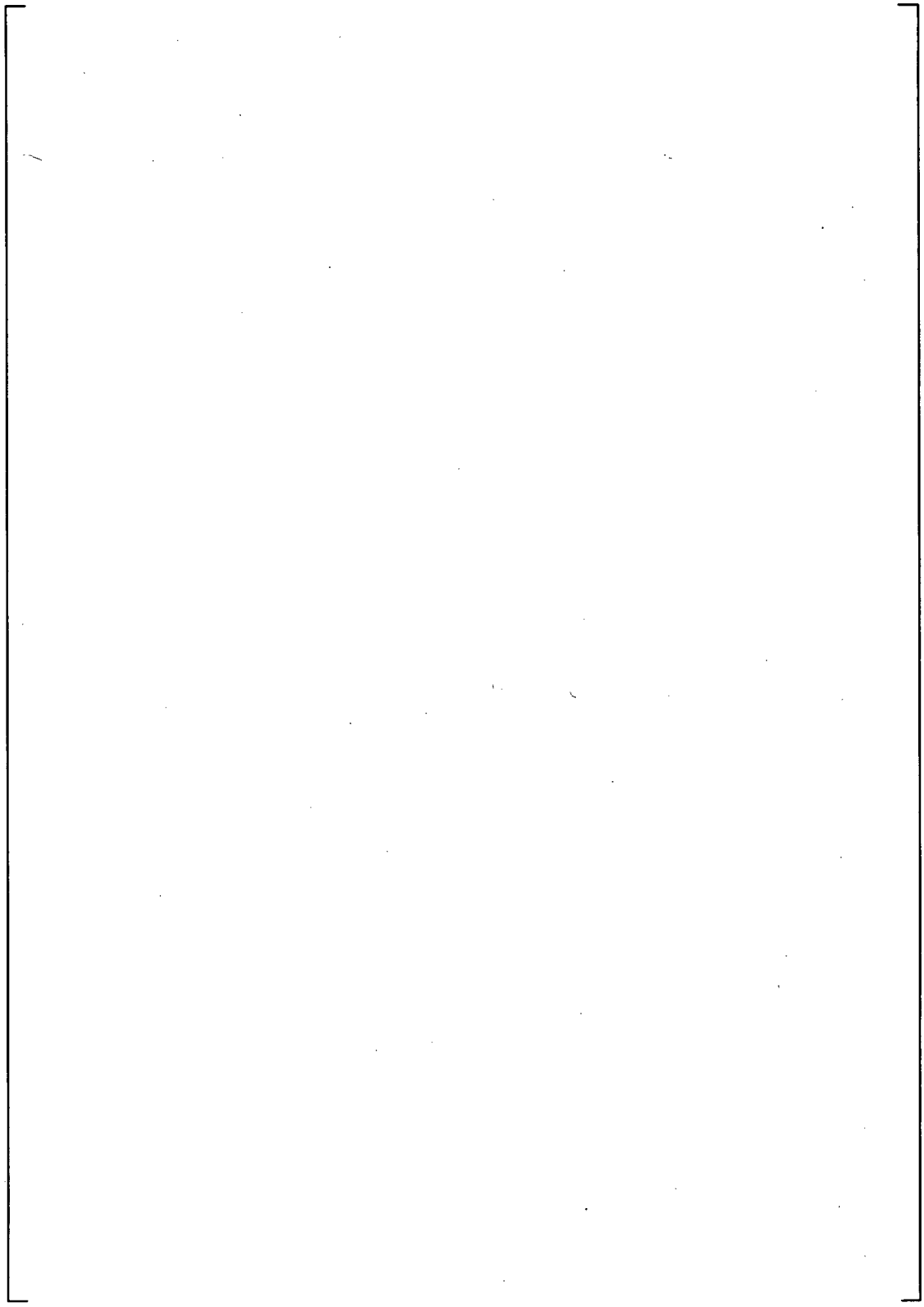

Figure 5-101: Run NRL09 Core Uncovery with Low Boric Acid Concentration (Cycle 1)

c

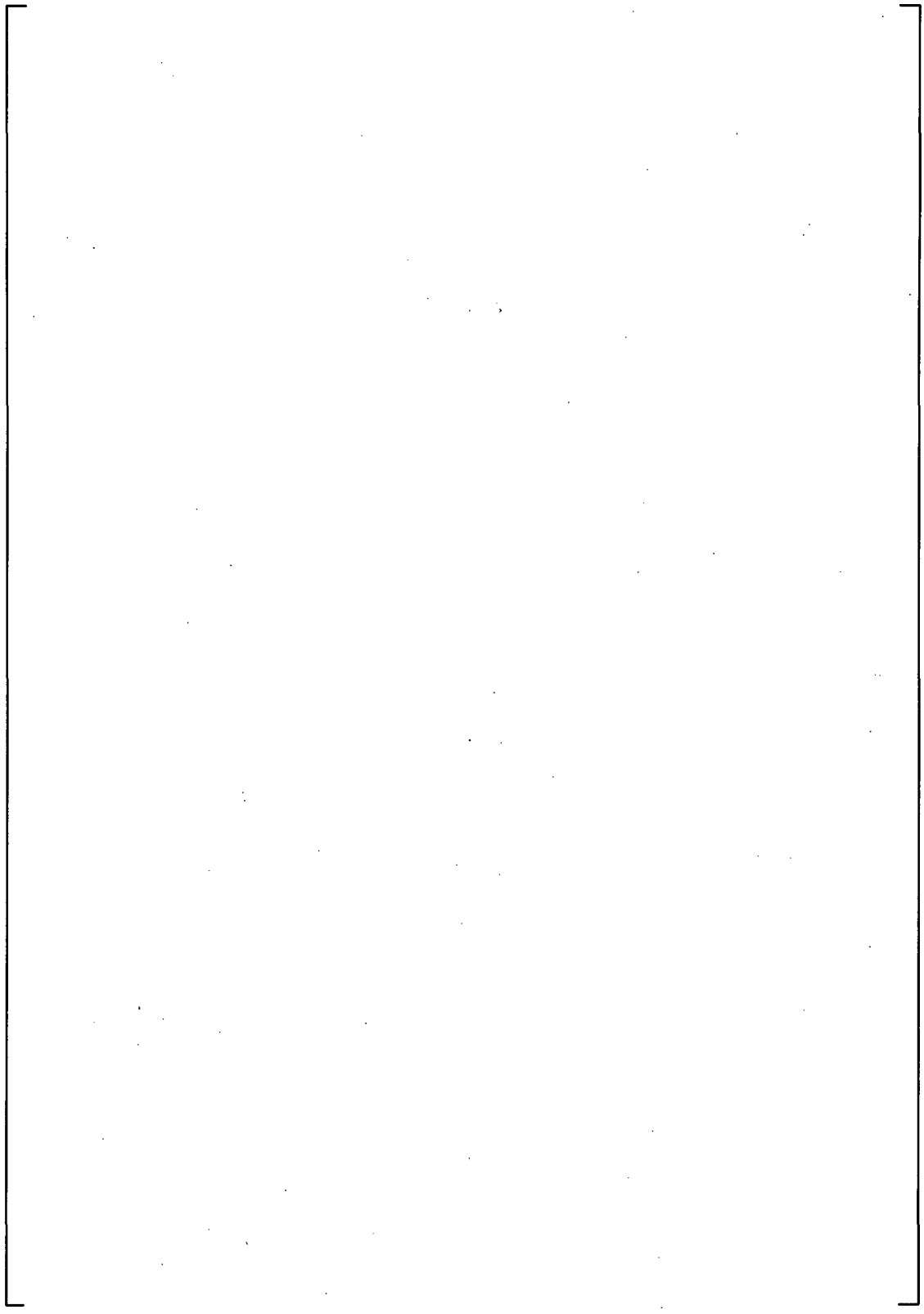

Figure 5-102: Run NRL09 Core Uncovery with High Boric Acid Concentration (Cycle 2)

c

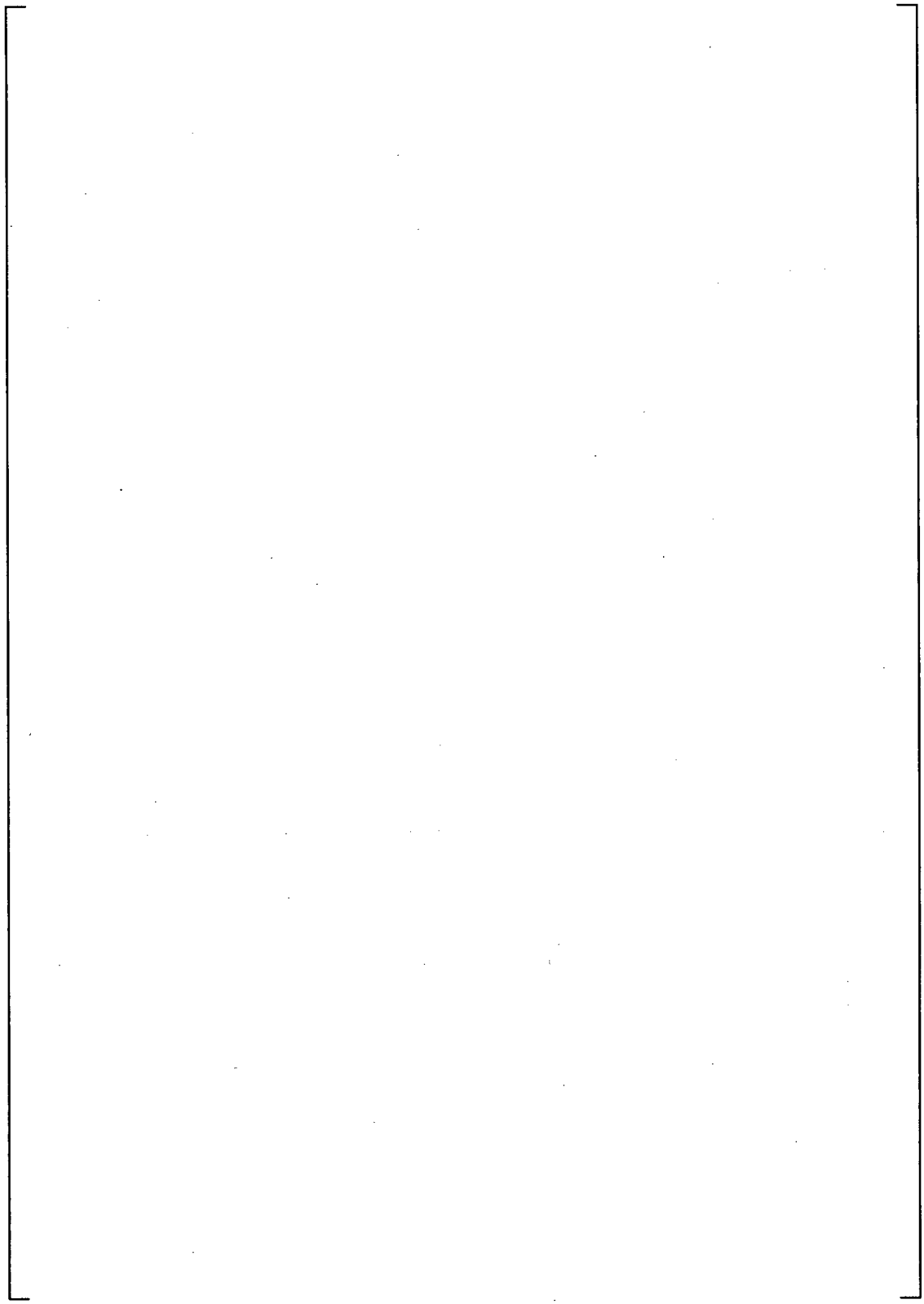

Figure 5-103: Run NRL09 Core Uncovery with High Boric Acid Concentration (Cycle 3)

[c

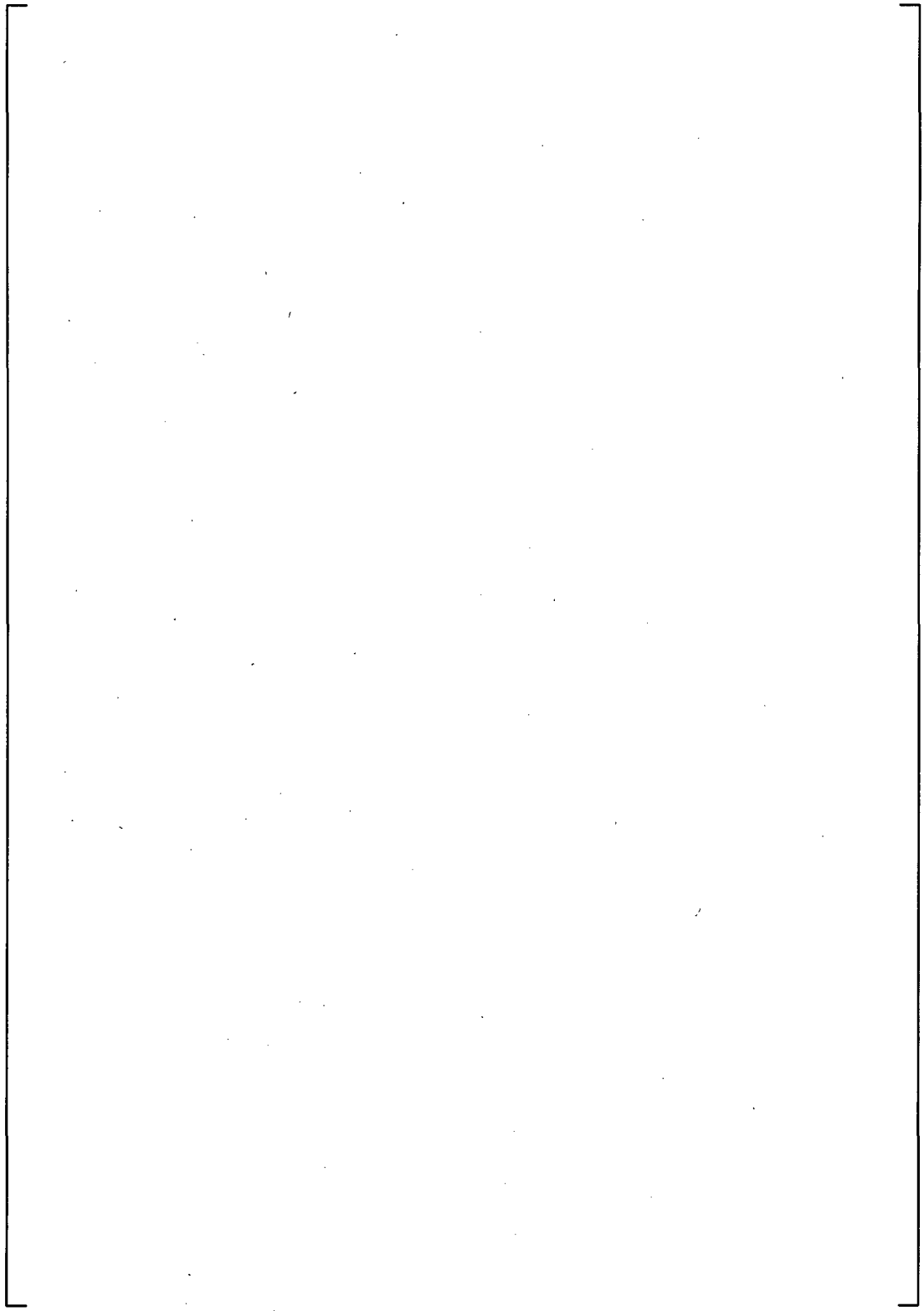

]

Figure 5-104: Run NRL09 Core Uncovery with High Boric Acid Concentration and [ ]^{c} (Cycle 4)

[

]^{c}

c

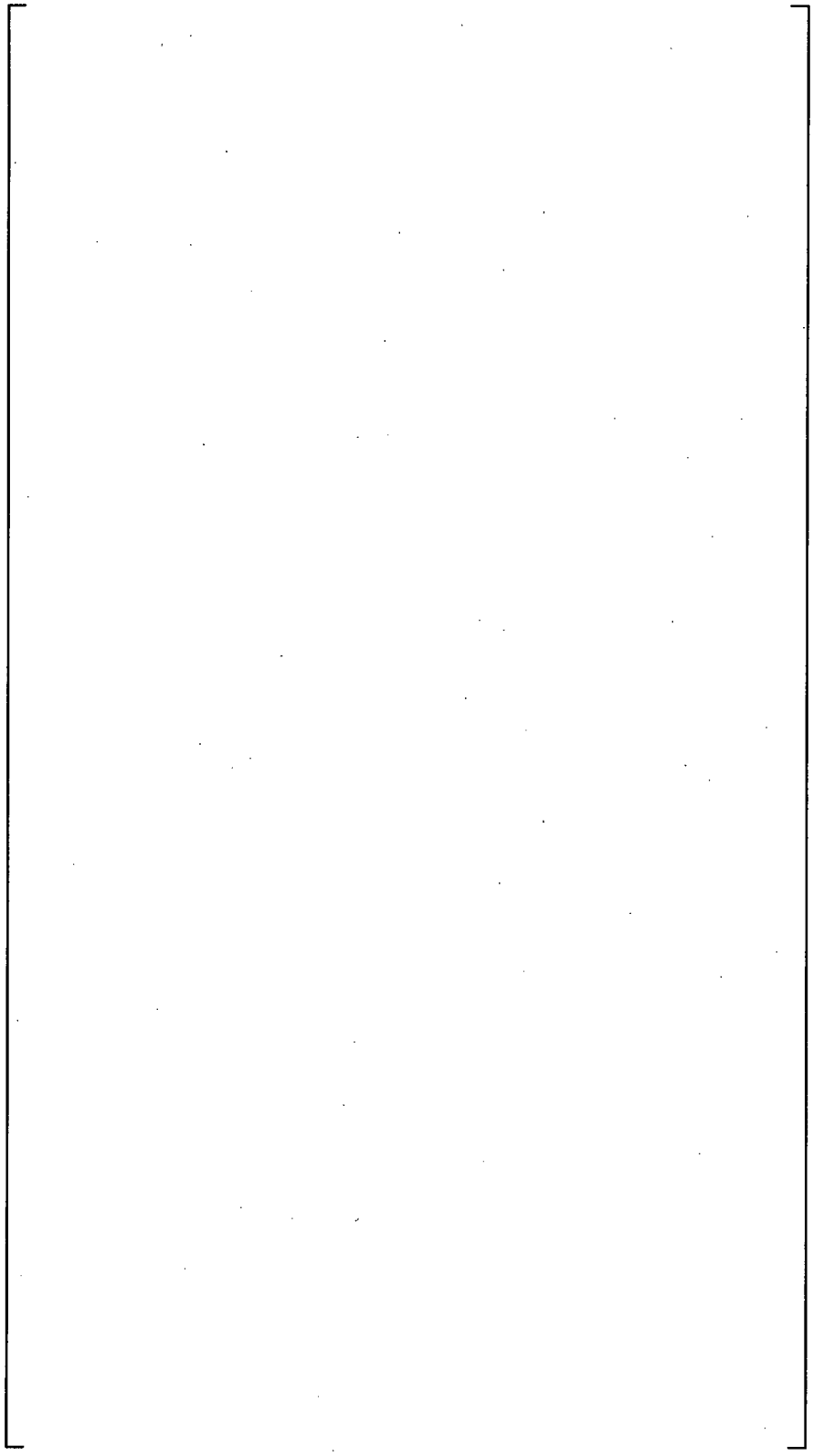

Figure 5-105: Run NRL09 Core Recovery and Precipitate Dissolution Process (Cycle 3)

6 DISCUSSION

In this chapter results from various experimental runs are compared to show the effects of unbuffered and buffered boric acid solutions with and without debris loadings on nucleate boiling heat transfer, heat and mass transport between the core to the lower plenum, precipitation and dissolution during core uncovery and recovery, and two-phase mixture level. Table 6-1 provides a summary of the solution composition and debris loading used for each run.

In Section 6.1 the effects of solution composition and debris loading on nucleate boiling heat transfer is discussed. First, runs NRL01, NRL02, and NRL03 are compared to show the effect of unbuffered boric acid with and without debris relative to de-ionized water. Next, runs NRL01, NRL06, and NRL09 are compared to show the effects of TSP buffered boric acid with and without debris relative to de-ionized water. Lastly, Runs NRL01, NRL05, and NRL08 are compared to show the effect of NaOH buffered boric acid with a debris loading relative to de-ionized water. In addition, comparison of runs NRL05, and NRL08 will identify any differences associated with the lower plenum design since NRL05 was conducted using the large lower plenum while NRL08 was conducted using the small lower plenum design.

In Section 6.2, fluid thermocouple measurements made in the core and lower plenum regions are compared for runs NRL01, NRL02, and NRL03 to highlight the observation that when unbuffered boric acid concentration builds in the core region due to boil-off, a point is reached in which higher temperature, higher concentration liquid in the core is transported to the lower plenum region and mixes with the cooler, less concentrated liquid contained in the lower plenum. This behavior was also observed in the buffered boric acid runs both with and without debris.

Table 6-1: Solution Composition and Debris Loading Test Matrix

c

In Section 6.3, precipitation and dissolution observations made during core uncovery and recovery cycles from runs NRL06, NRL08, and NRL09.

In Section 6.4, The impact of solution concentration on the two-phase mixture level is discussed by comparing images showing the two-phase mixture level height from run NRL09. During run NRL09, the power was initially held constant at 1400W then the power controller was set to follow the 10CFR50 Appendix K decay heat curve and a point was reached near the end of the run when the power decay reached 1400W. Therefore, it is possible to compare the mixture level at low and high solution concentrations under the same power level.

6.1 NUCLEATE BOILING WITH DEBRIS AND CHEMICALS

A major objective of this test program was to study the impact of debris and solution chemical components on nucleate boiling within the core region. When the core was covered no major degradation in heat transfer was observed due to solution composition or the presence of debris. In all experimental runs, the cladding temperature was a few degrees higher than saturation temperature, which is an indication of fully developed nucleate boiling. In this regime, most of the heat exchange is through direct transfer from the heater rod surface to the liquid in motion at the surface and not through the vapor bubbles shedding from the heated surface. In this section, the effect of debris and solution chemical composition on nucleate boiling heat transfer is examined.

Using power and temperature data collected during the experimental runs it is possible to create experimental boiling curves. A boiling curve consists of the surface heat flux plotted as a function of wall superheat. The wall super heat is usually defined as the difference between the heated surface temperature and the fluid saturation temperature, $(T_{wall} - T_{sat})$ (Reference 7). In the experiments, it was observed that boiling occurred during the entire experiment and it can be assumed that the fluid temperatures measured in the core region corresponds to the saturation temperature. The heater rod surface temperature, however, is not directly measured during the experiments. It is the heater rod cladding inside surface temperature that is measured during each experimental run.

[

]^{c}

To determine the heat flux, the first step is to calculate the heater rod surface area within the heated region. Using the heater rod geometry, the surface area of a single rod is calculated as:

$$A_s = (\pi D)L \tag{6-1}$$

where D is the heater rod diameter and L the heated length. Using the values for D and L given in Section 2.1 the heater rod surface area is calculated to be:

[ ]^c

Now the heat flux for a given time and decay heat can be determined by dividing the bundle power (P) at the given time by the number of heater rods (N) and the surface area:

$$q_w'' = \frac{P}{NA_s} \tag{6-2}$$

The wall heat flux was calculated using (Eq. 6-2) for a range of experimental times and decay heats as shown in Table 6-2.

Table 6-2: Calculated Heat Fluxes for given Experimental Times and Bundle Powers c

[ ]

6.1.1 Unbuffered Boric Acid with and without Debris

The first set of experimental boiling curves compares the results from runs NRL01, NRL02, and NRL03.

Run NRL01 was conducted using de-ionized water, run NRL02 was conducted using unbuffered boric acid, and run NRL03 was conducted using unbuffered boric acid with a debris loading. It should be noted that during run NRL03 the power was lost to heater rod 9. This resulted in an 11% decrease in bundle power and requires that the heat flux calculated after the power was lost to be adjusted to account for the power reduction.

[

]^{c}

[

]^{c}

Figure 6-1: Comparison of Experimental Boiling Curves for Runs NRL01, NRL02, and NRL03 Calculated at the [ ]^{c} Bundle Elevation

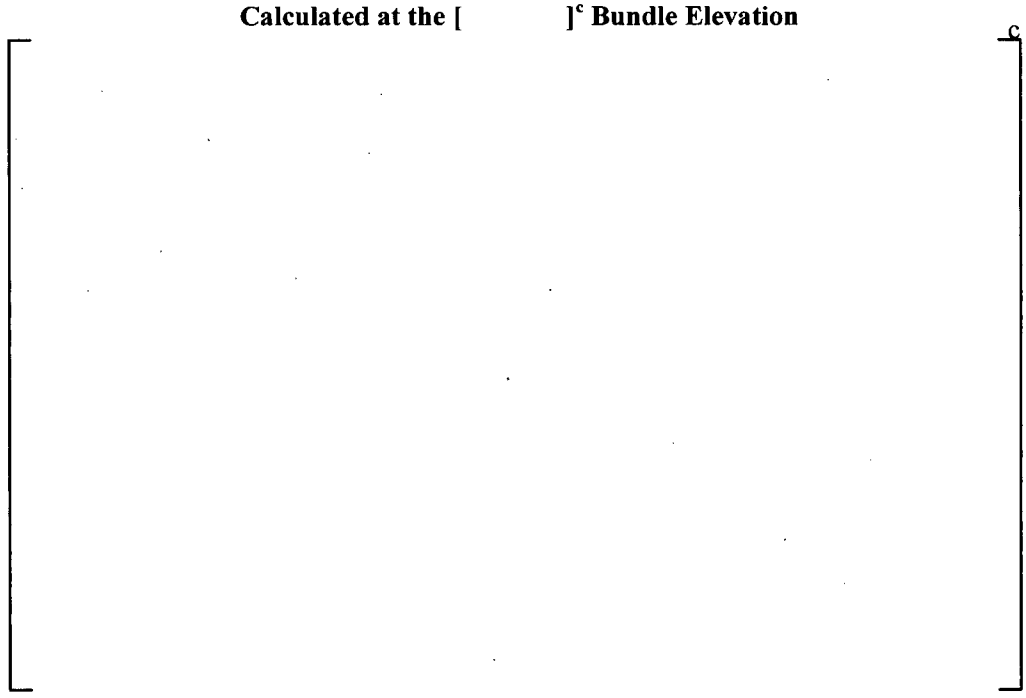

Figure 6-2: Comparison of Experimental Boiling Curves for Runs NRL01, NRL02, and NRL03 Calculated at the [ ]^{c} Bundle Elevation

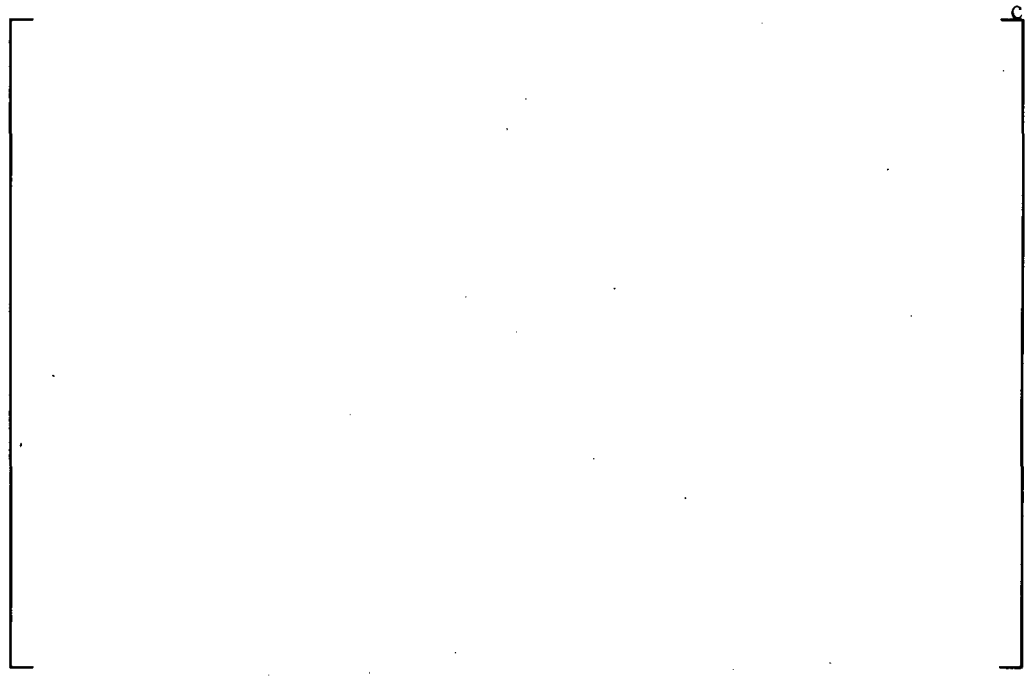

Figure 6-3: Comparison of Experimental Boiling Curves for Runs NRL01, NRL02, and NRL03 Calculated at the [ ]^{c} Bundle Elevation

Figure 6-4: Comparison of Core Fluid Temperature for Runs NRL01, NRL02, and NRL03 Measured at the [ ]^{c} Bundle Elevation

Figure 6-5: Comparison of Core Fluid Temperature for Runs NRL01, NRL02, and NRL03 Measured at the [ ]^{c} Bundle Elevation

Figure 6-6: Comparison of Core Fluid Temperature for Runs NRL01, NRL02, and NRL03 Measured at the [ ]^{c} Bundle Elevation

Figure 6-7: Comparison of Heater Rod Temperature for Runs NRL01, NRL02, and NRL03 Measured at the [ ]^{c} Bundle Elevation

Figure 6-8: Comparison of Heater Rod Temperature for Runs NRL01, NRL02, and NRL03 Measured at the [ ]^{c} Bundle Elevation

Figure 6-9: Comparison of Heater Rod Temperature for Runs NRL01, NRL02, and NRL03 Measured at the [ ]^{c} Bundle Elevation

6.1.2 Trisodium Phosphate Buffered Boric Acid with and without Debris

This set of boiling curves compares results from runs NRL01, NRL06, and NRL09. Run NRL01 was conducted using de-ionized water. Run NRL06 was conducted using boric acid buffered with TSP and has a debris loading. Run NRL09 was conducted using boric acid buffered with TSP but without any debris. Run NRL09 is unique in that [ ]^{c} was added near the end of the experiment. In order to compare the boiling characteristics of boric acid buffered with TSP with and without debris (NRL06 vs. NRL09) the data after the addition of the [ ]^{c} was removed before generating the boiling curve for run NRL09.

[

]^{c}

[

]c

(

Figure 6-10: Comparison of Experimental Boiling Curves for Runs NRL01, NRL06, and NRL09 Calculated at the [ ]^{c} Bundle Elevation

Figure 6-11: Comparison of Experimental Boiling Curves for Runs NRL01, NRL06, and NRL09 Calculated at the [ ]^{c} Bundle Elevation

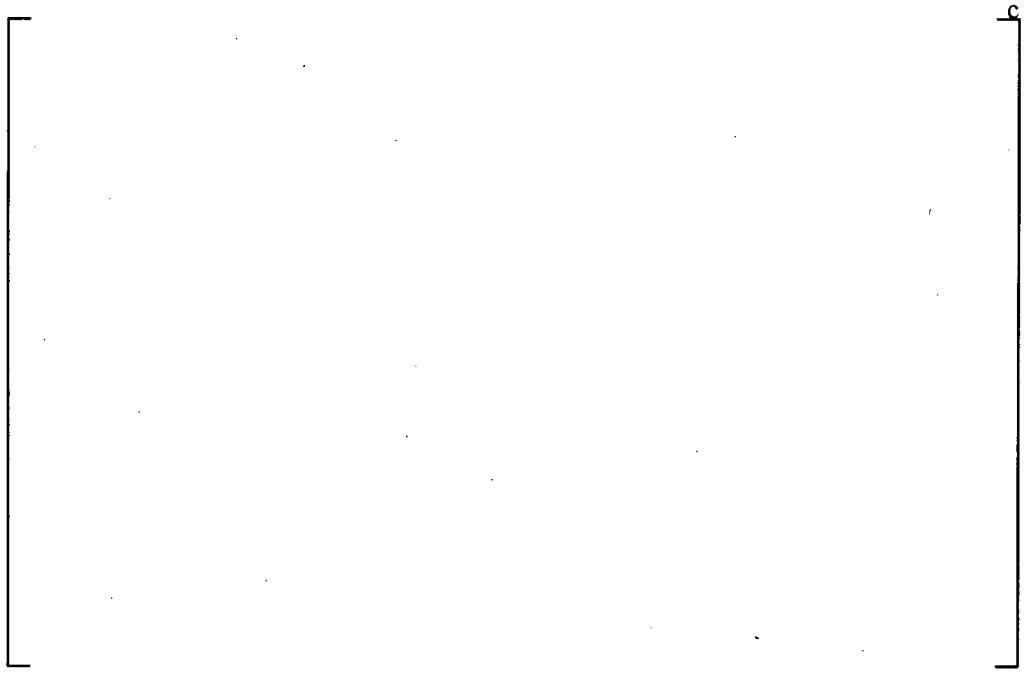

Figure 6-12: Comparison of Core Fluid Temperature for Runs NRL01, NRL06, and NRL09 Measured at the [ ]^{c} Bundle Elevation

Figure 6-13: Comparison of Core Fluid Temperature for Runs NRL01, NRL06, and NRL09 Measured at the [ ]^{c} Bundle Elevation

Figure 6-14: Comparison of Heater Rod Temperature for Runs NRL01, NRL06, and NRL09 Measured at the [ ]^{c} Bundle Elevation

Figure 6-15: Comparison of Heater Rod Temperature for Runs NRL01, NRL06, and NRL09 Measured at the [ ]^{c} Bundle Elevation

6.1.3 Sodium Hydroxide Buffered Boric Acid with Debris

This set of boiling curves compares results from runs NRL01, NRL05, and NRL08. Run NRL01 was conducted using de-ionized water and the large lower plenum design. Run NRL05 was conducted using boric acid buffered with NaOH, uses the large lower plenum design and has a debris loading. Run NRL08 was also conducted using boric acid buffered with NaOH and a debris loading but was conducted using the small lower plenum.

[

]^{c}

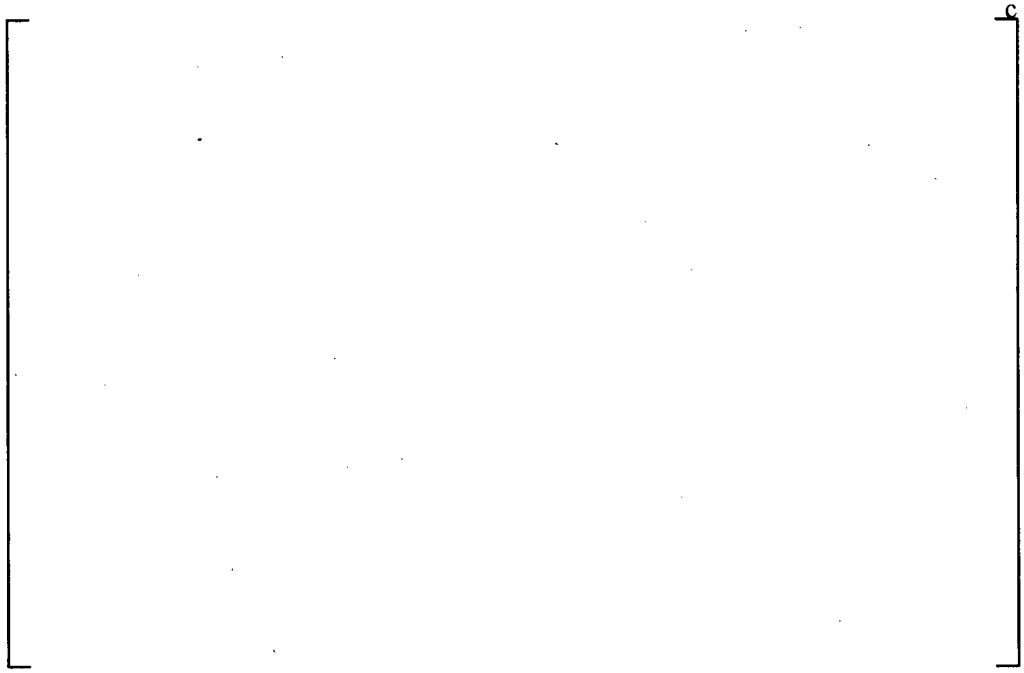

Figure 6-16: Comparison of Experimental Boiling Curves for Runs NRL01, NRL05, and NRL08 Calculated at the [ ]^{c} Bundle Elevation

Figure 6-17: Comparison of Core Fluid Temperatures for Runs NRL01, NRL05, and NRL08 at the [ ]^{c} Bundle Elevation

Figure 6-18: Comparison of Heater Rod Temperatures for Runs NRL01, NRL05, and NRL08 at the [ ]^{c} Bundle Elevation

6.2 BUOYANCY DRIVEN EXCHANGE

Fluid temperature in the lower plenum region depends highly on the core-to-lower plenum mass and heat transfer mechanisms. One important mechanism is buoyancy driven convection which is a result of density gradients between the fluids in the core and lower plenum. This convection mechanism has been studied experimentally and theoretically for simple configurations as described in Reference 12. The concentration of a buffered/unbuffered boric acid solution increases as water vaporizes in the core due to subcooled and nucleate boiling. The supply buffered/unbuffered solution from the downcomer feeds the lower plenum which has a lower concentration than in the core. Therefore, the core provides a source of higher density solution, while the lower plenum is a source of low density solution. The buoyancy force will drive the heavier fluid from the core to the lower plenum and circulate lighter fluid from the lower plenum to the core. Such buoyancy driven convection will continue until concentration in the core and lower plenum reach quasi-equilibrium. This buoyancy driven exchange between the core and lower plenum was observed in the larger scale VEERA (Reference 9) and BACCHUS [ ]^{c,e} test facilities.

[

]^{c,e}

[

]^{c,e}

Figure 6-19: Run NRL01 Fluid Temperature Measurements Made in the Core and Lower Plenum Regions

Figure 6-20: Run NRL02 Fluid Temperature Measurements Made in the Core and Lower Plenum Regions

Figure 6-21: Run NRL03 Fluid Temperature Measurements Made in the Core and Lower Plenum Regions

6.3 BORIC ACID PRECIPITATION AND DISSOLUTION

The uncovery and recovery cycles performed in runs NRL06, NRL08, and NRL09 demonstrated that chemical precipitation can accumulate on heater rod surfaces above the two-phase mixture level if the boric acid concentration is high. [

]^{c,e}

[

]c,e

Figure 6-22: Cladding Temperature Response during Core Uncovery and Recovery

6.4 IMPACT OF BORIC ACID CONCENTRATION ON TWO-PHASE MIXTURE LEVEL

The core two-phase mixture level is estimated by equating the static hydraulic head between the core and the downcomer. If the pressure loss from the top of the mixture level to vessel exit is ignored as well as frictional and acceleration pressure losses, the static hydraulic balance can be written as:

$$\int_0^{L_d} \rho_d dz = \int_0^{L_c} \alpha \rho_c dz \qquad (6\text{-}8)$$

where the integral on the left hand side of (Eq. 6-8) represents the static head in the downcomer and is expressed as the liquid density in the downcomer, ρ_d integrated across the entire length of the downcomer, L_d. The integral on the right hand side represents the static head in the core and is expressed as the liquid density in the core, ρ_c times the core average void fraction, α integrated across the core length, L_c.

The downcomer liquid density is assumed constant over the entire test. The core liquid density is the same as the downcomer liquid density at the beginning of the test but will increase as boric acid and debris concentrations build in the core region. The average core void fraction is proportional to the power and will decrease as the experiment progresses.

[

]^{c,e}

[

]^c,e

Table 6-3: Physical Properties of Buffered (TSP) Boric Acid	c

c

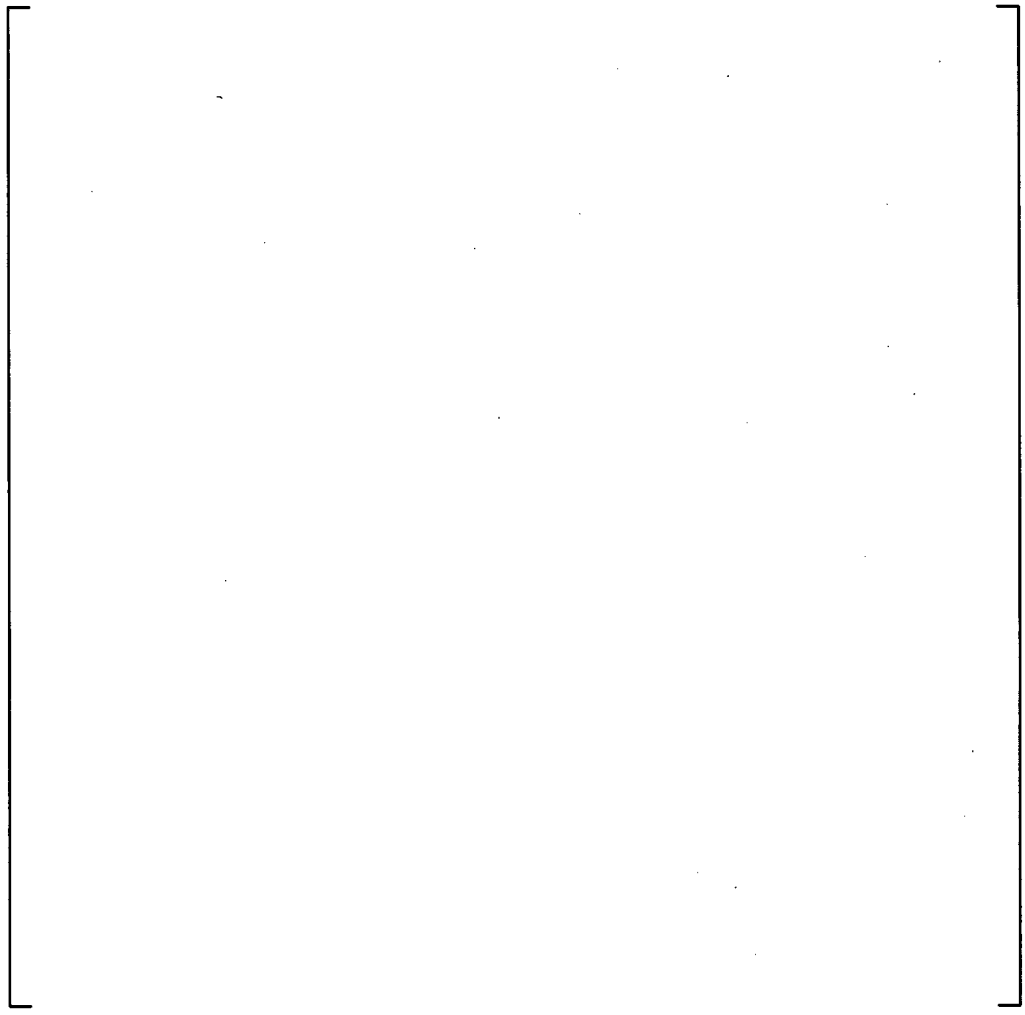

Figure 6-23: Run NRL09 Two-Phase Mixture Level at Similar Powers and Different Concentrations: (a) Low Boric Acid Concentration, (b) High Boric Acid Concentration

7 CONCLUSIONS AND RECOMMENDATIONS

[

]^{c,e}

[

]c,e

[

]c,e

8 REFERENCES

1. McCullough, C. et al., "Investigation of the Use of Aqueous Solutions as Emergency Coolants – Final Report," March 31, 1969.

2. WCAP-17021-NP, "Summary of Tests to Determine the Physical Properties of Buffered and Unbuffered Boric Acid Solutions," March 2009.

3. WCAP-17040-NP, "Small Scale Un-buffered and Buffered Boric Acid Nucleate Boiling Heat Transfer Tests with a Single Fuel Rod in a Vertical Channel," July 2009.

4. WCAP-16530-NP-A, "Evaluation of Post-Accident Chemical Effects in Containment Sump Fluids to Support GSI-191," March 2008.

5. WCAP-17047-NP, "Phenomena Identification and Ranking Tables (PIRT) for Un-Buffered/Buffered Boric Acid Mixing/Transport and Precipitation Modes in a Reactor Vessel During Post-LOCA Conditions," May 2009.

6. STD-MCE-07-53, "Reactor Coolant Chemistry after a LOCA and Issues with Core Cooling," September 25, 2007.

7. W. Rohsenow et al., "Handbook of Heat Transfer Fundamentals," 1985.

8. Walter C. Blasdale and Cyril M. Salansky, "Solubility Curves of Boric Acid and the Borates of Sodium," J. Am. Chem. Soc., 1939, 61(4), 917-920.

9. Tuunanen, J.; Tuomisto, H.; Raussi, P., "Experimental and Analytical Studies of Boric Acid Concentrations in a VVER-440 Reactor During the Long-Term Cooling Period of Loss-of-Coolant Accidents," Nuclear Engineering and Design, Vol. 148, July 1994, pgs. 217-231.

10. [ ]^{c,e}

11. WCAP-1570, "Literature Values for Selected Chemistry/Physical Properties of Aqueous Boric Acid Solutions," May 1960

12. Bird, R.B., Stewart, W.E. and Lightfoot, E.N., "Transport Phenomena," John Wiley & Sons, Inc., 1960.

13. Yeh H. C. "Modification of Void Fraction Correlation," Proceedings of the 4th International Topical Meetings on Nuclear Thermal Hydraulics Operations and Safety, Volume 1, Taipei, Taiwan, April 5-9, 1994.

14. [ ]^{c}

15. Astarita, G and Marrucci, G., Accademia Nazionale dei Lincei, Ser: VIII, 36, 836 (1964) Zuber, N., "An Integrated Structure and Scaling Methodology for Severe Accident Analysis, Appendix D, A Hierarchical Two-Tiered Scaling Analysis", NUREG/CR-5809, 1991.

16. WCAP-14270 Rev. 1, "AP600 Low Pressure Integral systems Test at Oregon State University, Facility Scaling Report," 1997.

17. WCAP-14727 Rev. 2, "AP600 Scaling and PIRT Closure Report," 1998.

18. Hochreiter, L. E., Cheung, F-B., Lin, T. F., Frepoli, C., Sridharan, A., Todd, D. R., Rosal, E. R., "Rod Bundle Heat Transfer Test Facility Test Plan and Design," NUREG/CR-6975, 2010.

19. Shames, I., "Mechanics of Fluids, "McGraw-Hill Inc., New York, 1962

20. Todreas, N., Kazimi, M., "Nuclear Systems I, Thermal Hydraulic Fundamentals," p. 373-379, Hemisphere Publishing, 1990.

21. Levy, S., "Two-Phase Flow in Complex Systems," p. 28-85, John Wiley & Sons, 1999.

22. RT-TR-11-21, "Property Measurement Analysis: The Assessment of Sodium Hydroxide and Trisodium Phosphate Solutions with and without the Presence of Solid Debris," October 2011.

23. LTR-LIS-11-686 Rev. 0a, "Preliminary Scaling Analysis and Conceptual Design of a Proposed PWROG Boric Acid Precipitation Program Test Facility," March 2012.

24. [

]^{c}

APPENDIX A
RESOLUTION OF ISSUES NOT ADDRESSED IN PREVIOUS BOILING CHANNEL TESTS

WCAP-17040-NP (Reference 3) documents the single rod boiling channel tests conducted with unbuffered and buffered boric acid solutions without debris. In Appendix A of Reference 3, three known scenarios of interest that were not investigated are described and it was recommended that future tests be conducted to investigate the additional scenarios of interest. The three additional scenarios recommended for future testing in Reference 3 are presented along with responses to addressing these scenarios:

1. [

]^{c,e}

2. [

]^{c,e}

3. [

]^{c,e}

[

]c,e

APPENDIX B
BORIC ACID SOLUBILITY

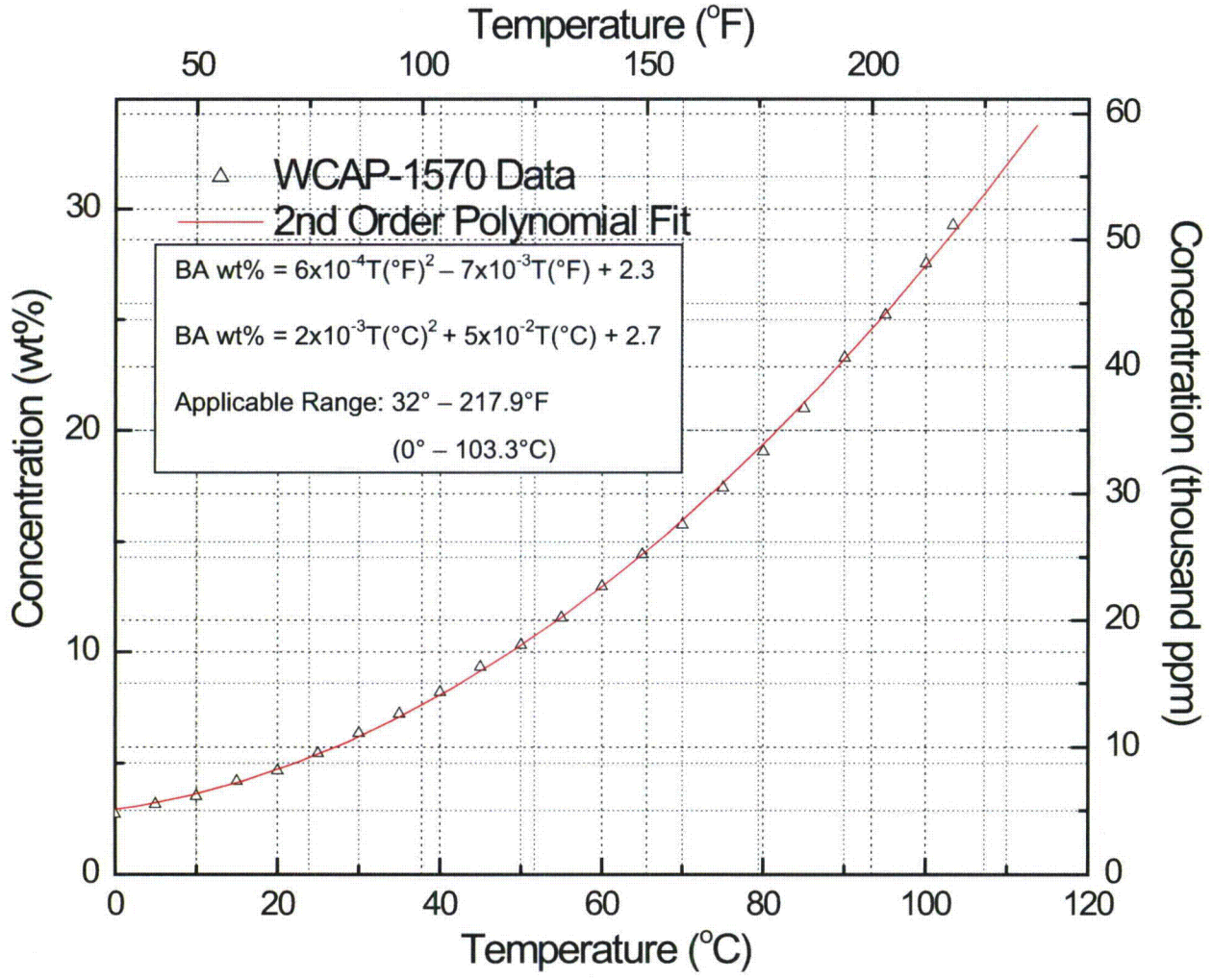

Figure B-1: Boric Acid (H_3BO_3) Solubility Limit as a Function of Temperature (Reference 11)

APPENDIX C
VISCOSITY DATA OF BUFFERED BORIC ACID SOLUTION WITH AND WITHOUT DEBRIS

The viscosity data of buffered boric acid solutions with and without debris are reported in RT-TR-11-21 (Reference 22) as part of PWROG program PA-ASC-0689. The methods of measurement, calibration and uncertainty associated with the measurement device are all discussed in Reference 22. Tables C-1 and C-2 show the chemical compositions for buffered boric acid (NaOH and TSP) solutions with and without debris used in the viscosity tests. Table C-3 shows the chemical composition of the AlOOH solution used in the testing. Three to six viscosity measurements were made for a given shear rate and solution temperature as described in Reference 22. In this appendix, average viscosity and standard deviation values derived from the given solution sample populations are presented.

Table C-4 summarizes the average viscosity and 2σ uncertainty obtained from the sample population for buffered (NaOH) boric acid solutions from 140°F to 212°F (60°C to 100°C). Figures C-1 to C-5 present the viscosity data graphically for the 5 solution temperatures measured. In the figures, the error bars represent ±2σ uncertainty.

Table C-5 summarizes the average viscosity and 2σ uncertainty obtained from the sample population for buffered (NaOH) boric acid solutions with debris from 140°F to 212°F (60°C to 100°C). Figures C-6 to C-10 present the viscosity data graphically for the 5 solution temperatures measured. In the figures, the error bars represent ±2σ uncertainty.

Table C-6 summarizes the average viscosity and 2σ uncertainty obtained from the sample population for buffered (TSP) boric acid solutions from 140°F to 212°F (60°C to 100°C). Figures C-11 to C-15 present the viscosity data graphically for the 5 solution temperatures measured. In the figures, the error bars represent ±2σ uncertainty.

Table C-7 summarizes the average viscosity and 2σ uncertainty obtained from the sample population for buffered (TSP) boric acid solutions with debris from 140°F to 212°F (60°C to 100°C). Figures C-16 to C-20 present the viscosity data graphically for the 5 solution temperatures measured. In the figures, the error bars represent ±2σ uncertainty.

[

]°

Table C-1: Chemical Additions for Solutions without Debris

c

Table C-2: Chemical Additions for Solutions with Debris

c

Table C-3: Chemical Additions for AlOOH

c

Table C-4: Viscosity of Buffered (NaOH) Boric Acid without Debris

c

Figure C-1: Viscosity of Buffered (NaOH) Boric Acid at 140°F

Figure C-2: Viscosity of Buffered (NaOH) Boric Acid at 158°F

Figure C-3: Viscosity of Buffered (NaOH) Boric Acid at 176°F

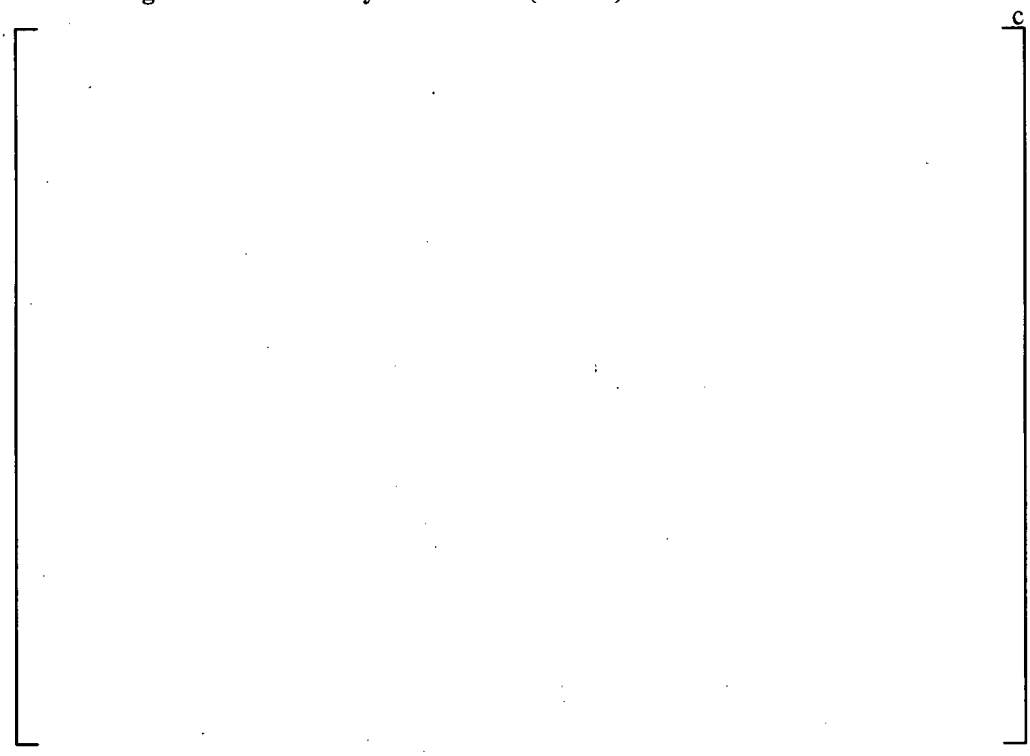

Figure C-4: Viscosity of Buffered (NaOH) Boric Acid at 194°F

Figure C-5: Viscosity of Buffered (NaOH) Boric Acid at 212°F

Table C-5: Viscosity of Buffered (NaOH) Boric Acid with Debris

c

Table C-5: Viscosity of Buffered (NaOH) Boric Acid with Debris (cont.)

c

c

Figure C-6: Viscosity of Buffered (NaOH) Boric Acid with Debris at 140°F

Figure C-7: Viscosity of Buffered (NaOH) Boric Acid with Debris at 158°F

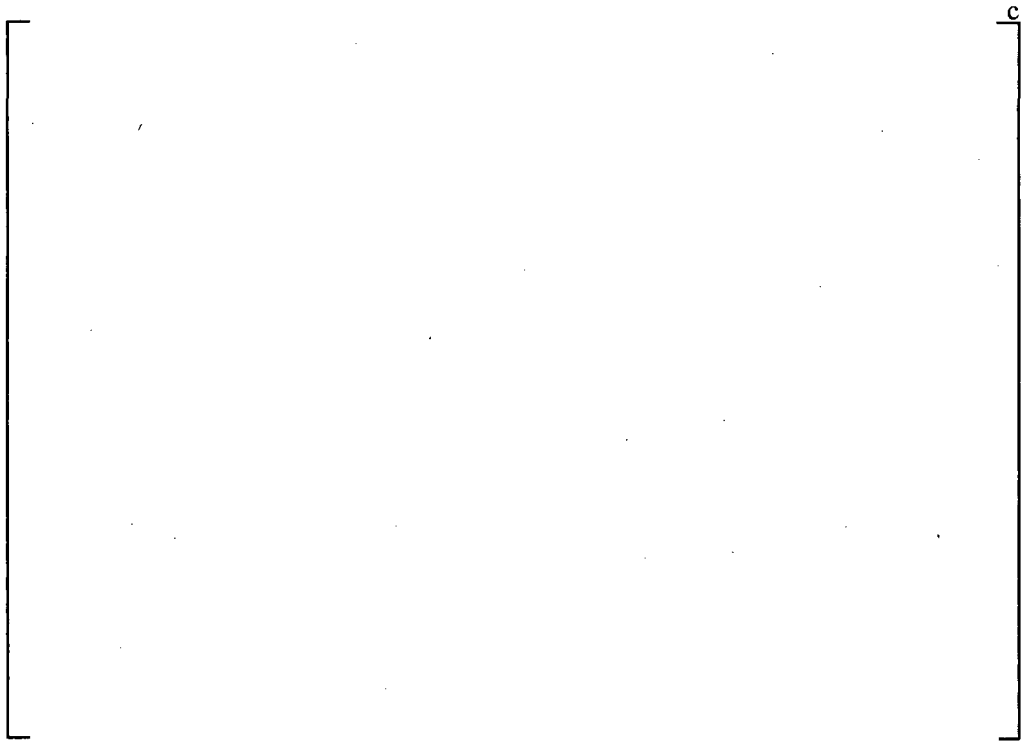

Figure C-8: Viscosity of Buffered (NaOH) Boric Acid with Debris at 176°F

[c]

Figure C-9: Viscosity of Buffered (NaOH) Boric Acid with Debris at 194°F

[c]

Figure C-10: Viscosity of Buffered (NaOH) Boric Acid with Debris at 212°F

Table C-6: Viscosity of Buffered (TSP) Boric Acid without Debris

c

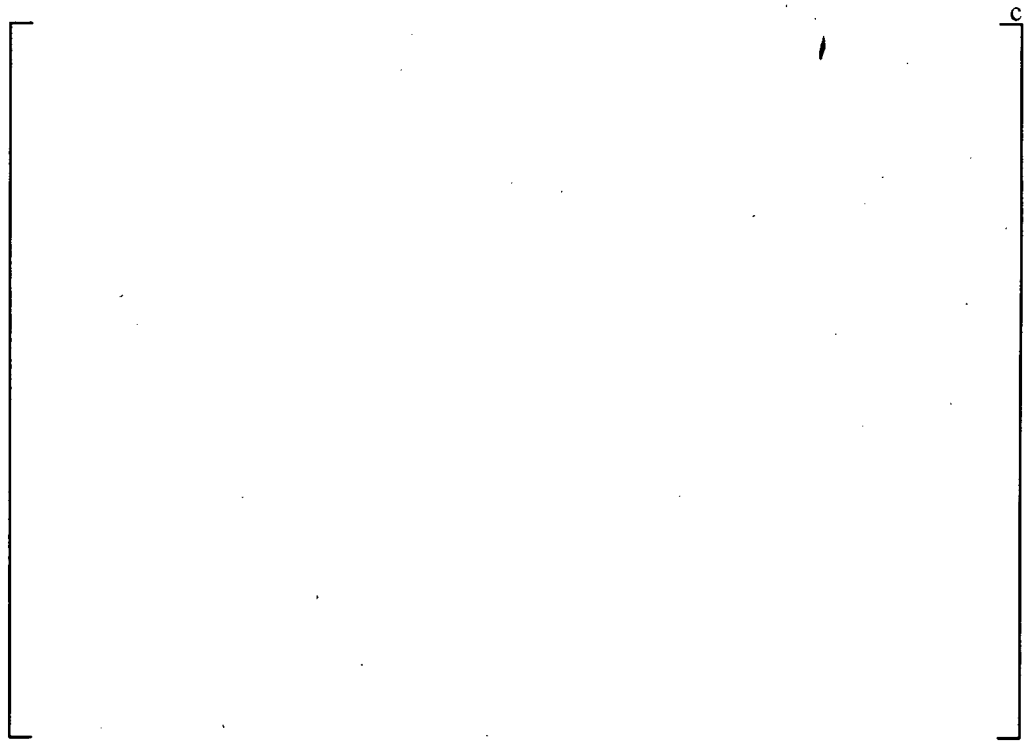

Figure C-11: Viscosity of Buffered (TSP) Boric Acid at 140°F

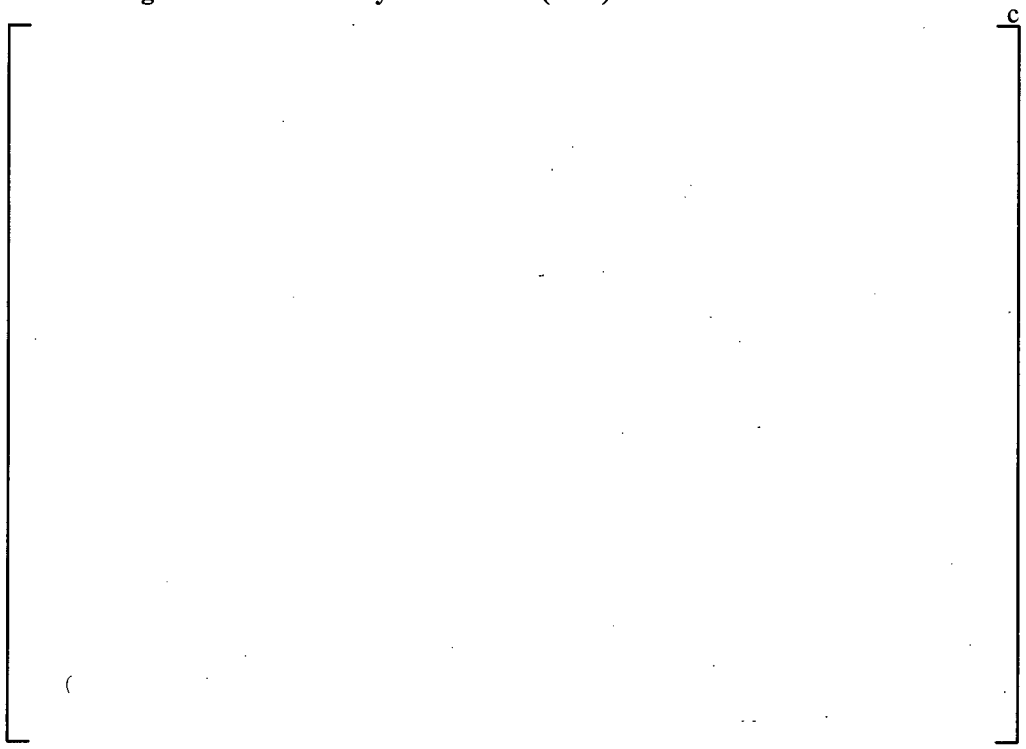

Figure C-12: Viscosity of Buffered (TSP) Boric Acid at 158°F

Figure C-13: Viscosity of Buffered (TSP) Boric Acid at 176°F

Figure C-14: Viscosity of Buffered (TSP) Boric Acid at 194°F

Figure C-15: Viscosity of Buffered (TSP) Boric Acid at 212°F

Table C-7: Viscosity of Buffered (TSP) Boric Acid with Debris

c

Table C-7: Viscosity of Buffered (TSP) Boric Acid with Debris (cont.)	
[	] c

[ ] c

Figure C-16: Viscosity of Buffered (TSP) Boric Acid with Debris at 140°F

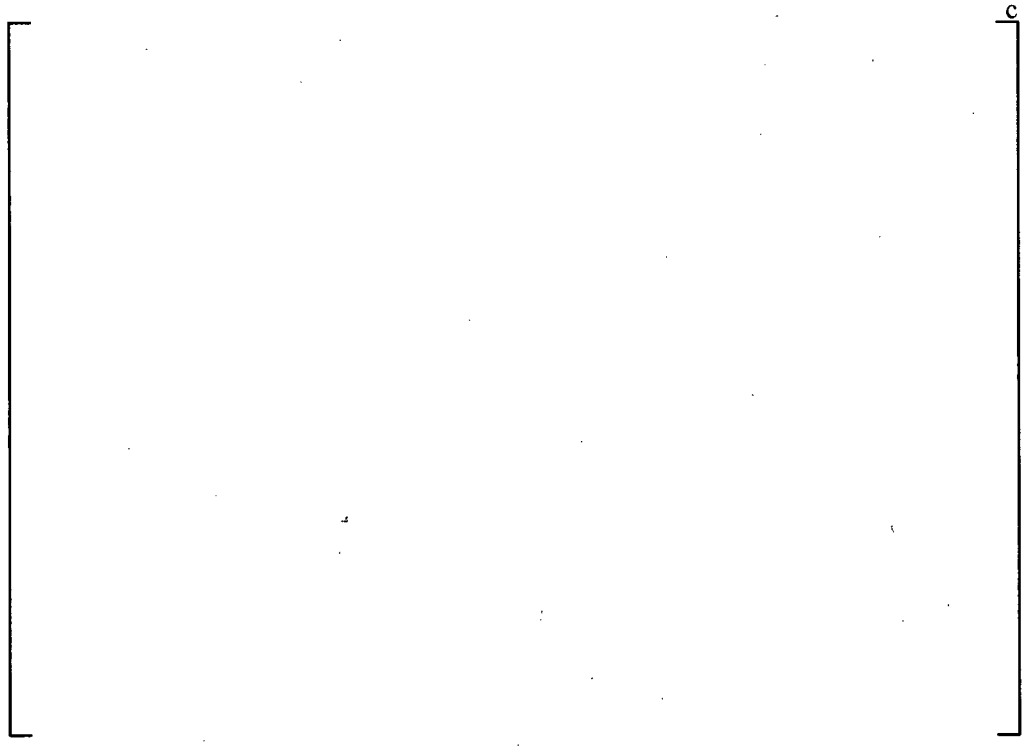

Figure C-17: Viscosity of Buffered (TSP) Boric Acid with Debris at 158°F

Figure C-18: Viscosity of Buffered (TSP) Boric Acid with Debris at 176°F

Figure C-19: Viscosity of Buffered (TSP) Boric Acid with Debris at 194°F

Figure C-20: Viscosity of Buffered (TSP) Boric Acid with Debris at 212°F

APPENDIX D
SURFACE TENSION DATA OF BUFFERED BORIC ACID SOLUTION WITH AND WITHOUT DEBRIS

The surface tension data of buffered boric acid solutions with and without debris are reported in RT-TR-11-21 (Reference 22) as part of PWROG program PA-ASC-0689. The methods of measurements, calibration and uncertainty associated with the instrument are all discussed in Reference 22. Tables D-1 and D-2 show chemical compositions for buffered boric acid (NaOH and TSP) with and without debris used for the surface tension testing. Table D-3 lists the chemical composition of AlOOH used in the testing. Surface tension measurements were made for a given solution temperature using 3 independent samples and each sample was measured 3 times resulting in a sample population of 9 for each solution composition as described in Reference 22. In this appendix, average surface tension and standard deviation values derived from the given solution sample populations are presented.

Table D-4 summarizes the average surface tension and 2σ uncertainty obtained from the sample population for all buffered boric acid solutions with and without debris from 140°F to 212°F (60°C to 100°C). Figures D-1 to D-4 present the surface tension data graphically for the 4 solution compositions and the 5 temperatures measured. In the figures, the error bars represent ±2σ uncertainty.

Figures D-1 and D-2 present surface tension test results for buffered boric acid (NaOH) with and without debris. The impact of debris on surface tension appears to be much less than its impact on viscosity. The same trend is true for TSP buffered boric acid solution as observed by comparison of Figures D-3 and D-4.

Table D-1: Chemical Additions for Solutions without Debris

c

Table D-2: Chemical Additions for Solutions with Debris

c

Table D-3: Chemical Additions for AlOOH c

[

]

Table D-4: Surface Tension of Buffered Boric Acid Solutions with and without Debris c

[

]

Figure D-1: Surface Tension of Buffered (NaOH) Boric Acid

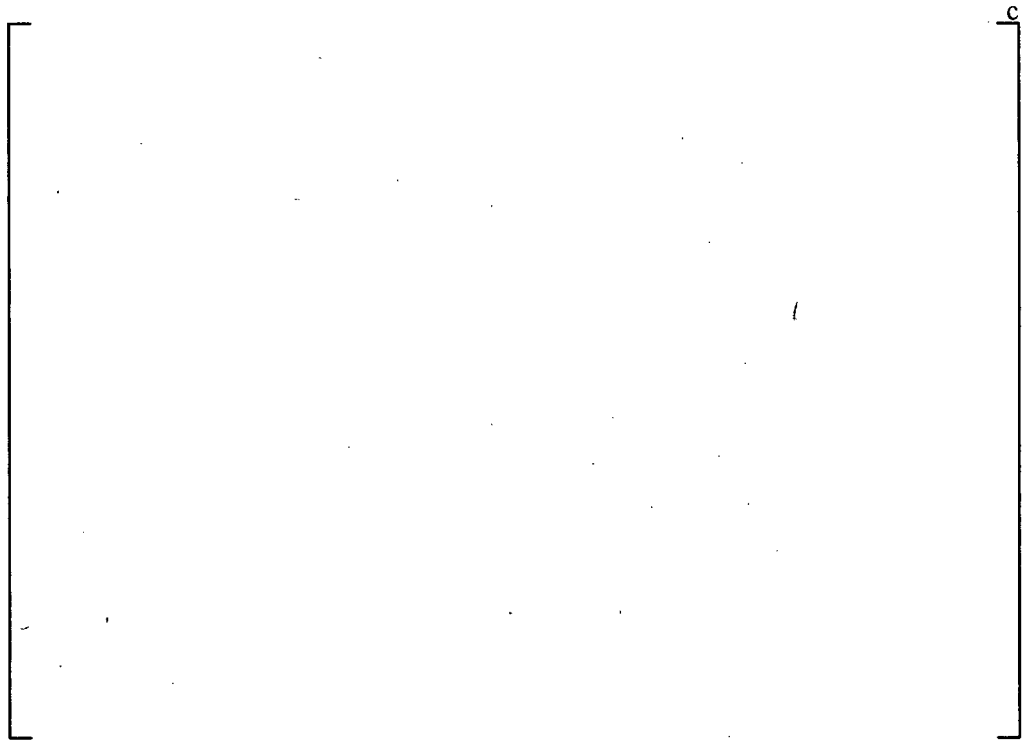

Figure D-2: Surface Tension of Buffered (NaOH) Boric Acid with Debris

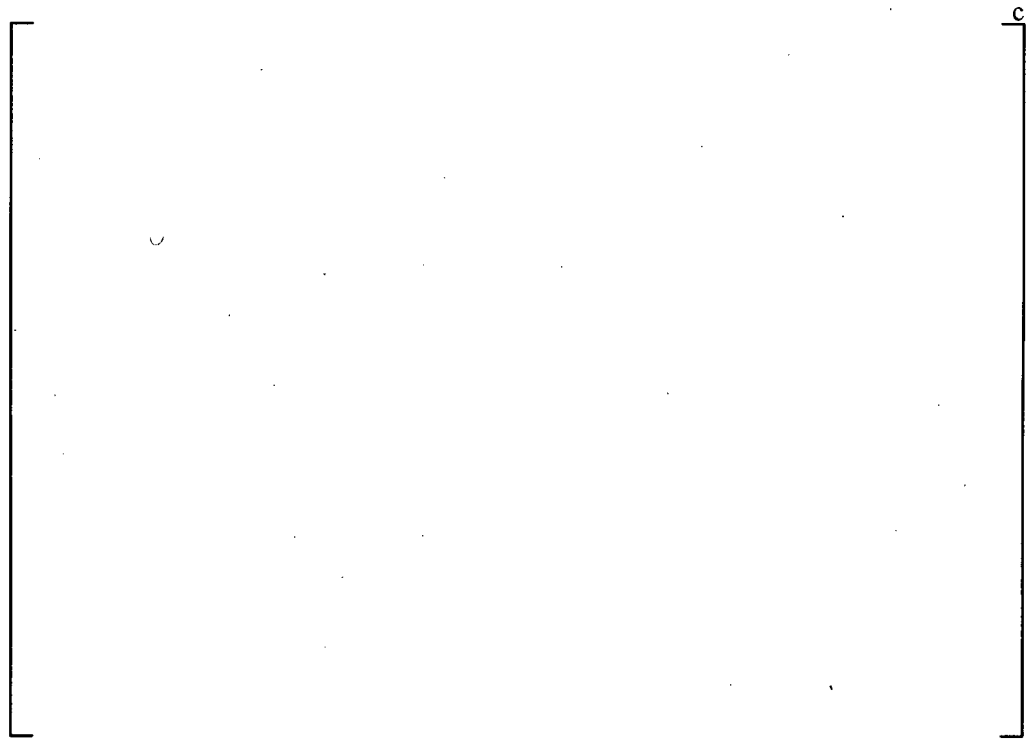

Figure D-3: Surface Tension of Buffered (TSP) Boric Acid

Figure D-4: Surface Tension of Buffered (TSP) Boric Acid with Debris